

Title of thesis

**Analysis of Pressure Drop and Heat  
Transfer of Annular Deposition Test Unit**

I, MUNZIR AHMED IBRAHIM ABDALLAH hereby allow my thesis to be placed at the Information Resource Center (IRC) of Universiti Teknologi PETRONAS (UTP) with the following conditions:

1. The thesis becomes the property of UTP.
2. The IRC of UTP may make copies of the thesis for academic purposes only.
3. This thesis is classified as

Confidential

Non-confidential

If this thesis is confidential, please state the reason:

---

---

---

The contents of the thesis will remain confidential for \_\_\_\_\_ years.


Remarks on disclosure:

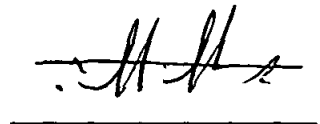
---

---

---

Endorsed by:

  
Signature of Author

  
Signature of Supervisor

Permanent Address:

AP. Dr. Hussain Al-Kayiem

Date: March 25, 2008

Date: March 25, 2008

UNIVERSITI TEKNOLOGI PETRONAS

Approval by Supervisor (s)

The undersigned certify that they have read, and recommend to The Postgraduate  
Studies Programme for acceptance, a thesis entitled:

Analysis of Pressure Drop and Heat Transfer of Annular  
Deposition Test Unit

submitted by:

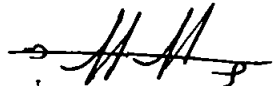
Munzir Ahmed Ibrahim Abdallah

for the fulfillment of the requirements for the degree of

Master of Science in Mechanical Engineering

Signature

:



Main Supervisor

:

AP. Dr. Hussain H. Jaafer Al-Kayiem

Date

:

March 25, 2008

Co-Supervisor

\_\_\_\_\_

UNIVERSITI TEKNOLOGI PETRONAS

ANALYSIS OF PRESSURE DROP AND HEAT TRANSFER  
OF ANNULAR DEPOSITION TEST UNIT


BY  
MUNZIR AHMED IBRAHIM ABDALLAH

A THESIS  
SUBMITTED TO THE POSTGRADUATE STUDIES PROGRAMME  
AS A REQUIREMENT FOR THE  
DEGREE OF MASTER OF SCIENCE IN MECHANICAL ENGINEERING

BANDAR SERI ISKANDAR,  
PERAK  
MARCH 2008

## DECLARATION

I hereby declare that the thesis is based on my original work except for quotations and citations which have been duly acknowledged. I also declare that it has not been previously or concurrently submitted for any other degree at UTP or other institutions.

Signature :   
Name : **Munzir Ahmed Ibrahim Abdallah**  
Date : **March 25, 2008**

## ACKNOWLEDGEMENT

All gratitude and thanks are due to “*ALLAH*” for his guidance throughout this work and for all the blessings he has bestowed upon me. This study would not have been done without the help of “*ALLAH*”.

I would like to thank my supervisor, Assoc. Prof. Dr Hussain H. Jaafer Al-Kayiem, you have helped me when I had questions and needed guidance.

Thank you Dr. Anwar Raja, for giving me the opportunity to join PETRONAS Research Sdn Bhd, PRSB. Thank you as well for your supervision and encouragement during the early steps of this work.

Thank you Dr. Toma, your knowledge in this field and your guidance have been mainly responsible for the success of this work. It was an amazing learning experience that I will never forget.

Thank you to staff members of Sub-Surface and Facility Engineering Group in PETRONAS Research Sdn Bhd, PRSB, for making their laboratory available for me. Thank you as well for helping in the experimental work of this study.

Thank you to all staff members of the postgraduate studies program. Appreciation is acknowledged for the assistantship opportunity provided by UNIVERSITI TEKNOLOGI PETRONAS.

Finally thank you to my parents, sisters and brothers for their prayers and supports. Thank you to my friends and many other who have in a way or another helped me.

## ABSTRACT

Deposition of wax on the internal wall of pipelines is often regarded as a problem since the tube diameter is reduced. Consequently, more power is needed to force the same amount of oil through the system. In order to design efficient sub-sea petroleum production facilities to achieve optimum production returns, it is necessary to understand the phenomena of the wax deposition and provide prediction for the nature of deposits.

PETRONAS High Temperature/High Pressure Model Pipeline and Wax Deposition Facility, HT/HPMPWDF, is designed and installed, to investigate and model the process of the wax deposition. In this system, pressure drop and heat transfer are proposed as the key parameters to model the process of the wax deposition. Experiments were carried out to investigate and characterize the hydrothermal performance of the test section of the system. Pressure drop and temperature variation data throughout the test section of the deposition apparatus with varying flow condition were measured and processed analytically. Also, pressure drop and heat transfer data were predicted based on the available correlations. Comparison was made between the two models. For each parameter involved in the pressure drop calculations, a parametric analysis was performed to study its effect on the pressure drop estimation. The discrepancies between the measured and calculated pressure drop results were justified and a realistic pressure drop correlation was developed based on the equivalent length technique. The heat transfer was investigated in terms of the steady state energy balance. Also, several heat transfer correlations were used to predict the heat transfer. Comparison between the theoretical and experimental results reveals that *Sandal et. al.* correlation for the convective heat transfer is produced the best agreement with the experimental results.

The system is proved to provide an experimental data within an accuracy of 7 % AAPE for the pressure drop and 5% AAPE for the turbulent convective heat transfer. A steady state thermal energy balance of 6 % AAPE is achieved. It could be concluded that the proposed correlations have brought the system to the capability of modeling and predicting the wax deposition formation.

## ABSTRAK

Pengenapan wax pada dinding dalam sesuatu paip sering dianggap sebagai masalah apabila diameter dalamannya berkurangan. Akibatnya, lebih tenaga diperlukan untuk memaksa pengaliran minyak dalam sistem perpaipan walaupun pada jumlah yang sama. Untuk merekabentuk kemudahan pengeluaran petroleum dasar lautan yang berkesan dalam mencapai pulangan pengeluaran yang optimum, adalah penting untuk memahami fenomena enapan wax dan pemberian ramalan enapan semulajadi.

Model Perpaipan dan Kemudahan Enapan Wax Suhu Lampau / Tekanan Lampau PETRONAS (HT/HPMPWDF) telah direkabentuk dan dipasang bagi menyiasat dan memodelkan proses enapan wax ini. Dalam model tersebut, penurunan tekanan dan pemindahan haba telah dicadangkan sebagai parameter utama dalam memodelkan proses enapan wax. Ujikaji dijalankan untuk menyiasat dan mencirikan pencapaian hidro-haba pada bahagian ujikaji di dalam sistem. Kepelbagaian data penurunan tekanan dan suhu di sepanjang bahagian ujikaji berserta kepelbagaian keadaan pengaliran telah diukur dan diproses secara analitikal. Selain daripada itu, penurunan tekanan dan pemindahan haba diramalkan berdasar kepada formula persamaan (correlation) yang sedia ada. Perbandingan telah dibuat di antara dua model. Untuk setiap parameter yang digunakan dalam pengiraan penurunan tekanan, analisa "parametric" dilakukan untuk mengkaji kesannya kepada penganggaran penurunan tekanan. Perbezaan antara penurunan tekanan yang diukur dan yang dikira telah dihurai dan dibuktikan; formula persamaan (correlation) penurunan tekanan yang realistik telah dibangunkan berdasarkan kepada teknik panjang setara. Pemindahan haba telah diselidiki dalam erti kata penyeimbangan tenaga pada keadaan stabil. Tambahan pula, beberapa formula persamaan (correlation) pemindahan haba digunakan dalam meramalkan pemindahan haba. Perbandingan yang dibuat di antara keputusan teori dan ujikaji menunjukkan bahawa formula persamaan (correlation) *Sandal et. al.* bagi pemindahan haba konvektif telah menghasilkan persetujuan yang terbaik dengan keputusan ujikaji.

Sistem ini telah terbukti mampu menghasilkan data ujikaji yang berketepatan 7% AAPE untuk penurunan tekanan dan berketepatan 5% AAPE bagi pemindahan haba konveksi tidak stabil (turbulent convection). Penyeimbangan tenaga haba berkeadaan stabil pada kadar 6% telah dicapai. Dapat dirumuskan bahawa formula persamaan (correlation) yang telah dicadangkan telah menjadikan sistem ini berkeupayaan dalam memodelkan dan meramalkan pembentukan enapan wax.



## TABLE OF CONTENTS

<b>STATUS OF THESIS</b> .....	<b>I</b>
<b>APPROVAL PAGE</b> .....	<b>II</b>
<b>TITLE PAGE</b> .....	<b>III</b>
<b>DECLARATION</b> .....	<b>IV</b>
<b>ACKNOWLEDGEMENT</b> .....	<b>V</b>
<b>ABSTRACT</b> .....	<b>VI</b>
<b>ABSTRAK</b> .....	<b>VII</b>
<b>TABLE OF CONTENTS</b> .....	<b>IX</b>
<b>LIST OF TABLES</b> .....	<b>XI</b>
<b>LIST OF FIGURES</b> .....	<b>XII</b>
<b>1. INTRODUCTION</b> .....	<b>1</b>
1.1 PIPELINE WAX DEPOSITION .....	1
1.2 PARAFFIN/WAX DEPOSITION MECHANISIM .....	4
1.3 PROBLEM STATEMENT .....	5
1.4 RESEARCH OBJECTIVES .....	7
1.5 RESEARCH METHODOLOGY .....	7
1.6 DISSERTATION STRUCTURE.....	8
<b>2. LITERATURE REVIEW</b> .....	<b>9</b>
2.1 PREDICTION OF PARAFFIN/WAX DEPOSITION .....	9
2.2 FLUID FLOW IN ANNULUS .....	15
2.3 HEAT TRANSFER IN ANNULUS .....	21
<b>3. EXPERIMENTAL TEST FACILITY</b> .....	<b>25</b>
3.1 OIL SYSTEM .....	26
3.2 BASE-LINE DIFFERENTIAL PRESSURE SECTION (DP-1).....	29
3.3 PARAFFIN DEPOSITION TEST SECTION (SEC-1).....	30
3.4 COOLING SYSTEM.....	32

3.5 HEATING SYSTEM .....	35
3.6 AUXILIARY SYSTEM.....	38
3.7 DATA ACQUISITION AND CONTROL SYSTEM .....	39
<b>4. PRESSURE DROP EXPERIMENTAL INVESTIGATIONS.....</b>	<b>44</b>
4.1 INTRODUCTION .....	44
4.2 EXPERIMENTAL PROCEDURES.....	45
4.3 ANALYTICAL MODELING PROCEDURE.....	50
4.4 THEORETICAL ANALYSIS .....	54
4.5 RESULT AND DISCUSSION .....	56
4.6 PARAMETERIC ANALYSIS.....	62
4.7 DEVELOPMENT OF REALISTIC PRESSURE DROP CORRELATION ....	74
<b>5. HEAT TRANSFER EXPERIMENTAL INVESTIGATIONS .....</b>	<b>86</b>
5.1 INTRODUCTION .....	86
5.2 EXPERIMENTAL PROCEDURE .....	89
5.3 THEORETICAL ANALYSIS .....	93
5.4 EXPERIMENTAL ANALYSIS .....	95
5.5 ENERGY BALANCE INVESTIGATIONS .....	98
5.6 HEAT TRANSFER CORRELATION INVESTIGATIONS .....	104
<b>6. CONCLUSIONS AND RECOMMENDATIONS.....</b>	<b>120</b>
<b>7. REFERENCES.....</b>	<b>126</b>
<b>8. APPENDIXES .....</b>	<b>132</b>

## LIST OF TABLES

<b>Table</b>	<b>Title</b>	<b>Page</b>
4.1	Test matrix for three test runs performed at different temperatures	47
4.2	Dimensions of Deposition Apparatus (DA)	65
4.3	Statistical Error Analysis	81
4.4	Experimental-measured data Average Absolute Percent Error	83
5.1	Fully-Developed Turbulent Convective Heat Transfer Correlations	106
5.2	Theoretical-Experimental error analysis of the heat transfer correlation	117

## LIST OF FIGURES

Figure	Title	Page
1.1	Pipeline Petroleum Transport Plugging (Mansoori et al., 2003)	2
1.2	Schematic of the wax deposition process (Ramachandran, 2004)	4
1.3	Photograph of the oil tank storage.	6
2.1	Eccentricity Degrees in Annuli (Boone, 2004)	15
2.2	Thermal boundary layer in a concentric annulus - idealized model	23
3.1	Schematic of Oil Flow Control System	28
3.2	Schematic of the Base-Line Differential Pressure Section	29
3.3	Cross sectional view of the Paraffin Deposition Test Section	31
3.4	Schematic of Paraffin Deposition Test Section	31
3.5	Schematic of the Cooling System	33
3.6	Photograph of the Cooling System	34
3.7	Schematic of the Heating System	36
3.8	Photograph of the Heating System	37
3.9	The process control equipment	40
3.10	LabVIEW, Driver Software and Measurement Hardware	41
3.11	The Process Control Main Graphical User Interface - Labview	42
3.12	The PID Panel Interface Window for Control of Fluid Process Pump Speed, Flow Rate and Fluid Temperature	43
4.1	Typical stepwise variation of flowrate during a non-deposition test	46
4.2	Pressure Drop and Flow Rate for Mineral Oil Run at 50 °C	48
4.3	Pressure Drop and Flow Rate for Mineral Oil Run at 60 °C	48
4.4	Pressure Drop and Flow Rate for Mineral Oil Run at 70 °C	49
4.5	Schematic of the test section	55
4.6	Measured and Calculated Pressure Drop Values in Laminar Flows at 50 °C	57
4.7	Measured and Calculated Pressure Drop Values in Turbulent Flows at 50 °C	57

<b>Figure</b>	<b>Title</b>	<b>Page</b>
4.8	Measured and Calculated Pressure Drop Values in Turbulent Flows at 60 °C	58
4.9	Measured and Calculated Pressure Drop Values in Turbulent Flows at 70 °C	58
4.10	Measured Versus Calculated pressure drop across DA (laminar, transition and turbulent regime) for white oil recirculated at 50 °C	60
4.11	Measured Versus Calculated pressure drop across DA (laminar, transition and turbulent regime) for white oil recirculated at 60 °C	60
4.12	Measured Versus Calculated pressure drop across DA (laminar, transition and turbulent regime) for white oil recirculated at 70 °C	61
4.13	The effect of different friction factor correlations	63
4.14	The effect of the various equivalent diameter models to the turbulent regime length	67
4.15	The effect of various equivalent diameter models used for the annular duct (Regression Analysis)	68
4.16	The effect of the correction factor on the calculation of the pressure drop	71
4.17	The effect of the correction factor on the calculated pressure drop	72
4.18	Solver parameter window	77
4.19	Measured Versus Calculated pressure drop across DA (laminar, transition and turbulent regime) for white oil recirculated at 50 °C	78
4.20	Measured Versus Calculated pressure drop across DA (laminar, transition and turbulent regime) for white oil recirculated at 60 °C	78
4.21	Measured Versus Calculated pressure drop across DA (laminar, transition and turbulent regime) for white oil recirculated at 70 °C	79
4.22	Measured Versus Calculated pressure drop across DA (turbulent regime) for white oil recirculated at 50 °C	79
4.23	Measured Versus Calculated pressure drop across DA (turbulent regime) for white oil recirculated at 60 °C	80

<b>Figure</b>	<b>Title</b>	<b>Page</b>
4.24	Measured Versus Calculated pressure drop across DA (turbulent regime) for white oil recirculated at 70 °C	80
4.25	Experimental-measured data error reduction in terms of the AAPE	83
4.26	Isothermal and diabatic pressure drop data comparison (turbulent, transition and laminar regime)	84
5.1	Schematic of the test section with temperature and pressure drop measurement	87
5.2	The information flux adopted for thermal experimental stage	88
5.3	Mineral oil temperature measurement	91
5.4	Cold glycol temperature measurement	91
5.5	Working fluids inlet-outlet temperature differences	92
5.6	Mineral oil (FT04), cold glycol mixture (FT02) and hot glycol mixture (FT03) flow rate measurements	92
5.7	Comparison of heat transfer rate, oil inlet temperature at 50 °C, glycol inlet temperature 15 °C and 1 m <sup>3</sup> /h flow rate	99
5.8	Comparison of heat transfer rate, oil inlet temperature at 60 °C, glycol inlet temperature 15 °C and 1 m <sup>3</sup> /h flow rate	99
5.9	Comparison of heat transfer rate, oil inlet temperature at 70 °C, glycol inlet temperature 15 °C and 1 m <sup>3</sup> /h flow rate	100
5.10	comparison of heat transfer rate, oil inlet temperature at 70 °C, glycol inlet temperature 15 °C and 3 m <sup>3</sup> /h flow rate	100
5.11	Comparison of heat transfer rate, oil inlet temperature at 70 °C, glycol inlet temperature 15 °C and 5 m <sup>3</sup> /h flow rate	101
5.12	Comparison of measured and calculated heat rate, oil inlet temperature at 70 °C, glycol inlet temperature 15 °C and 5 m <sup>3</sup> /h	103
5.13	Comparison of measured and calculated heat rate, oil inlet temperature at 70 °C, glycol inlet temperature 15 °C and 5 m <sup>3</sup> /h	103
5.14	Experimental and theoretical turbulent Nusslet Number data	108
5.15	Experimental vs. Calculated Nusselt Number for Petukhov Correlation	110

<b>Figure</b>	<b>Title</b>	<b>Page</b>
5.16	Experimental vs. Calculated Nusselt Number for Dittus-Boelter Correlation	110
5.17	Experimental vs. Calculated Nusselt Number for Gnielinski Correlation	111
5.18	Experimental vs. Calculated Nusselt Number for Sider and Tate Correlation	111
5.19	Experimental vs. Calculated Nusselt Number for Bernado and McAdams Correlation	112
5.20	Experimental vs. Calculated Nusselt Number for Webb Correlation	112
5.21	Experimental vs. Calculated Nusselt Number for sandall et. al. Correlation	113
5.22	Experimental vs. Calculated Overall Heat Transfer Coefficient for Petukhov Correlation	113
5.23	Experimental vs. Calculated Overall Heat Transfer Coefficient for Dittus-Boelter Correlation	114
5.24	Experimental vs. Calculated Overall Heat Transfer Coefficient for Gnielinski Correlation	114
5.25	Experimental vs. Calculated Overall Heat Transfer Coefficient for Sider and Tate Correlation	115
5.26	Experimental vs. Calculated Overall Heat Transfer Coefficient for Bernado and McAdams Correlation	115
5.27	Experimental vs. Calculated Overall Heat Transfer Coefficient for Webb Correlation	116
5.28	Experimental vs. Calculated Overall Heat Transfer Coefficient for sandal et. al. Correlation	116
5.29	Comparison of AAPE of the Convective Heat Transfer Correlations for obtaining Nusslet Number	118
5.30	Comparison of AAPE of the Convective Heat Transfer Correlations for obtaining the Overall Heat Transfer Coefficient	118

---

## CHAPTER I

### INTRODUCTION

Petroleum crude oil, commonly referred to as crude oil, contain a significant amount of high molecular weight hydrocarbons (also called paraffin, heavy components or waxes). These heavy components have a low solubility in organic solvent at room temperature and atmospheric pressure. However, because of the high temperatures and pressure in crude oil reservoir, these heavy components have enough solubility in the crude oils.

#### 1.1 PIPELINE WAX DEPOSITION

When crude oil production occurs in a cold climate region and in offshore platforms, the crude oil being pumped out of the reservoirs and through the pipelines is exposed to low temperature in the environment. The temperature drops of the crude oil due to heat loss and decrease the solubility of the heavy component in the crude oil. As long as the temperature of the oil remains above the Cloud Point (CP) Temperature, the heavy component remains in solution and no precipitation occur. The Cloud Point temperature also called Wax Appearance Temperature (WAT) is defined as the temperature at which the first precipitation or crystal of solute start developing (Reistle, 1927, Ajiienka, 1999, Sadeghazad, 2000) and the oil become "cloudy". The temperature at which the oil (solution) will not flow when tilted to a horizontal position in the bottle, is called the Pour Point (PP) Temperature. When the temperature of the crude oil falls below the CP the heavy component crystallize and precipitate out of the crude oils. Paraffin deposition occurs when these precipitated heavy component in the crude oil form a layer of deposits on pipelines wall and equipment during crude oil transport and production.

Paraffin deposition has adverse effects on the economic of the crude oil production. The deposits of heavy components reduce the pipeline cross-sectional area available for fluid flow, resulting in a reduced flow efficiency. At a sufficiently cold pipeline temperature, a deposit may continue to grow in thickness inside the pipe, such that gradually a complete



wax blockage forms in the pipe, ceasing the flow. Figure 1.1 show severe case of pipeline that is plugged due to paraffin deposition and this to occur, a certain condition must be fulfilled (Mansoori *et al.*, 2003). The best known is:

1. The temperature of the wall is below the cloud point of the particular oil.
2. A negative radial temperature gradient is present in the flow. A zero gradient implies that approximately no deposition will occur.
3. The wall friction is high enough for wax crystals to stick to the wall.

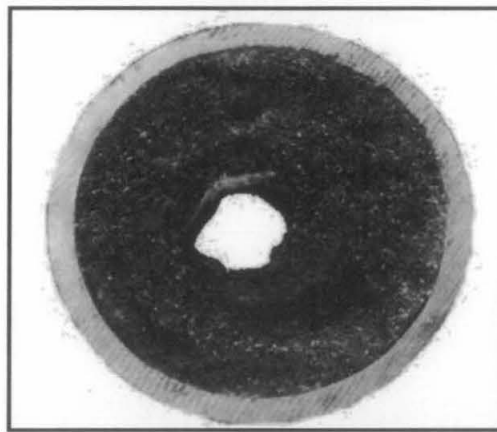


Figure 1.1: Pipeline Petroleum Transport Plugging (Mansoori *et al.*, 2003)

The precipitation of paraffin/wax in petroleum fluid production and transportation may give rise to a variety of problems. Misra *et al.* (1994) on their review of the paraffin problems encountered in the crude oil production, they pointed out three major problems that may cause by the wax crystallization. These problems are:

**High viscosity and pressure losses**, High viscosity and wax deposition on pipe surfaces are primary causes of high flow pressure besides turbulent flow behavior. Crystallization of wax suddenly increases the crude viscosity because of the gel-forming tendency of the waxy crystallites. This results in increased viscosity and pressure loss, leading to a reduction in the effective capacity of the line. Sometime pumping pressure can increase beyond the limits of the system, and crude transportation is stopped.

---

**High yield stress for restarting the flow**, the problem can be called the “restartability” of the flow in a line when the static oil contained therein is allowed to cool to temperatures below its pour point. In such cases, certain pressure, called the restarting pressure, is required to break the gel and resume flow. Sometimes this pressure exceeds the pressure limits of the pump and pipelines. The line appears to be choked. This problem is compounded by wax deposited in the line.

**Deposition of wax crystallites on surfaces**, when the oil temperature goes below cloud point, the wax crystals start precipitating out. These crystals deposit at the surface of handling system (e.g. on tubing, flowlines, tank bottom, process equipment, and sucker rod assemblies). Wax can deposit even if the bulk is at a temperature above its cloud point and the outer surface of the line. Oil near the pipe wall may experience a temperature below its cloud point, and wax crystallization will occur. Deposition is preferred state for such crystals because it is a low-energy state; it occurs at a lower temperature and the lattice obtained is stable. Lattice stability results from the availability of surface for deposition (adhesion) and further interlocking of crystals (cohesion).

Since the oil producers have been aware of the difficulties of pipelining waxy crude oil and fuel oils for several decades; there are several methods have been addressed to improve the flow and the handling of the waxy crudes when the ambient temperature is appreciably lower than the PP (Reistle, 1927). Usually alternative methods are tried until one is found to be successful. All the common methods are either one or a combination of the following general methods:

1. Thermal pre-treatment of the crude to change the wax crystal structure.
2. Preheating the crude with subsequent heating of the line.
3. Adding a less-waxy crude or light distillate.
4. Injection of additives to modify the wax structure of the crude.
5. Preheating the crude and pumping it hot through a buried pipeline.
6. Injecting water to form a layer between the pipe wall and the crude.
7. Mixing the molten crude with water to produce an emulsion which on further cooling becomes slurry.

## 1.2 PARAFFIN/WAX DEPOSITION MECHANISIM

Wax deposition is a complex phenomenon affected by several processes. Ramachandran, 2004, described the phenomenon of the wax deposits formation as a combination of five steps, shown in Figure 1.2. These steps are:

1. Formation of an incipient gel layer on the surface of the cold wall due to wax precipitation near the wall.
2. Mass flux of dissolved waxes towards the gel layer due to the radial concentration gradient induced by the precipitation.
3. Internal diffusion of some of these wax molecules inside the gel.
4. Precipitation of these wax molecules within the gel deposit.
5. Counter-diffusion of de-waxed oil out of the gel deposit.

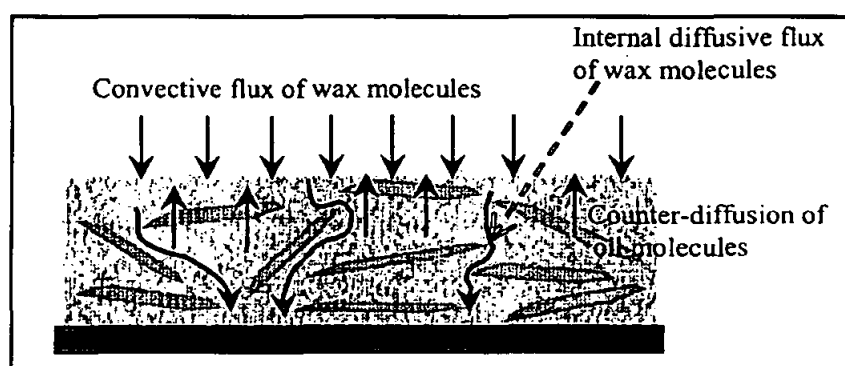


Figure 1.2: Schematic of the wax deposition process (Ramachandran, 2004)

There are a number of mechanisms have been proposed to describe the lateral transport and formation of wax deposits on the pipe walls. These mechanisms include molecular diffusion, shear dispersion, Brownian diffusion, and gravity settling (Ramachandran, 2004, Kristofer, 2005, Hamouda *et al.*, 1995, Burger *et al.*, 1981, Brown *et al.*, 1993, Mustafa *et al.*, 2000, Solaimany *et al.*, 2001). Mechanisms such as shear dispersion, Brownian diffusion and gravity settling will be important if wax deposition were to occur in particulate state. Burger (1981) reported that molecular diffusion dominants at high temperature and heat flux conditions, whereas the shear dispersion is the dominant mechanism at the lower temperature and low heat flux. The contribution of the Brownian diffusion is small compared to other mechanisms.

---

### 1.3 PROBLEM STATEMENT

In 1997 PETRONAS High Temperature/High Pressure Model Pipeline and Wax Deposition Facility, HT/HPMPWDF, was designed and installed in PRSS (PETRONAS Research and Scientific Services) Bangi. This project was joint venture between PRSS and ARC (Alberta Research Council) Canada. The HT/HPMPWDF is designed to assess the paraffin deposit test method to mitigate it in the field. The deposition test section of the HT/HPMPWDF is 3m in length and consists of an annular shaped flow element where test fluid (waxy crude) pumped and re-circulated consciously from relatively large tank Figure 1.3. Preliminary observation resulted from operating the PETRONAS and ARC deposition apparatus (Appendix A) are suggesting that the system can be confidently used for assessing field operations (pipeline and offshore) and mitigation strategies (Toma *et al.*, 2006).

Further on, this equipment is dedicated to produce the required background data for developing suitable numerical modeling procedure. In this scenario the model is used to transfer laboratory data to field and for assessing optional operations strategies in the field. Continuous monitoring of pressure drop and heat transfer (via temperature and pressure drop measurement performing during the operation of the HT/HPMPWDF) are proposed to be used for model validation operations as scalar, because neither Reynolds number nor shear rate or shear stress are working well as scalar. The theory behind the pressure drop and heat transfer methods to be used as scalar is (Cem and Michael, 2004).

**The pressure drop method** is based on the concept that wax deposition in the pipe section reduces the hydraulic diameter of the flowing fluid inside the pipe, resulting in an increase on frictional pressure drop over the pipe section. The wax thickness on the inner pipe wall can be calculated with the aid of the flow parameters and pressure drop equation.

**The heat transfer method** is based on the concept that when a layer of wax deposit is formed in the pipe wall, convective heat transfer with paraffin solidification will take place on the interface between the flowing fluid and the deposited wax layer. A thermal

resistance term due to heat transfer from the flowing fluid to cooling fluid. This added thermal resistance to approximately in direct proportion the thickness of the wax layer on the pipe wall can be determined from measurement of relevant thermal parameters by solving the heat transfer equations.



Figure 1.3: Photograph of the oil tank storage

The present study aims at developing rational operation and data validation criteria of the HT/HPMPWDF and in view of developing field strategies and assessing improved deposition models. This involves a number of “base-line” experiments (no paraffin deposition involved) and detailed pressure drop and heat transfer calculations using existing literature models. Results will be further used as base-line for continuous assessment of paraffin deposition in a subsequent study.

A particular feature of this study is the annular shape of HT/HPMPWDF Measuring Section. This shape offers the advantage of improved control of wall/boundary temperature, however the particulars related to flow – heat transfer laboratory – field transfer condition will be discussed.

---

Annular flow is also of interest because it is a flow case which may provide some insight into the general problem of fully developed turbulent shear flows. It combines two boundary layers that may be very different from each other in distributions of velocity, shear stress, and turbulence quantities. Studying this flow type is also relevant since its limiting cases are flow in circular pipe and flow between parallel plates, which have been extensively studied (Brighton and Jones, 1964).

#### 1.4 RESEARCH OBJECTIVES

This systematic experimental study aiming to reveal advantages and limitations of using the laboratory equipment for simulating particular field situations. The experimental component of this study will improve the confidence of using the HT/HPMPWDF for assessing field mitigation strategies, therefore the following objectives are adopted:

1. Investigating the hydraulic-thermal performance of the HT/HPMPWDF via comparisons between various empirical correlations and the experimental data to come out with suitable characterizing criteria.
2. Assessing and improving the pressure drop and heat transfer accuracy of the HT/HPMPWDF to a level suitable for wax deposition simulation and prediction.

#### 1.5 RESEARCH METHODOLOGY

A detailed experimental investigation of the pressure drop and heat transfer characteristics of single-phase Newtonian flow has been carried out through the following adopted methodology:

1. Develop standard and reliable operation of the HT/HPMPWDF.
2. Check and improve instrumentations reading.
3. Troubleshooting.
4. Check pressure drop model(s) (base-line against literature).
5. Check heat transfer model(s) (base-line against literature).
6. Prepare a standard test procedure for deposition experiments.

---

## 1.6 THESIS STRUCTURE

Chapter II reviews and discusses literature relevant to the prediction of the wax deposition rate and the aspect of fluid flow and heat transfer in the annulus as it addressed as particular feature in this work.

Chapter III shows the experimental program of this work with the details of the working fluids and the test facility.

Chapter IV dedicated for the investigation of the pressure drop aspect of the wax deposition test facility, which include experimental procedure, modeling and equations derivation, measured-calculated pressure drop comparisons and parametric analysis. A realistic pressure drop correlation is developed and presented in this chapter a long with its statistical error analysis.

In Chapter V the heat transfer of the wax deposition test facility is investigated in three steps: temperature measurements, heat transfer balance and the convective heat transfer behavior.

Finally, Chapter VI concludes and summarizes the findings of this study and discusses potential future work.

---

## CHAPTER II

### LITERATURE REVIEW

This chapter reviews the progress in the modeling and prediction of the wax deposition encountered in the oil and gas industry. The shortage on the scalar used to transfer laboratory data to field is explained in this chapter. Fluid flow and heat transfer in annulus are also discussed.

#### 2.1 PREDICTION OF PARAFFIN/WAX DEPOSITION

In order to design efficient sub-sea petroleum production facilities and remediation system to achieve optimum production returns, it is necessary to understand the phenomenon of the wax deposition and provide prediction for the nature of deposits formed (Misra, 1994). For example, knowledge of the rate of deposition and deposit properties such as mechanical strength and melting enthalpies provides guidance in selecting appropriate remediation and prevention technologies.

Typically in-situ remediation technologies are mechanical pigging and melting the deposit using hot oil or heat produced by a chemical reaction (Reistle, 1927). Pigging is a well established method of using mechanical device to physically remove the wax deposits from the pipe wall. The design of mechanical pigs differs from hard or soft wax deposits. If a wax deposits becomes too hard by the process of aging which is defined as the change of the deposit structure and properties with time (Ajiienka, 1991), then mechanical methods of remediation may be ineffective and a pig may become lodged in a petroleum production line, exacerbating the flow restriction. Hardened deposits may require thermal or chemical solvent methods of remediation to dissolve the wax deposit completely, or to soften the deposit for subsequent pigging. Thus, being able to predict the strength of a deposit without opening a flowline is crucial for the successful remediation of the wax deposition.



---

Laboratory-scale experiments such as cold finger and flow loop testing are often used to assess the deposition potential of a petroleum fluid (Ajienka, 1991 and Brown *et al.*, 1993). Deposition rates measured in the laboratory can not be directly scaled up to field condition, because of differences in the shear and thermal conditions which have a large impact on the morphology of the wax deposit. Therefore, mathematical models have been developed that appropriately account for shear and thermal history effects (Toma *et al.*, 2006, Ramachandran, 2004, Kristofer, 2005, Hamouda *et al.*, 1995, Burger *et al.*, 1981, Brown *et al.*, 1993, Mustafa *et al.*, 2000, Solaimany *et al.*, 2001). Early deposition model did not account for aging phenomenon, and subsequently were unable to provide a priori predictions of wax deposition (Misra, 1994 and Hsu *et al.*, 1995). The early models utilized the oil content of the deposit as an adjustable parameter in order to match flow loop result to the model prediction.

Hsu *at el.* (1994), developed laboratory test method for measuring the wax deposition rate under turbulent flow conditions without knowing oil properties or disassembling the system for the wax deposition measurement. This work was of essential need since that most study most deposition study in laboratory are conduct with flow loop under laminar flow conditions. They used a system given the name “High Pressure Wax Deposition Turbulent Flow Loop (HPTFL)”, in this system a two tube unit are installed and connected in series, one of the tube given name “Test Tube” was dedicated for collecting wax deposited from the oil, the other tube given name “Reference Tube” was kept at condition of no deposition by maintaining the ambient temperature above the cloud point of the flowing oil. A technique of monitoring the difference in the pressure drop through the two tubes is used to calculate the amount of the wax deposited in the test tube.

Hsu *at al.* (1994) concluded their experimental study with most important observations concerning the effect of the turbulence on the wax deposition process. They reported that under turbulent flow conditions the pseudoplastic non-Newtonian behavior of a cold waxy crude significantly affects wax deposition rate. Wax deposition from a waxy crude can be reduced significantly under turbulent flow conditions. The flow turbulent depresses the temperature at which maximum wax deposition occurs. They also

---

concluded that the sloughing effect generated under turbulent flow conditions has significant impact on wax deposition rate and can not be neglected in wax deposition modeling. The sloughing of deposits occurs when the shear rate is high enough that the shear stress at the wall exceeds the strength of the wax deposit (Weingarten *et al.*, 1988). The onset of sloughing is not related to a transition from laminar to turbulent flow.

Many investigators (Toma *et al.*, 2006, Hsu *et al.*, 1995, Hsu *et al.*, 1994, Weingarten *et al.*, 1988) through the experimental study, pointed out the strong evidence of shear removal on paraffin deposition (decreasing deposition rates, arrest of deposition, and tearing off of deposits). Shear removal is not explicitly considered in many of the deposition models, specifically, no functional dependence of shear removal on fluid properties and flow rates has been formulated.

Hsu and Brubaker (1995), in subsequent study found that wax deposition scale-up parameters: shear rate, shear stress, and Reynolds number can not be used as scalar.

The wall shear rate for laminar flow conditions is expressed as  $8V/D$  ( $V \equiv$  flow velocity,  $D \equiv$  pipe ID). It is only valid under laminar flow conditions. Under turbulent flow conditions, the shear rate near the wall but outside of the laminar layer is very large and changes sharply with distance from the wall. It is difficult to predict or calculate the shear rate and determine where the wax deposition is affected.

The wall shear stress is expressed as  $\Delta PD/4L$ . This was considered as a promising factor to explain the shear effect. At the equilibrium state the wax strength (tension) at a temperature may be balanced with a certain shear stress. However the scale up results show that the shear stress obtained with large pipe under turbulent flow conditions is small and similar to that obtained with laboratory small tube under laminar flow conditions. Therefore, wax deposition predicted by scaling up from shear stress parameters is unreasonably high.

The problems of scale-up from shear rate and shear stress can be verified by the following equations (Hsu and Brubaker, 1995):

The Fanning friction factor,  $f$ , is defined as:

$$f = \frac{\Delta PD}{2\rho LU^2} \quad (2.1)$$

Where  $\Delta P$  = pressure drop,  $\rho$  = fluid density. This definition is valid for either laminar or turbulent flow. For a smooth pipe and Reynolds number  $Re$ , up to 100,000, the friction factor can be expressed as.

$$f = \frac{k}{Re^n} \quad (2.2)$$

Where,  $k$  and  $n$  are constants. Substituting equation (2.2) to (2.1) gives:

$$\frac{\Delta PD^{1+n}}{U^{2-n}L} = K\rho^{1-n}\mu^n \quad (2.3)$$

For a given oil and a temperature the term on the right hand side of equation (2.3) is constant by neglecting shear rate effect on oil viscosity. Then the right term can be scaled up and expressed as:

$$\left(\frac{\Delta PD^{1+n}}{U^{2-n}L}\right)_F = \left(\frac{\Delta PD^{1+n}}{U^{2-n}L}\right)_M \quad (2.4)$$

The subscript F means full scale, and M means model or laboratory data.

The wall shear stress is expressed as:

$$\tau_w = \frac{\Delta PD}{4L} \quad (2.5)$$

Substituting equation (2.5) to (2.4) gives:

$$\frac{(\tau_w)_F}{(\tau_w)_M} = \left(\frac{D_M}{D_F}\right)^n \left(\frac{U_M}{U_F}\right)^{2-n} \quad (2.6)$$

---

Where,  $n = 1$  for laminar flow, and  $n = 0.25$  for turbulent flow according to Blasius friction factor equation. So, the term,  $2-n$ , is greater than zero.

If shear stress is a scaler, then the shear stress is the same for a given oil and temperature in a model and a full scale pipeline.

Hsu and Brubaker (1995) discussed a special case by using shear stress as a scaler. They assumed the full scale pipe is an infinitely large pipe, then the velocity to be applied in the 1/4" model tube must be infinitely small (Eq. 2.6). Their experimental data (Hsu *et al.*, 1994) showed that the tube has plugging problems at low flow rates due to high wax content in the tested oils. In other words, at infinitely small flow rates the tube or pipe will be clogged if the amount of wax precipitated at the given temperature is larger than the volume of the tube. This is the reason why the wax deposition predicted is unreasonably high, when either shear rate or shear stress is used as a scaler even in the case under turbulent flow conditions. This is not true for the real pipeline, especially under turbulent flow conditions. Therefore, it is concluded that neither shear rate nor shear stress can be used as a scaler for wax deposition scale-up.

If Reynolds number is used as a scaler, then  $(VD)_M = (VD)_F$ . Similar to the above discussion, if  $(D)_F$  becomes infinitive large, then, flow velocity applied to a 1/4" model tube is also infinitive large. However, under infinitive large velocity wax will not deposit on the pipe wall. Therefore, Reynolds number can not be used as a scaler.

Hsu and Brubaker (1995) based on the fact – they deduced and explained in the preceding paragraph - that none of the shear stress, shear rate and Reynolds number can be used as scaler, they developed a wax deposition scale-up model to scale-up laboratory wax deposition results for waxy crude oil production lines by heat flux and flow velocity.

In this model the critical wax tension concept had been proposed as scaler. Wax tension is defined as a force required to break a fixed thickness of wax cake. Since that during the

deposition, hard wax is deposited first due high initial high heat flux conditions; the wax tension in the radial direction is different in each layer.

The shear force per unit length of pipe (called shear force gradient) required to break a layer of wax deposit is defined as critical wax tension at the term given oil and measured by equation (2.7):

$$\frac{\Delta PD^{1+n}}{\Delta L} = K\rho^{1-n}\mu^n U^{2-n} \quad (2.7)$$

Equation (2.7) can be rearranged for a given oil and temperature as:

$$\frac{\left(\frac{\Delta PD^{1+n}}{\Delta L}\right)_F}{\left(\frac{\Delta PD^{1+n}}{\Delta L}\right)_M} = \frac{\left(U^{2-n}\right)_F}{\left(U^{2-n}\right)_M} \quad (2.8)$$

If using the critical wax tension as a scaler, then flow velocity in the model tube and full scale pipe must be the same according to equation (2.8). Therefore, wax deposition test in the laboratory can be conducted at the same flow velocity and ambient temperature as that in the field production line. The data can be used to scale-up to the pipeline operating conditions to predict wax deposition profile.

## 2.2 FLUID FLOW IN ANNULUS

Annuli are characterized by the existence of two circular pipes, where the flow area is bounded by the inner wall of the outer pipe and the outer wall of the inner pipe. Annuli can be eccentric, partially eccentric, or concentric, as shown in Figure 2.1. A concentric annulus occurs when the pipe centers are coincident and the eccentricity value is zero. When an annulus is fully eccentric, the eccentricity value is equal to one and both pipe walls have a point of contact.

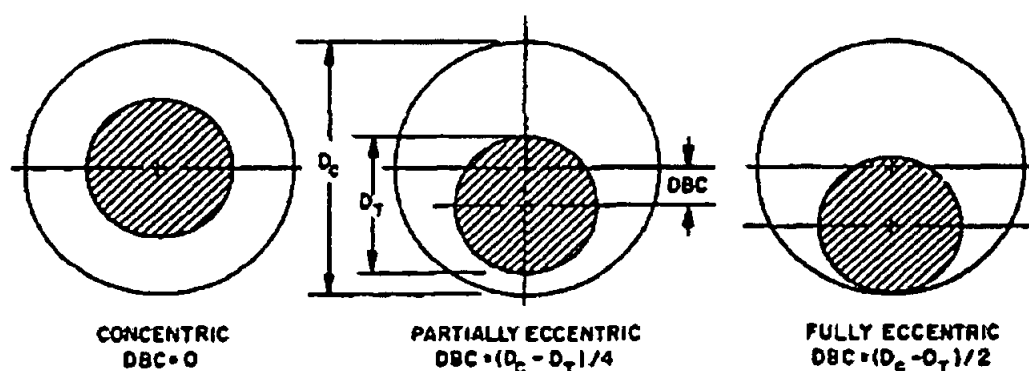


Figure 2.4: Eccentricity Degrees in Annuli (Boone, 2004)

Flow through an annulus is encountered in various industrial applications, including the oil and gas industry. Although it is often encountered in practical applications, little literature has been published on the subject. The oil and gas industry's past interest in this subject was limited to investigating high productivity wells flowing through the casing-tubing annulus, but more recently people are becoming interested in this topic for other reasons such as looking into underbalanced drilling technology. Since the accurate prediction of downhole pressure is very important for this technology, annular flow is becoming more relevant (Boone, 2004).

Annular pipe flow is of interest not only because of its direct engineering applications, but also because in two ways it is a flow case which might provide insight into the general problem of fully developed turbulent shear flows. First fully developed annular pipe flow involves the combination of two boundary layers (each extending from a wall

---

to appoint of maximum velocity) which, unlike those that meet at the center of a pipe or midway between parallel planes, may be quite different from each other in distribution of velocity, shear stress and turbulence quantities. Also, the two one dimensional fully developed turbulent flows which have been studied in detail – flow in circular and between parallel planes – are both limiting case of annular pipe flow.

The asymmetry of an internal flow is in general imposed by the dissimilar conditions of the solid surfaces bounding the flow. In the case of an annulus it appears basically due to the unequal wall curvatures and is therefore particularly pronounced if the radius ratio of the inner and outer wall is small. The same effect however, may be generated if the roughness composition or the porosity of the walls are unequal (Hanjalić, 1974). As a consequence of the flow asymmetry, the diffusion transport causes the zero and stationary values of the various characteristic flow properties to occur at different positions in the flow.

In the past annuli have been evaluated on the basis of hydraulic diameter, but this may not always be the best way to represent the dimension for flow in an annulus. To more appropriately determine this parameter, a better understanding of flow through an annulus is required (Lawn and Elliot, 1972, Jones and Leung, 1981).

Brighton and Jones (1964) studied fully developed turbulent flow in annuli with a range of Reynolds numbers from 46,000 to 327,000. The test section included two concentric aluminum pipes. The outer pipe had an 8 inch (0.2032 m) nominal inside diameter and four different inner pipe sizes were used. Friction factors were determined with a water flow apparatus for Reynolds numbers between 4,000 and 17,000 and were found to be six to eight percent higher than what was generally accepted for flow through an annulus with smooth walls in this range. Brighton and Jones (1964) found that friction factors for air flows through an annulus with smooth walls were one to ten percent higher than the pipe flow values for those with same Reynolds numbers. They found that these results depended very little on the ratio of the inner pipe radius to the outer pipe radius.

Velocity profiles were studied by Brighton and Jones (1964) and were found to deviate from the normal correlations when the radial distribution of Reynolds stress is nonlinear. They also found that in turbulent flow, the point of maximum mean velocity will occur at a smaller radius than in laminar flow. They were also able to determine mixing lengths from accurate measurement of the velocity gradients. Physically, the mixing length is the distance a particle travels before exchanging momentum with fluid particles of different layers. Brighton and Jones (1964) found that the mixing length goes to infinity as the maximum velocity is approached. Mixing lengths of this magnitude would be physically impossible and hence their findings support the findings of the physical incorrectness of the mixing length theory.

Roy and Gangopadhyay (1971) based on available accurate experimental data at that time, derived new correlation for finding the friction factor in a smooth annulus  $f$  in the form:

$$\frac{f - f_c}{f_c} = c \text{Re}^p n^q \quad (2.9)$$

In which  $f_c$  denotes the friction factor for the circular tube with a diameter equal to the hydraulic diameter of an annulus at the corresponding Reynolds number. The developed correlation showed that for the same radius ratio the deviation from that of circular tube, based on hydraulic diameter, increase with the increase of the Reynolds number. They concluded that the proposed correlation should be accepted as more dependable because it represents the qualitative aspects and quantitative results better than other available equations.

Lawn and Elliot (1972) performed an experimental investigation of fully developed turbulent flow through concentric annuli, they were focused to know whether the curvature of the inner wall of an annulus of small radius ratio (ratio of inner to outer radii) has the effect of the modifying the velocity profile, so that the 'law of the wall' (Eq. 2.10) no longer applies to any extent, or if it dose apply, whether or not it is of the 'universal' form thought to be common to nearly flat surfaces.

$$U^+ = 5.50 \log y^+ + 5.45 \quad (2.10)$$



in which is the dimensionless velocity and is the dimensionless distance from the wall. The experimental result of Lawn and Elliot (1972) showed for the first time that the positions of zero shear stress and maximum velocity are non-coincident even in the case of smooth annuli. Lawn and Elliot used the hot wire technique to measure the shear stress distribution; the “sliding sleeve” method was used only for comparison. Lawn and Elliot concluded from their study that zero shear stress occurred closer to the inner surface than the maximum velocity, the position of the zero shear stress were in excellent agreement with the Kay’s-Leung (1963) equation and that there were considerable deviations from universal laws of the velocity profiles of the inner zone.

Rehme (1974) experimentally investigated fully developed turbulent flow through three concentric annuli for Reynolds number ranged  $Re = 2 \times 10^4 - 2 \times 10^5$ . In Rehme’s investigation the measurement of pressure drop, the position of the zero shear stress and maximum velocity, and the velocity distribution in the annuli of different radius ratios were made. The results for the key problem in the flow through annuli, the position of zero shear stress, showed that this position is not coincident with the position of maximum velocity as was supposed for asymmetric velocity. The position of the zero shear stress found to be in every case is distinctly closer to the inner tube than the position of the maximum velocity. Also the measured position of the zero shear stress showed deviation from that one predicted by Kays and Leung (1963).

The pressure drop for the flow through three annuli was investigated by Rehme (1974) over a length  $L = 2106 \text{ mm}$ . the pressure-drop coefficient  $\lambda$  evaluated from the measurement using the equation:

$$\lambda = \frac{\Delta P / \Delta L}{\frac{1}{2} \rho u_m^2 / d_h} \quad (2.11)$$

where  $d_h$  is the hydraulic diameter,  $\rho$  is the fluid density and  $u_m$  is the fluid average velocity. Rehme’s conclusion was that the pressure drop coefficients increase slightly with increasing radius ratio, the experimental pressure-drop coefficient have been

---

reported to be in coincidence with the circular tube values at  $Re = 10^5$  and radius ratio of 0.2. Moreover, a conclusion drawn by Lawn and Elliott (1972) according to which the pressure-drop coefficients of parallel plates are about 5% higher than the circular tube value proved to be true.

Jones and Leung (1981) developed an improved method of calculating turbulent friction in smooth concentric annuli. Because hydraulic diameter is known to be insufficient in correlating frictional pressure drop in turbulent flow, many authors still do not agree on a method to be used. There are in agreement that radii ratio's does indeed play a significant role, but correlations applied to various data sets available do not yield the same results.

Jones and Leung (1981) modified the Colebrook (1979) equation for flow in smooth annulus by using a modified Reynolds number they reported significant improvement over the studies available at that time and tried to show the geometric similarity for both circular tubes and concentric annular in laminar, steady state and fully developed flow. A laminar equivalent diameter ( $d_L$ ) is used in their study, which is expressed in terms of hydraulic diameter and the shape factor,  $\phi$ . Although not perfect, the study commented on the followings:

1. Lack of knowledge of the annular gap may present difficulty since the friction varies with the cube thereof. (Data will tend to lie parallel with the theoretical line).
2. Eccentricity, especially in small annular spaces will result in smaller friction factors.
3. Inlet swirl caused by distorted inlet conditions will cause friction to appear higher than expected. The insertion of flow straighteners was suggested to eliminate the problem.
4. Secondary flow will inevitably cause deviation from the laminar theory above some Reynolds number, which varies from case to case.

---

Only few studies of the flow of a fluid in the entrance region of a concentric annulus are found in the literature; these have been reported by Rothfus *et al.* (1955) and Lee and Park (1971).

Rothfus *et al.* (1955) indicate entrance region behavior which is quite different than that of turbulent flows in circular tubes and between parallel plates. Their results were based on the ratio of the local apparent shear stress to the fully developed value and used annuli of radius ratios, 1.78 and 2.97. The entrance lengths appear to be larger by a factor of ten than the typical circular tube entrance lengths and strongly affected by the Reynolds number. Since the circular tube and parallel plate channel are special cases of the annulus, it is not clear why the results from concentric annuli are so different.

Lee and Park (1971) studied the problem from an integral view point, based on a modified model for the eddy diffusivity of momentum together with a new ratio of eddy diffusivity obtained from experiment. Comparisons were made between experiments and analytical computations conducted on the effects of various factors on the turbulent flow in the developing regions of concentric annuli. Air was used as the working fluid and four annuli having radius ratios ( $r_o/r_i$ ) of 1.61, 2.31, 3.83 and 15.32 were used over a range of Reynolds numbers between about 20,000 and 110,000. The hydrodynamic entrance lengths based on friction measurements were obtained for approximately 6 to 12 equivalent diameters, which agreed with his prediction. Velocity profiles in the inner region of a concentric annulus were significantly affected by the Reynolds numbers, radius ratio and entrance length.

---

### 2.3 HEAT TRANSFER IN ANNULUS

Forced convection heat transfer problems in ducts may be classified as either thermally developing or thermally fully developed. The first case may be further divided depending upon whether the velocity profile is developing or fully developed. Simultaneous development of velocity and temperature profiles is the most difficult problem to analyze. Most solutions to this type of problem have been obtained using numerical methods. The second type of thermally developing flow occurs when the velocity profile is established. This type of problem is easier to solve and is often referred to as the Graetz problem or Graetz-Nusselt problem (Sadik and Yaman, 1995). Finally, for the case of fully developed flow, both velocity and temperature profiles are fully developed. This is the case for very long flow passages.

An annular passage is a simple geometrical form used in practice for the purpose of heat transfer between two fluids. In double pipe heat exchanger, for example, while one fluid flows in the inside tube, another one at different temperature flows in the annular space between the two tubes for heating or cooling purpose.

Although the number of works on annulus problems is quite limited, various limiting cases (circular pipes or parallel-plate channels) have received considerable attention.

In certain annulus problems, flow has been found to remain laminar for about 11 times the hydraulic diameter with a Reynolds number over 2900 with transition occurring a little sooner on the inner wall than on the outer wall. Therefore, any investigation of heat transfer near the entrance of an annular duct should include considerations of laminar flow (Sadik and Yaman, 1995).

In most heat transfer applications, there are mainly two kinds of simple boundary conditions; constant-heat flux and constant temperature. Since there are two boundary conditions in the annulus, various combinations of these two boundary conditions are possible.

---

Kays and Leung (1963) solved this problem for the fundamental solutions of the second kind\*. In this work for four annulus radius ratio, 0.192, 0.255, 0.376, 0.500, the fundamental solutions of the second kind are developed for air ( $Pr = 0.76$ ) entirely from experimental data. An asymptotic solution is then developed analytically (velocity and temperature profiles fully-developed) for Prandtl numbers from 0 to  $10^3$ , Reynolds numbers from  $10^4$  to  $10^6$  and radius ratios from 0.1 to 1.0.

The thermal entrance region has been defined, either as the distance required for the local heat transfer coefficient to approach that of the fully developed value or as the distance from the entrance to the cross section where the non-dimensionalized temperature profile becomes independent of the flow direction. Most of the thermal entry region solutions so far considered have been based on the assumption that the velocity profile is fully developed. Since the velocity profile of the fluid entering a heat transfer passage is already fully developed, it is often called a "purely thermal entrance region" to distinguish it from a simultaneously developing region. In a simultaneously developing region, the heat transfer occurs near the actual entrance of a tube or annulus where the velocity profile is not developed but rather developing. Often the design of a heat transfer sections (flow conditions) are such that the entire section is simultaneously developing, but with very long flow passages, the entry length is only a small fraction of the whole length and its influence is negligible. However, with certain fluid and thermal boundary conditions, these entry effects might be very important and cognizance of them must be taken.

Deissler (1955) analytically investigated the effects of various factors on turbulent heat transfer and friction in the entrance regions of smooth passages. He used the integral heat transfer and momentum equation for calculating the thickness of the thermal and boundary layers. The influence of the Reynolds number, the Prandtl number, initial velocity distribution, wall-boundary conditions, and variable fluid properties were

---

\* The linearity of the energy equation for constant property flows, any axisymmetric surface temperature or surface heat flux boundary can be satisfied by superposing one or more solutions of so-called four fundamental problems. One of these four fundamental problems is the second kind problem in which one surface with a constant flux, the other surface insulated. And there are two solutions of the second kind.

studied. His results indicate that fully developed heat transfer and friction are obtained in an entrance length approximately less than 10 diameters. The effect of initial velocity distribution on heat transfer in the entrance region was that the values of  $Nu_x/Nu_d$ , for a uniform initial velocity distribution were higher than those for a fully developed velocity distribution.

Lee (1967) investigated the problems of the thermal boundary-layer, for hydrodynamically fully developed turbulent flow in concentric annuli. He applied the means of the momentum and heat transfer integral equations, along with a modified universal velocity profile, to the case of thermal entrance region heat transfer from the core of a concentric annulus. The investigation was conducted for a range of radius ratios from 1.01 to 5, Prandtl numbers from 0.01 to 30 and a Reynolds number range of from  $10^3$  to  $2 \times 10^4$ , Fig. 2.2 shows the idealized model used in the analysis.

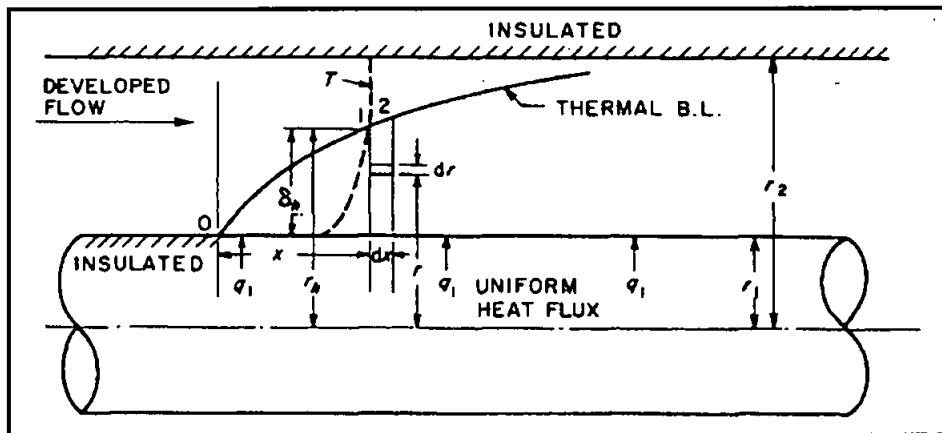


Figure 2.5: Thermal boundary layer in a concentric annulus - idealized model (Lee, 1967)

Lee's results revealed that in general the heat transfer coefficient attains the fully developed values in less than thirty equivalent diameters; also that the entrance length is moderately dependent upon radius ratio. Lee also concluded that the increase in the radius ratio leads to decrease in the thermal entrance length with increase in the Nusselt number.

---

The problem of developing turbulent flow and heat transfer in the simultaneously developing regions of concentric annuli were studied both analytically and experimentally by Park (1971). The fully developed heat transfer was attained from both the analytical and experimental studies in entrance lengths of less than 40 equivalent diameters for the air flow. For very small Prandtl numbers, "pseudo thermal entrance lengths" were predicted. This showed that, even though the thermal boundary layer had extended itself across the flow duct, the generalized temperature profile continued to change until the flow was hydrodynamically fully developed. The Nusselt numbers for the heated inner wall were always greater than those for the heated outer wall.

---

## CHAPTER III

### EXPERIMENTAL TEST FACILITY

PETRONAS High Temperature/High Pressure Model Pipeline and Wax Deposition Facility, HT/HPMPWDF, is designed in 1997 to assess the paraffin deposit and test methods to mitigate it in the field. This test facility – generally - consists of three main systems: oil, cooling and heating system, and two test sections, wax deposition test section and pressure drop monitoring section in addition to auxiliary system include the heat tracing and pressure boosting elements.

The deposition test section is 3m in length and consists of an annular shaped flow element where the test fluid (waxy crude) is continuously pumped and re-circulated from a relatively large volume vertical tank, while coolant mixture is flowing in the inner pipe simulating cold wall conditions in the field. Pumping, heating and cooling systems ensure control of flow rates and temperatures.

The maximum operating conditions of the HT/HPMPWDF are:

System operating temperature	160 °C
System operating pressure	17238 kPa
Design system pressure	20685 kPa
Oil flow rate	30 m <sup>3</sup> /h



---

### 3.1 OIL SYSTEM

Crude oil is stored in a vertical pressure vessel (Oil Tank TK-1). This vessel has an outside diameter OD of 0.20 m (8 in) and is 2.00 m (78 in) high. Oil drained from this vessel and pressure boosted by an Autoclave Centrifugal Packless (CP) pump having maximum capacity of 9 m<sup>3</sup>/h (150 L/min). This pump has been designed to fulfill additional requirements not obtained in the conventional packed pump such as leakage, contamination and packing heat generation problems. The pump suction and discharge are 3.81 mm (1.50 in) and 2.41 mm (0.95in) in diameter, respectively. A Baldor adjustable (Variable Frequency) drives (VFD) control unit controls the drive motor speed.

A bypass line with control valve (HV16) is used to put the oil on bypass mode between the oil tank and the oil heater (H1) to maintain the desired oil temperature, also the bypass mode can be use for conditioning the re-circulating oil to “live” saturation state by using the venture element if a multiphase (liquid + gas) fluid used. A Micro Motion mass flowmeter (FT01) is used to meter the flowing oil. This Micro motion flowmeter is sized for low mass flow rates of 0 – 27300 kg/h. The Micro Motion meter also measures the density of the oil.

The oil storage tank and all the oil flow lines are insulated and heat traced to avoid any paraffin deposition that might occur in the feed lines.

After the oil is metered it flows through the differential pressure section (DP-1), this section is pipe-shell type heat exchanger and is operated in countercurrent flow of hot glycol water mixture (50% + 50%), with oil in the pipe side. The hot glycol temperature and flow rate is controlled from the heat system to maintain the flowing oil at a temperature above the oil WAT. The oil can be bypassed from the differential pressure section if so desired. The differential pressure section structure and functions is described in more details in later paragraph.

---

The oil system, later, equipped with additional oil line given the name “2-inch high flow-rate line”. This is line was needed to fulfill the requirements of high flow rate and pumping of high viscous fluid, and for this requirements a 3-stage, 3-inch gear-width pump. The high flow-rate line was 5.08 mm (2 in) in diameter. The oil sucked from the high pressure vessel (TK-1) by a 3-stage, 3-inch gear-width gear pump. This pump was configured with parallel 5.08 mm (2 in) suction and discharge manifold. This pump has been measured to deliver 17 m<sup>3</sup>/hr at 1500 RPM and the total flow recorded to be 50 m<sup>3</sup>/h at 1525 RPM with output pressure rated up to 17238 kPa. A WEG electrical motor drives the pump and its speed controls by a WEG frequency inverter. The flow rate and density of the oil flowing in the high flow rate section is metered by Micro Motion flowmeter (FT04) sized for high flow rate of 0 – 30 m<sup>3</sup>/h. After the oil is metered it flows directly to the test section.

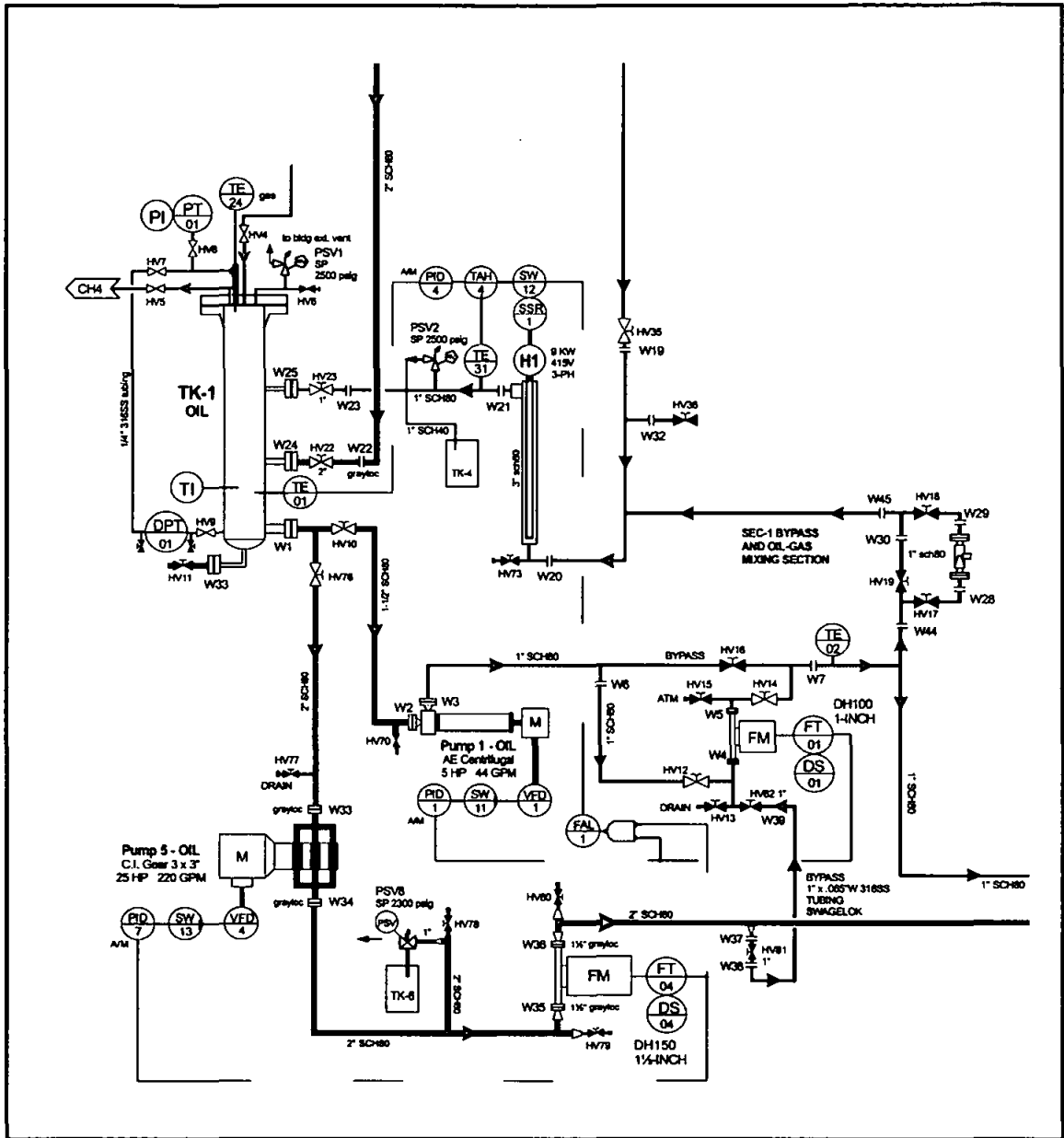


Figure 3.6: Schematic of Oil Flow Control System

### 3.2 BASE-LINE DIFFERENTIAL PRESSURE SECTION (DP-1)

The base-line differential pressure section is a 3m length pipe-shell type heat exchanger consists of two parallel lengths of process tube; one has inside diameter of 11.05 mm (0.44 in) and outside diameter of 12.70 mm (0.50 in), and one has inside diameter of 17.49 mm (0.69 in) and outside diameter of 19.05 mm (0.75 in), inside 76.20 mm (3in) pipe shell. A differential pressure transducer (DPT02) is installed across this section to monitor any changes occur due to wax deposition in the main test section. Figure 3.2 show the Schematic of the Base-Line Differential Pressure Section.

The DP-1 is designed to be used in line with the low flow rate section, as reference for measurement of wax deposition thickness in the main test section, and also the rheology. For this purpose this section all time must be kept at a temperature above the WAT to prevent any wax deposition and this condition is achieved by re-circulating hot glycol mixture in the shell pipe.

This section has two oil temperature transmitters (TE03, TE04) and two glycol transmitters (TE22, TE23) located at the inlet and out let of the section of each fluid respectively.

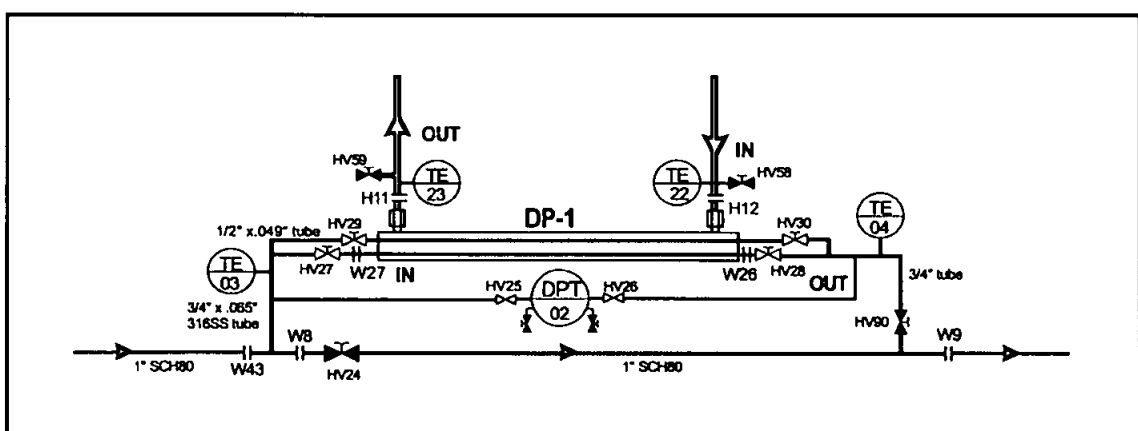


Figure 3.7: Schematic of the Base-Line Differential Pressure Section

---

### 3.3 WAX DEPOSITION TEST SECTION (SEC-1)

The Paraffin deposition test has a 3-m long, annulus shape cross section. The test section is fully jacketed permitting the test fluid to flow over the outer wall of the inner wax deposition pipe and a chilled glycol-water mixture to flow countercurrent in the inner wax deposition pipe. The heating jacket temperature, test fluid temperature and chilled glycol-water mixture temperature are monitored at the inlet and outlet of the wax deposition test section. A cross sectional view of the test section with the dimensional details is shown in Figure 3.3, and Figure 3.4 show the schematic of the test section.

A chilled mixture of glycol and water (50% + 50%) is circulated in the core tube, countercurrent to the oil flowing in the test section. A hot mixture of glycol and water (50% + 50%) is circulated in the heating jacket. This hot mixture is always circulated at a temperature as high as enough to control the wall of the test section at a temperature above the bulk oil temperature, aiming to provide adiabatic conditions at the outer boundary (wall) of the flowing oil, and thereby, prevent heat loss to surroundings. With this configuration the paraffin deposition test section has the capability of experiencing a cold pipe wall similar to what would be encountered at real pipelines world.

The wax deposition pipe of the test section can also be used as take-out section for visual inspection and sampling of the wax deposition. The inclination position of the test section is adjustable so that the system is capable to mimic vertical and the deviated wells flow.

A Rosemount differential pressure transducer (DPT03) is installed across the oil section to monitor the pressure drop resulted from the changes in its effective flow diameter due to wax deposition. The oil section has four temperature transmitters (TE07, TE08, TE09, TE10) located at the inlet, flowing oil mid-stream, inner wall and the outlet of the oil section respectively. Two glycol temperature transmitters (TE12, TE13) are also installed at the inlet and outlet of the cold finger, in addition to other transmitters (TE15, TE16) installed at the inlet and the outlet of the heating jacket. The inlet of the oil section is also equipped by pressure transmitter (PT02). And the whole SEC-1 is externally insulated and heat traced.

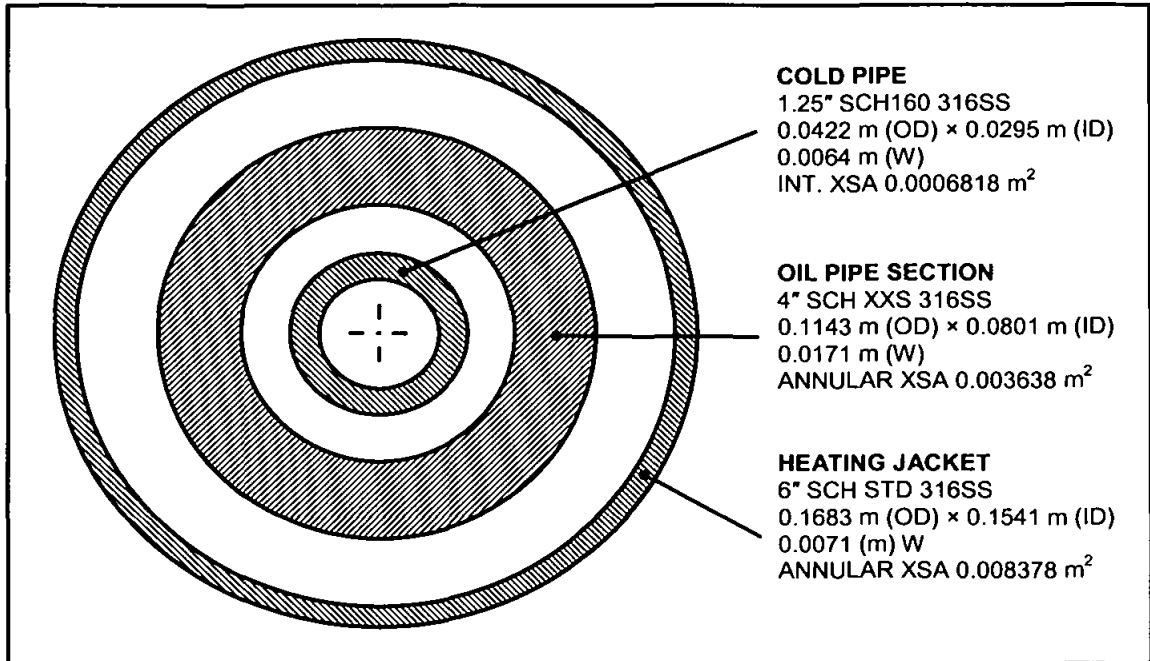


Figure 3.8: cross sectional view of the Paraffin Deposition Test Section

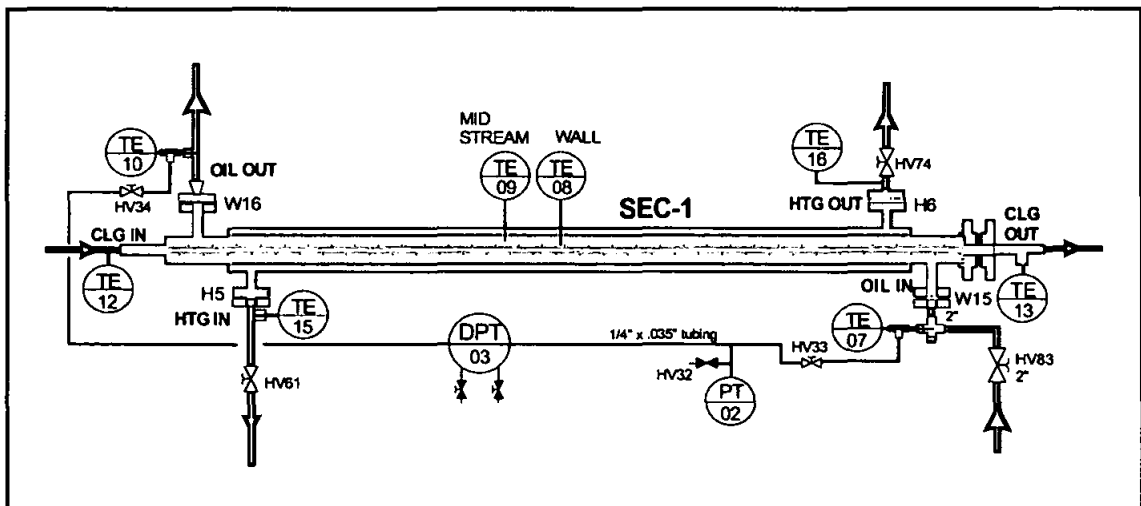


Figure 3.9: Schematic of Paraffin Deposition Test Section

---

### 3.4 COOLING SYSTEM

The cooling system used in the test facility encompasses primary and secondary circulation system. A schematic of the cooling system is shown in Figure 3.5. The purpose of this system is to supply the cold core tube in the test section with cold mixture to provide cold wall conditions at the surface of the core tube. The primary re-circulation system consists of: cold glycol storage tank (TK-2), a re-circulation pump and heater (H2).

The primary re-circulation system circulates a chilled glycol-water (50% + 50%) mixture in the inner pipe of the test section (cold finger). The glycol mixture is fed to the re-circulation pump from the cold glycol tank (TK-2). A bypass line with a control valve (HV38) is used to keep the cold glycol mixture flow in bypass mode to maintain its temperature until it required flowing to the system. The primary glycol is then directed to the metering unit where it can flow to the test section and/or to heat exchanger (HEX-3) if a temperature trim is required for the re-circulated oil. Cold glycol mixture also can be flow to the heat exchanger (HEX-1) by using control valve (HV69) or/and heat exchanger (HEX-2) by using control valve (HV65). A Barton First Rate Flow Totalizer, turbine meter type, is used to meter the cold glycol mixture (FT02).

Since the primary glycol returns at high temperature after the heat exchanging process with the hot oil, it is cooled in the secondary re-circulation system to be supplied again to primary re-circulation system. The secondary re-circulation system is consists of a cold glycol tank (TK-2), a pump, compressor and a 7.06 kW chiller unit.

A temperature controller located at the DAC cabinet front panel; adjust the temperature of the cooling tank liquid to the required value by activating on/off operation of the chiller compressor, thereby regulating the amount of chilling required for the glycol mixture in the primary re-circulation system.

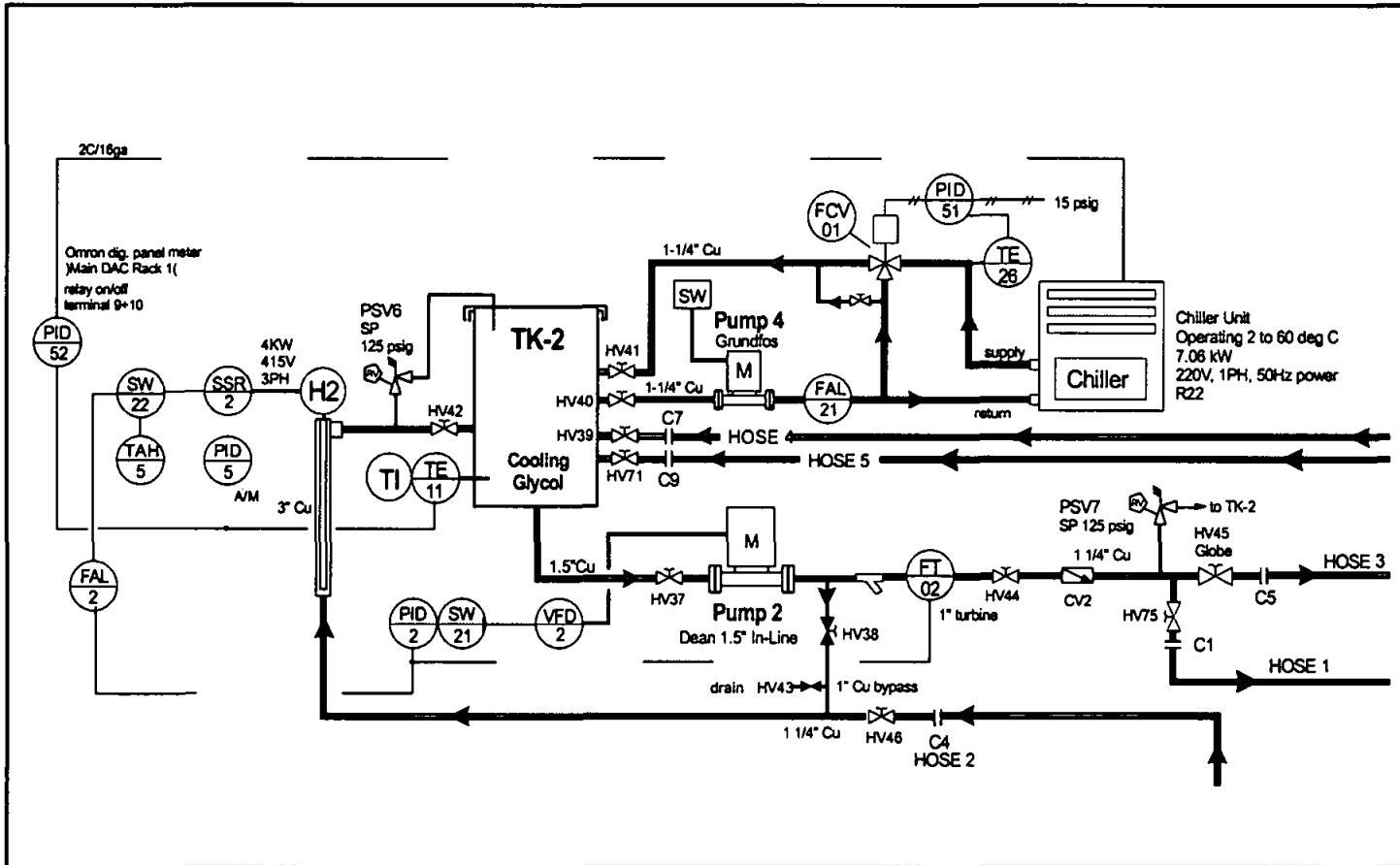


Figure 3.10: Schematic of the Cooling System



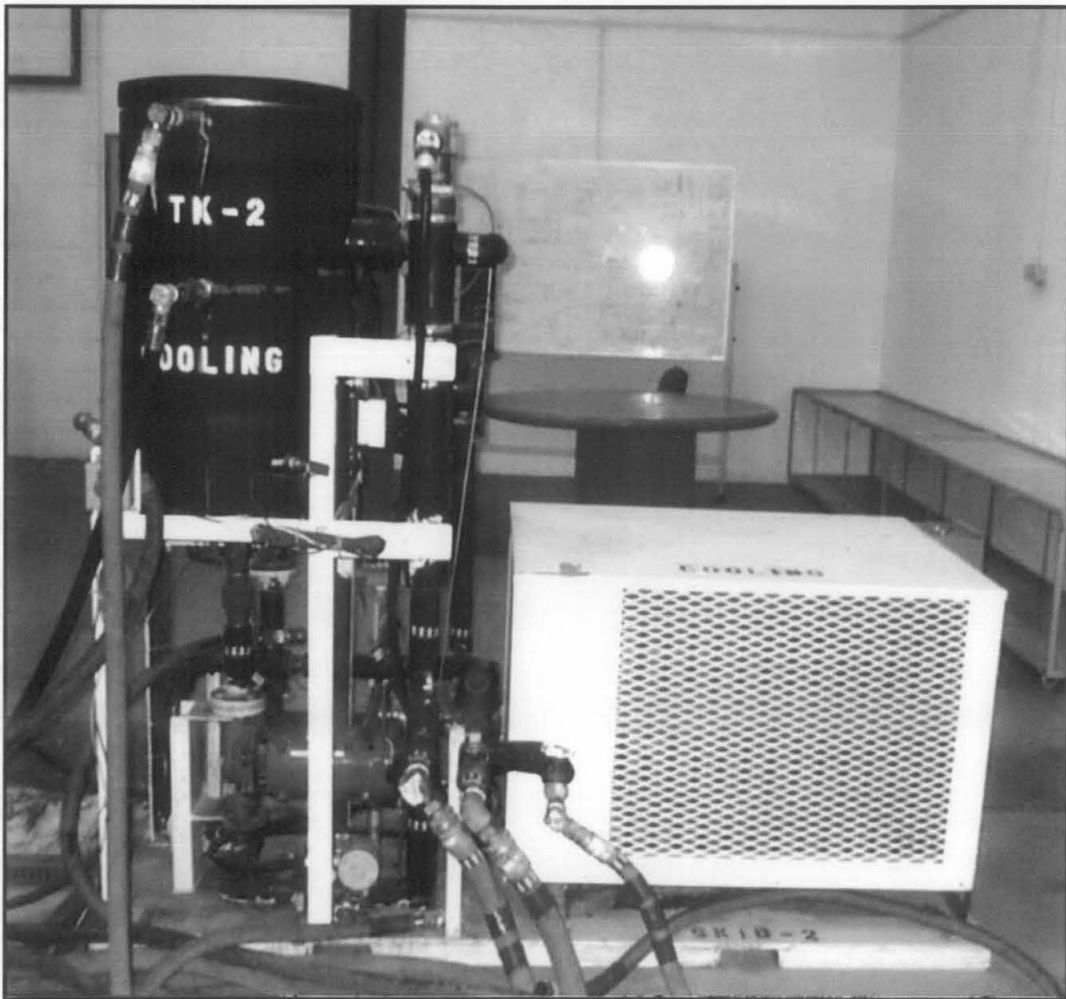


Figure 3.11: Photograph of the Cooling System

---

### 3.5 HEATING SYSTEM

The heating system used in the test facility is consists of hot glycol storage tank (TK-3), re-circulation pump and electrical heater (H3). Figure 3.7 presents schematic of the heating system. A mixture of glycol and water (50% + 50%) is fed to re-circulation pump from the hot glycol tank. A by pass line with globe valve (HV50) is used to keep the glycol mixture in a bypass mode to maintain the required temperature of the heating fluid at the system restart stage. The hot mixture is heated by using a Caloritech (9 kW, 415 V) immersion heater (H3).

The heating system circulates hot glycol mixture in the heating jacket of the deposition test section (SEC-1) to control the oil section wall at a temperature above the bulk oil temperature, and also circulates hot glycol mixture in the base-line differential pressure section (DP-1) to prevent any wax deposition in this section. The required amount of heating is automatically controlled by adjusting the temperature in heating tank (TK-3).

The hot glycol mixture can also be circulated simultaneously in the cold finger to remove or melt all wax deposited from the previous test. The hot glycol mixture was metered by a Barton First Rate Totalizer same type used for metering the cold glycol mixture in the cooling system.

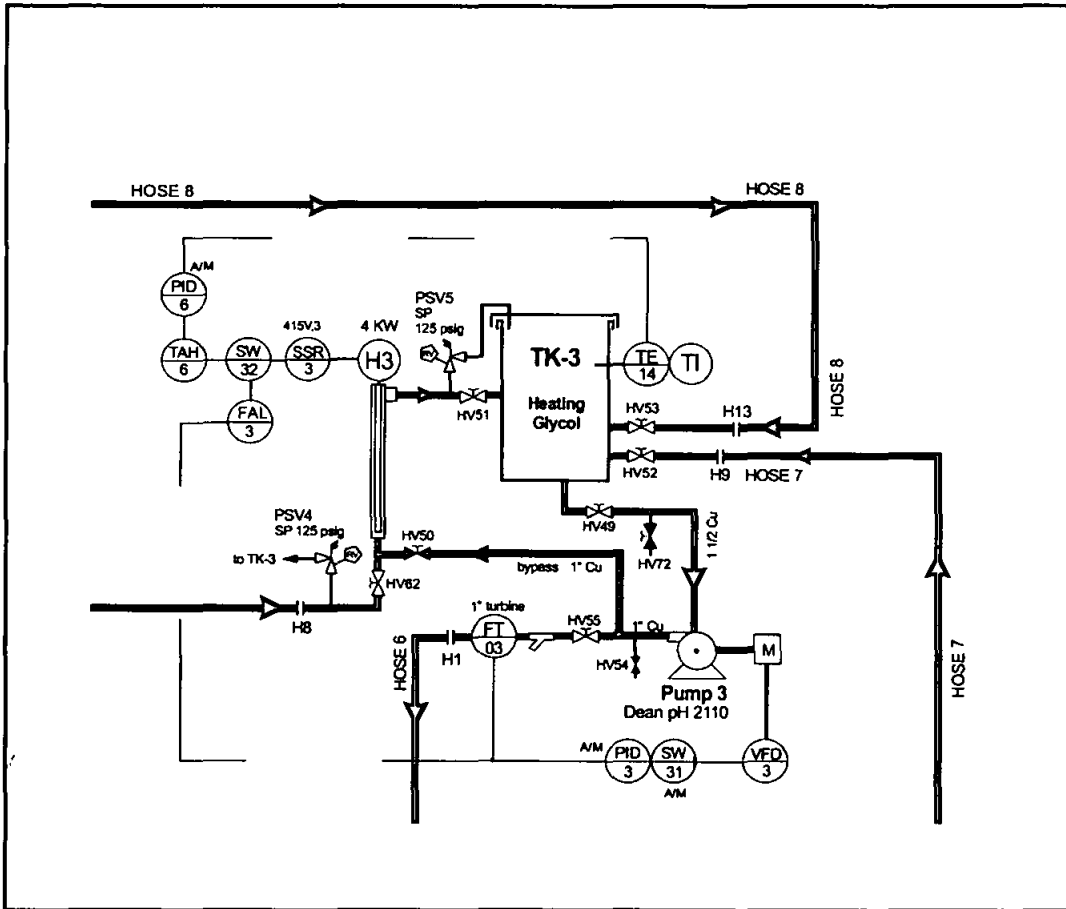


Figure 3.12: Schematic of the Heating System



Figure 3.13: Photograph of the Heating System

---

## 3.6 AUXILIARY SYSTEM

The auxiliary system consists of: pressure boosting system and heat tracing system. In addition, the entire flow loop is equipped with a large number of safety devices.

### 3.6.1 Heating tracing unit

Although the main tank and all oil re-circulation pipes are insulated, electrical heat tracing is installed to preheat TK-1 and oil re-circulation pipes to a temperature above the WAT of the oil to prevent the possibility of paraffin deposition outside the test section.

A 2.09 kW flexible silicon heating tape is used to heat the high pressure oil vessel TK-1. The heat tracing system consists of constant wattage heating tape wrapped underneath the insulation of the pipes. Dedicated percentage power controllers at the plug end of the tapes control each heat trace unit individually.

### 3.6.2 Pressure boosting unit

The oil system is equipped with “Wainbee” gas booster system. This system is designed to take gas flow from 700 kPa (100 psig) at the inlet up to a 17500 kPa (2500) psig discharge pressure. A gas bottle on the discharge side of the system allows for storage of the high-pressure gas (up to 2500psig).

---

### 3.7 DATA ACQUISITION AND CONTROL SYSTEM

The hardware of the data acquisition and control system (DAC) comprises: PC (Pentium 4, 2.5GHz, Windows 2000 Professional OS controller), signal conditioning cabinet and several I/O modules.

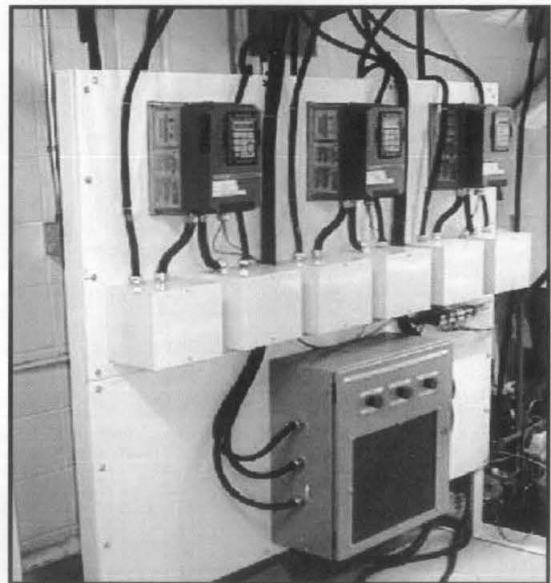
Several sensors and the transmitters were distributed among the test facility. These devices convert the physical signal (measurement) into electrical signal. The SCXI \* system that located at the signal conditioning cabinet receives the electrical signals coming from the field termination box -located at the test facility- and conditions it close to the signal source and increase the number of the analog and digital signal that the DAC device can analyze. The SCXI system consists of: SCXI chassis that house the signal conditioning modules, terminals blocks that plug directly to into the front of the modules, and cables assembly that that connects the SCXI to the front panel process signal indicators and to the parallel port of the PC.

---

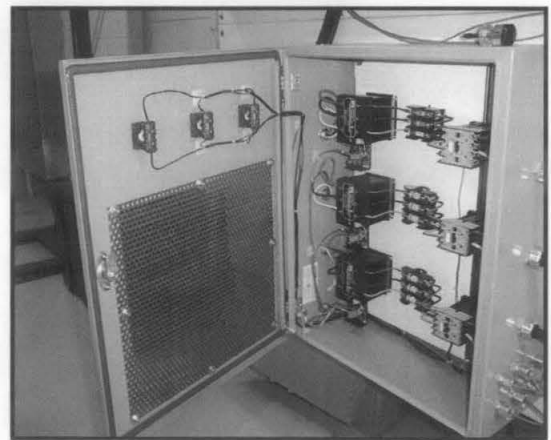
\* SCXI: Signal Conditioning eXTensions for Instrumentation. The national instruments product line for conditional low level signals within in an external chassis near sensors, s only high-level signals in a noisy environment are sent to data acquisition boards.



(a) Data acquisition cabinet



(b) Pump motor adjustable speed drives



(c) Heater power controller panels

Figure 3.14: The process control equipment.

The DAC software was LabVIEW6.1. LabVIEW programs are called virtual instruments, or VIs \*, because their appearance and operations imitate physical instruments. Every VI uses functions that manipulate input from the user interface or other source and display that information or move it to other files or other computers.

Using the labVIEW software many virtual instruments (VIs) were constructed and executed to have a friendly control panel that allow the user to view the schematic of the all test facility sections. Figure 3.11 views the main VI, given name “Delog VI”. It shows the main oil tank (TK-1) level, the oil path of low and high flow-rate sections, the path of the cooling fluid, the path of the heating fluid, along-with the relevant temperature and pressure probs. By toggling the front panel Booleans, the operator can view the desired waveform chart for temperature, flow-rate and pressure variable. The PID control panel (Figure 3.12) of the oil, cooling and heating system can be accessed by clicking PID button on the Delog VI panel.

National Instrument Data Acquisition (NI-DAQ), driver software was built in on the NI-DAQ device. The driver software communicates the application software (LabVIEW 6.1) VI's with the NI-DAQ device. The labVIEW soft ware call into the driver software which communicates with the measurements hardware. Figure 3.10 show the relationship between labVIEW VIs, driver software and measurement hardware.

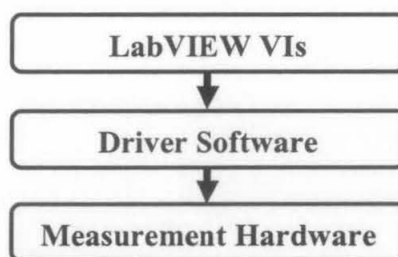


Figure 3.15: LabVIEW, Driver Software and Measurement Hardware Relationship.

\* The VI contains the following three components:

- **Front panel** – serves as user interface.
- **Block diagram** –contains the graphical source code of the VI that defines it functionality.
- **Icon and connector pane** – identifies the VI so that you can use the VI in another VI. A VI within another VI is called a subVI. A subVI corresponds to a subroutine in text-based programming languages.



The system flow-rates, pressures, temperatures were retrieved by execution of the flow-rates and pressures VI (Meas FT-PT-rev3.vi) and (Meas TEMP-rev3.vi). the main VI 'DELOG5.vi' was constructed and executed to scan and log to file a 50 data sets of flow-rate, pressure and temperature for the entire test facility. The data monitored at 2 second intervals in the master loop and recorded at the user defined interval in a slave loop.

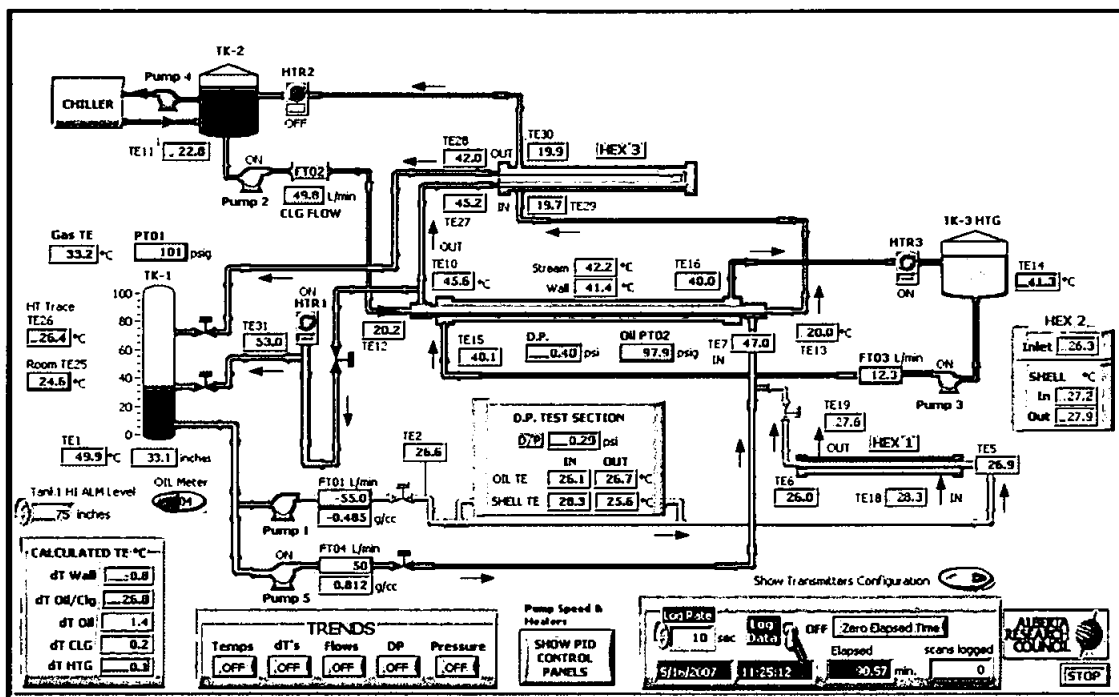


Figure 3.16: The Process Control Main Graphical User Interface - Labview

A Proportional Integral Derivative (PID) control virtual instruments, for the oil, heating, cooling systems are performed by executing those VIs co-currently with this VI. PID controllers were programmed to automatically control process variables such as flow-rate, temperature and pressure. These were set to the range of operating conditions of the test facility to ensure that they can be operated within the desired range. An emergency shutdown system and alarms with minimum and maximum set point were also incorporated into the DAC program to ensure optimum and safe operation.

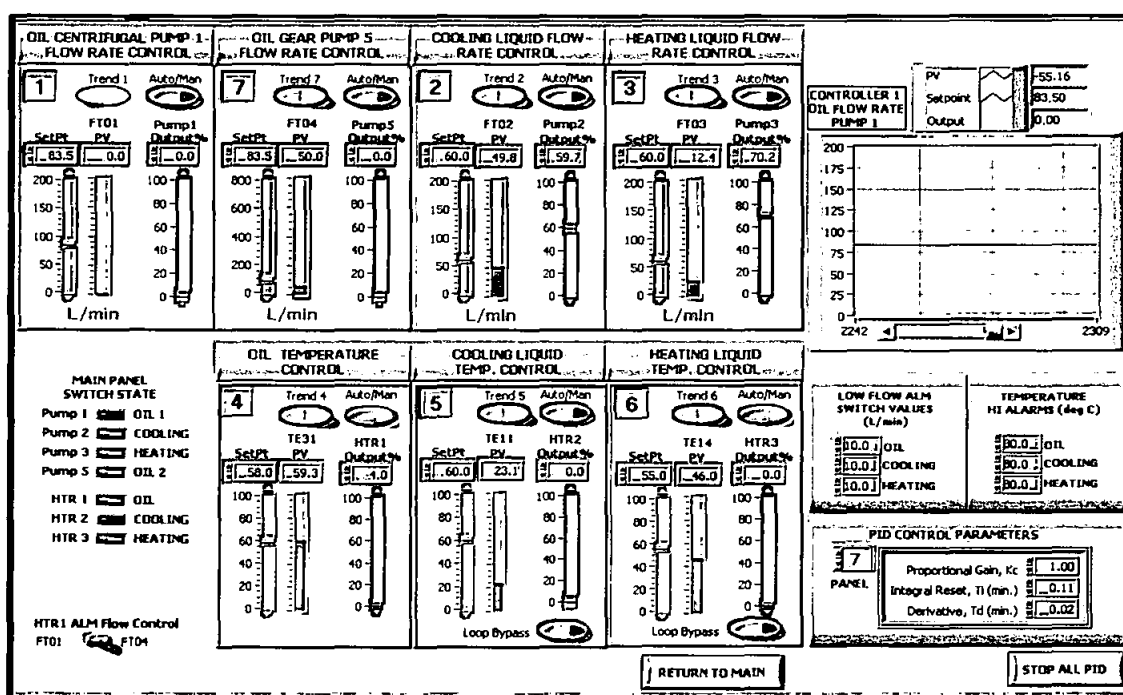


Figure 3.17: The PID Panel Interface Window for Control of Fluid Process Pump Speed, Flow Rate and Fluid Temperature

A list of mass flow meters, temperature, pressure and differential pressure instruments specifications used in the test facility are given in the appendix B. Micro Motion mass flow meters were used to measure the oil and glycol (hot/cold) flow-rates. An absolute pressure and differential pressure were measured using Rosemount transducer. Temperatures were measured with thermocouples. The accuracy limits of these transmitters are also provided in Appendix B.

---

## CHAPTER IV

### PRESSURE DROP EXPERIMENTAL INVESTIGATIONS

This chapter investigate on the pressure drop aspects of the test facility (HT/HPMPWDF). By checking the accuracy of the flow data measurement and compare the pressure drop experimental data with the calculated values will determine the accuracy limitation of the test facility and the confidence in the prediction of the wax deposited layer.

#### 4.1 INTRODUCTION

In order to ensure that the pressure drop measured across the test section of HT/HPMPWDF would closely reflect the deposition of paraffin conditions, non-deposition experiments are carried out. The pressure drop data collected during this group of experiments, carried on at various temperatures and flowrates, was further compared to calculated data. In this way, both the accuracy of calculation model and the confidence of experimental data have been improved.

The main objective of this task was to reduce the differences between the measured and calculated pressure drop values. Therefore, operation achieved using the following main steps:

- Improving the calculation procedure (to better reflect the specific design of deposition apparatus).
- Improving the calculation of re-circulated oil properties.
- Introducing acceptable modifications to initially used calculation procedure (after discussing the procedure).
- Observing and reducing the cause of errors with the aid of sensitivity studies of main involved parameters.

---

These experiments are necessary to improve the confidence of measurements and calculation routines in view of using the measured pressure drop as main parameter for assessing deposition of wax. The study confirms that the data collected from the flow loop agrees with the published theoretical widely accepted pressure drop models.

## **4.2 EXPERIMENTAL PROCEDURES**

Before starting the oil flow experimental programme, the pressure drop main sensor DPT03 was checked to ensure its reliability and readiness and to eliminate any causes of error or uncertainty. This step is needed to eliminate erroneous negative pressure gradients values generated at small (lower than calibration threshold values) flow rates. By checking the transducer, these errors were found to be as a result of shifting in the output signal range of the transducer. When the output signal range was calibrated to the original range of the measuring (4 - 20 mA which is equivalent to 0 - 40 psi), it was found that the data begins to approach the expected calculated results.

During the experiment, the pressure drop and inlet-outlet temperatures in re-circulated oil and cooling glycol circuits are continuously measured and logged while the flow rate of oil is increased in steps. This is shown in Figure 4.1, which indicates four operation stages consisting of stepwise increasing and decreasing of re-circulated oil flow rate. The adopted experimental procedure requires that each flow rate level is to be maintained for approximately 30 - 40 minutes, before a new flow rate level is activated.

This adopted procedure allows for temperature stabilization and for assessing repeatability of measured pressure drop and heat transfer data collected at similar flow rate-temperature conditions.

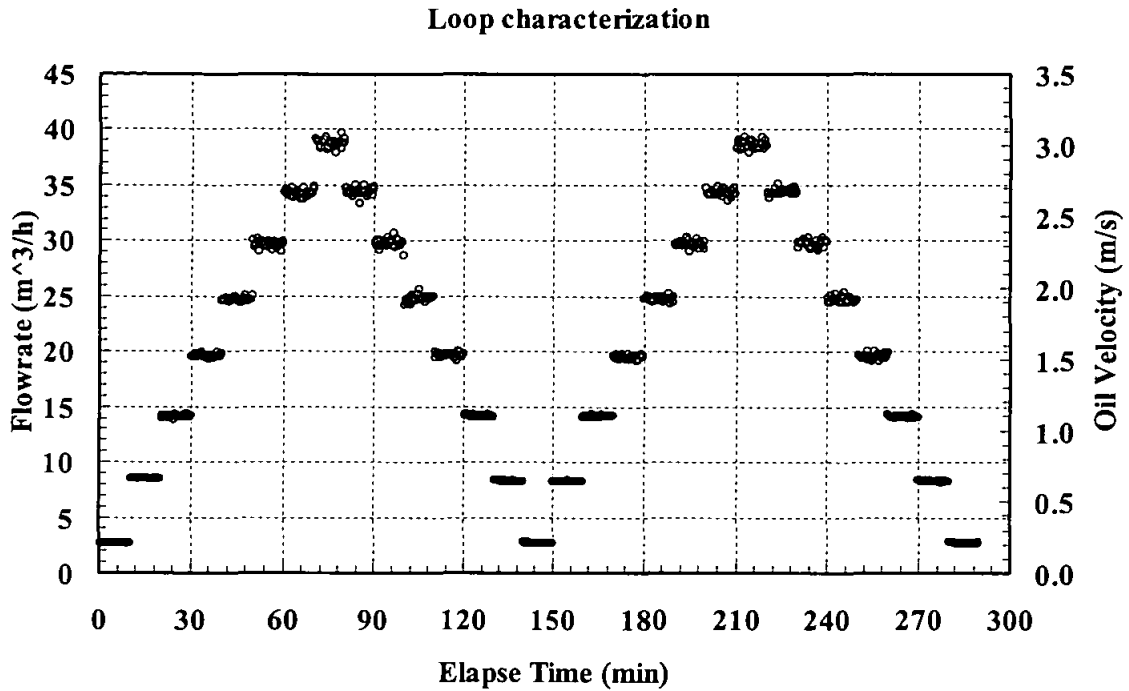


Figure 4.1: Typical stepwise variation of flow rate during a non-deposition experiment.

A series of experiments executed during a stepwise increase and decrease of flow rates, controlled by the speed of oil pump, were carried out. For each set of experiments, as illustrated in Fig. 4.1, the flow rate was varied from a minimum of approximately  $3 \text{ m}^3/\text{h}$  to a maximum of approximately  $40 \text{ m}^3/\text{h}$ . A variation of pump speed related flowrate from 100 rpm up to 1500 rpm was selected.

For consistency, a test matrix was generated and used throughout the entire experimental program. Table 4.1 illustrates the basic test matrix used. To observe the repeatability, for each experiment carried out, more than one set of data was collected.

Table 4.1: Test matrix for three test runs performed at different temperatures

Oil Inlet Temperature (°C)	50	60	70
step	Flow Rate (LPM) <sup>*</sup>		
1	54.0	50.3	44.7
2	100.4	96.3	104.8
3	141.4	148.4	146.8
4	175.9	195.1	185.0
5	211.7	238.0	222.8
6	245.2	278.5	275.7
7	322.4	319.5	316.1
8	362.9	357.0	355.2
9	405.8	395.6	393.5
10	452.7	433.1	448.6
11	496.3	489.2	486.2
12	534.8	534.0	535.7
13	573.2	574.2	574.8
14	610.3	610.2	608.4
15	644.8	642.4	642.7

(\*) LPM=litre per minute

Pressure drop versus flow rate, termed “flow characteristics” for different temperature conditions are depicted in Figures 4.2, 4.3 and 4.4. From these figures a good flow rate-pressure drop data grouping is observed. After a new flow rate level was achieved (by changing the pump speed via a Variable Frequency Drive VFD), the set level was maintained unchanged for 30 - 40 minutes. This time is required to achieve a new temperature-pressure equilibrium. The stabilization time was extended to 60 – 120 min when a real crude oil was used.

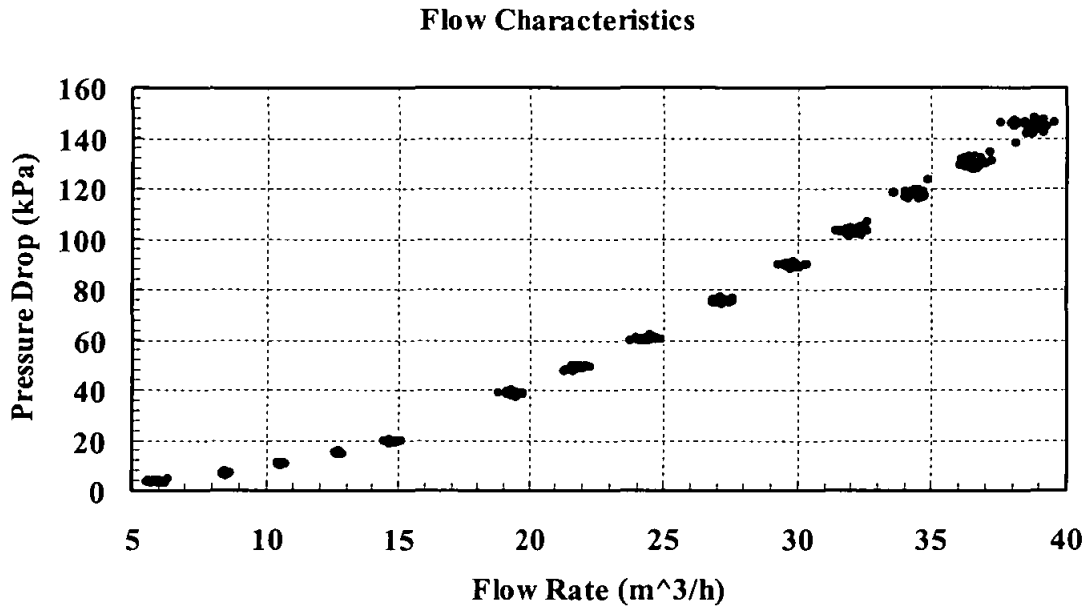


Figure 4.2: Pressure Drop and Flow Rate for Mineral Oil Run at 50 °C.

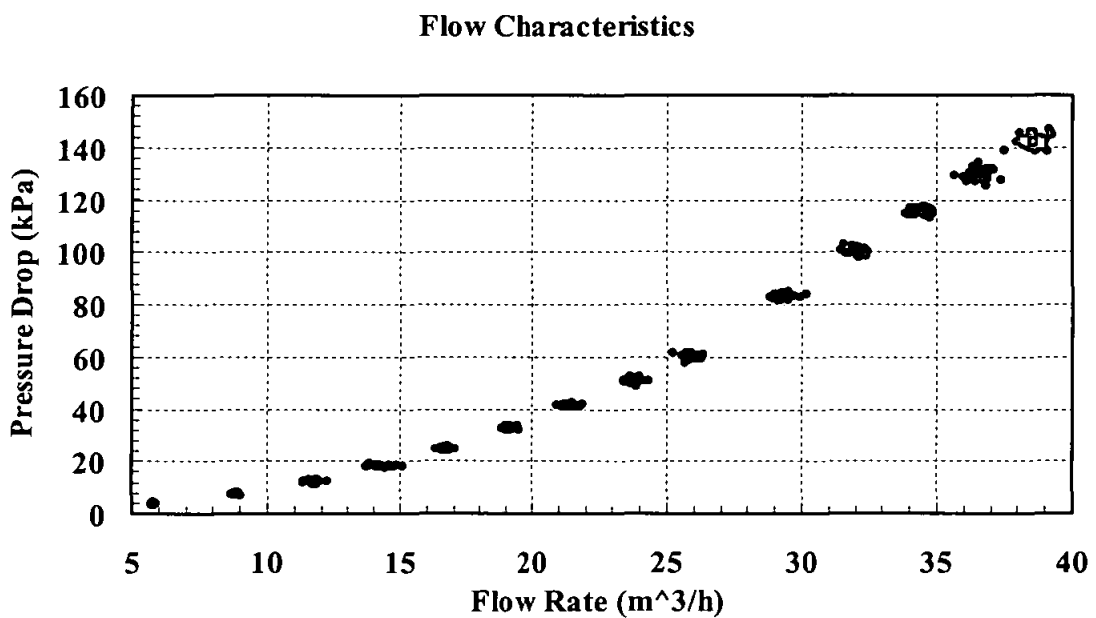


Figure 4.3: Pressure Drop and Flow Rate for Mineral Oil Run at 60 °C.

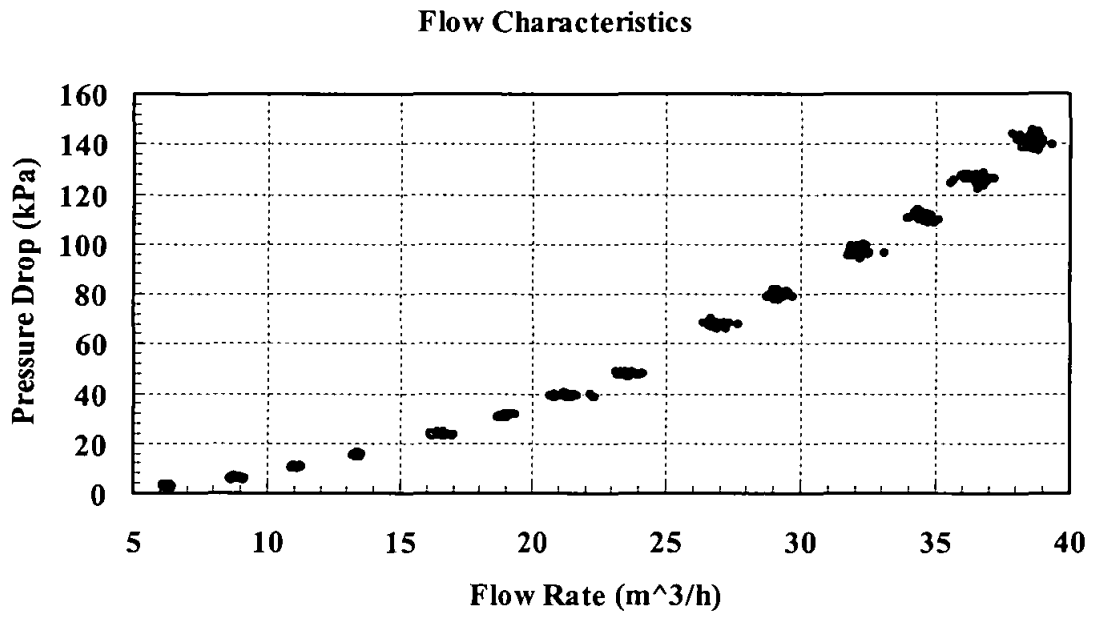


Figure 4.4: Pressure Drop and Flow Rate for Mineral Oil Run at 70 °C.



### 4.3 ANALYTICAL MODELING PROCEDURE

Pressure drop calculations were performed using the actual (measured) flowrate-temperature as well as the density and viscosity of “white oil” preliminary determined in laboratory as function of temperature. This calculation is required to compare the measured and calculated values, during non-deposition experiments. This preliminary validation of experimental and calculated data, is considered essential for assessing the onset and development of wax deposition from differences between measured and calculated (as non-deposit) pressure drop values.

The friction factor,  $f$  (the “*Moody’s*” evaluation of frictional pressure drop was used in fact) was calculated by different correlations used for calculating the frictional pressure drop in annular conduits were compared and results are further discussed.

The Bernoulli equation assumes inviscid and steady flow along a streamline, constant density and viscosity, and an inertial reference frame. The Bernoulli equation is used with external flows around objects submerged in fluids, or for internal duct/pipe flow over relatively short distances (such that all physical properties are kept constant), and with flow from a plenum (White, 1999).

The Bernoulli equation expresses the conservation of the sum of pressure, kinetic, and potential energy according to Eq. 4.1.

$$\frac{1}{\rho} \int_1^2 dP + \frac{1}{g} \int_1^2 v dv + \int_1^2 dz = 0 \quad (4.1)$$

Integrating Eq. 4.1, knowing that the flow is incompressible, Eq. 4.2 is obtained. This equation is also known as the Bernoulli equation.

$$P + \frac{1}{2} \rho v^2 + \rho g z = \text{Const} \quad (4.2)$$

The first term in Eq. 4.2 represents the pressure head, the second term represents the velocity head, and the final term represents the static head differences. The constant of

integration is called the Bernoulli constant and relies heavily on steady, frictionless, incompressible flow (Hodge and Taylor, 1998).

The Bernoulli equation cannot be used when general losses in the system are to be accounted for. An equation derived from the conservation of energy formula should be used for such situations. The conservation of energy equation used is shown in Eq. 4.3 (Hodge and Taylor, 1998):

$$\frac{\partial q}{\partial t} - \frac{\partial W_s}{\partial t} = \frac{\partial}{\partial t} \int_{cv} \rho e dV + \int_{cs} \left( e + \frac{P}{\rho} \right) \rho \bar{V} \cdot d\bar{A} \quad (4.3)$$

Considering the specific total energy,  $e$ , including the specific internal energy, the potential energy, and the kinetic energy; in the absence of heat transfer, the energy equation becomes Eq. 4.4 (Hodge and Taylor, 1998):

$$dW_s = \frac{dP}{\rho} + VdV + gdz = d(\text{losses}) = 0 \quad (4.4)$$

Integrating Eq. 4.4, we obtain Eq. 4.5 (Hodge and Taylor, 1998).

$$\frac{P_1}{\gamma} + \frac{V_1^2}{2g} + z_1 = \frac{P_2}{\gamma} + \frac{V_2^2}{2g} + z_2 + \frac{W_s}{g} + \text{losses} \quad (4.5)$$

The total pressure losses in a system are including both “major” and “minor” losses. Major losses are associated with pipe wall friction over the entire length of a pipe (Hodge & Taylor, 1998). Pressure losses due to friction are the major contributor that effects flow. Frictional pressure loss can be calculated according to the *Darcy-Weisbach* equation for the frictional pressure drop in pipes, which is expressed by Eq. 4.6.

$$\frac{dP}{dx} = \frac{f\rho v^2}{2D} \quad (4.6)$$

This equation is specific to circular pipes. Similar forms of equation have been applied for annular ducts. The appropriate characteristic length replacing the circular pipe internal diameter ID for non-circular conduit, used to evaluate the Reynolds number and, then, the friction factor  $f = F(\text{Re})$  is the *hydraulic diameter*. The hydraulic diameter  $D_h$  is defined

as the cross sectional area divided by the wetted perimeter of the pipe multiplied by four (Eq.4.7):

$$D_h = \frac{4A}{P} = \frac{4 \times \text{flow area}}{\text{wetted perimeter}} \quad (4.7)$$

The hydraulic diameter is an approximation that used to calculate the frictional pressure drop for non-circular conduit produce results close to measured values, particularly for turbulent flows regimes; greater errors being recorded for laminar flow conditions (Hodge & Taylor, 1998).

Rearranging and integrating Eq. 4.6, and incorporating the hydraulic diameter expressed by Eq. 4.7, the following is obtained:

$$\Delta P_f = f_M \frac{L}{D_h} \frac{\rho v^2}{2} \quad (4.8)$$

Where:

- $\Delta P$      $\equiv$     frictional pressure gradient (Pa)
- $f_M$      $\equiv$     friction factor (Moody evaluation)
- $L$      $\equiv$     pipe lengthy (m)
- $D_h$      $\equiv$     the hydraulic diameter (m)
- $\rho$      $\equiv$     Fluid density ( $\text{kg/m}^3$ )
- $v$      $\equiv$     Fluid velocity (m/s)

For laminar flow the friction factor is only a function of the Reynolds number, shown in Eq 4.9, but for turbulent flow it may depend on both the Reynolds number and the relative roughness  $\varepsilon / D$  of the pipe (White, 1999).

$$f_M = \frac{64}{\text{Re}_D} \quad (4.9)$$

Fully developed turbulent flow in rough ducts, the experimental values of  $f = F[\text{Re}, (\varepsilon / D)]$  may be calculated using the Colebrook correlation (curve-fit), an

---

implicit equation, that has been accepted as the most accurate representation of the Moody experimental diagram (Appendix F) for turbulent pipe flow (Hodge & Taylor, 1998).

$$\frac{1}{\sqrt{f}} = \log \left( \frac{\varepsilon}{3.7 D} + \frac{2.51}{\text{Re}_D \sqrt{f}} \right)^{-2} \quad (4.10)$$

This expression, although highly accurate, is not very amenable to design due to its implicit nature that must be solved iteratively and, also due to discontinuities inherent to transition from laminar to turbulent flow regimes.. Some alternate explicit forms have been proposed by Swamee and Jain (1966), Churchill (1977), Haaland (1981), and others. Most of these explicit equations have their own range of Reynolds numbers and roughness values for which they are valid.

#### 4.4 THEORETICAL ANALYSIS

To calculate the pressure drop according to Darcy equation, the friction factor is calculated first. An explicit alternate expression for the friction factor given by equation 4.11 is proposed by Churchill (Hodge and Taylor, 1998), is used instead of Colebrook expression.

It represents the friction factor for laminar, transitional, and turbulent flows. This explicit expression can be solved if Reynolds number and the relative roughness are known and is advantageous since the friction factor in the transition region is a continuous function, which (arbitrarily, for calculation purposes only) smoothly links the value of friction factors calculated for laminar and turbulent flow regions:

$$\left. \begin{aligned} f_F &= 2 \left[ \left( \frac{8}{\text{Re}_D} \right)^{12} + \left( \frac{1}{(A+B)^{3/2}} \right) \right]^{1/12} \\ A &= \left[ 2.457 \ln \left( \frac{1}{(7/\text{Re}_D)^{0.9} + (0.27\varepsilon/D)} \right) \right]^{16} \\ B &= \left[ \frac{37530}{\text{Re}_D} \right]^{16} \end{aligned} \right\} \quad (4.11)$$

where  $A$  and  $B$  constants,  $f_F$  is Fanning friction factor. Accordingly, Moody friction factor is:

$$f_M = 4 \times f_F$$

and Reynolds number is:

$$\text{Re} = \frac{\rho v D_h}{\mu} \quad (4.12)$$

In the present work, the working fluid was white mineral oil and its properties (density and viscosity) were determined according to standard laboratory tests analysis; “ASTM 4052 – 96” for density and “ASTM D 445 – 06” for kinematic viscosity. For detailed tests instructions and procedures see appendix D.

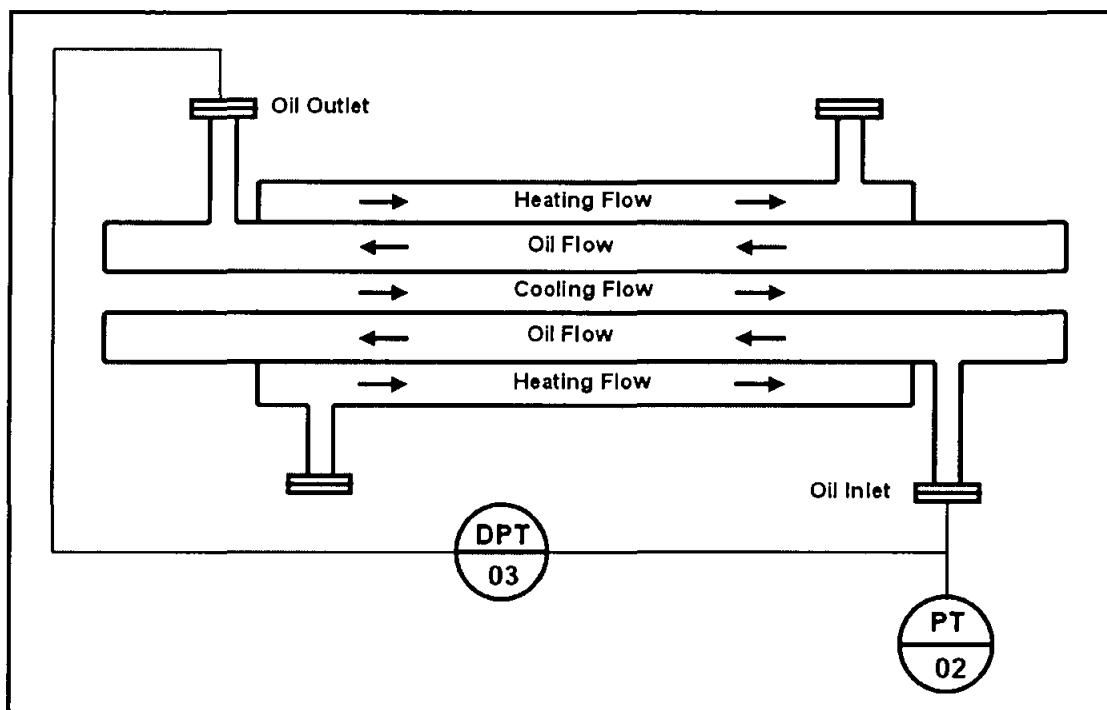


Figure 4.5: Schematic of the test section.

---

#### **4.5 RESULT AND DISCUSSION**

The frictional pressure drop measurements and calculations for a non-deposition experiment performed at various flow rates are compared. Calculated and measured pressure drop at different temperatures are plotted against Reynolds number as in Figures 4.6 for laminar flow regime and Figures 4.7 through 4.9 for turbulent flow regime. It is noted that the calculated pressure drop values are considerably higher than the measured ones. The measured-calculated pressure drop differences increase with the flow rate increments. This increase is even steeper for turbulent flow regimes.

Although the analysis during turbulent flow is more important for scaling the results to the field conditions, the laminar flows regimes were also considered. The special interest given to laminar flow conditions mainly related to assessment of frictional pressure drop for noncircular, annular duct geometry. Jones & Leung (1981) are strongly recommending obtaining sufficient data in the laminar flow region in order to insure the adequacy of the experimental procedure.

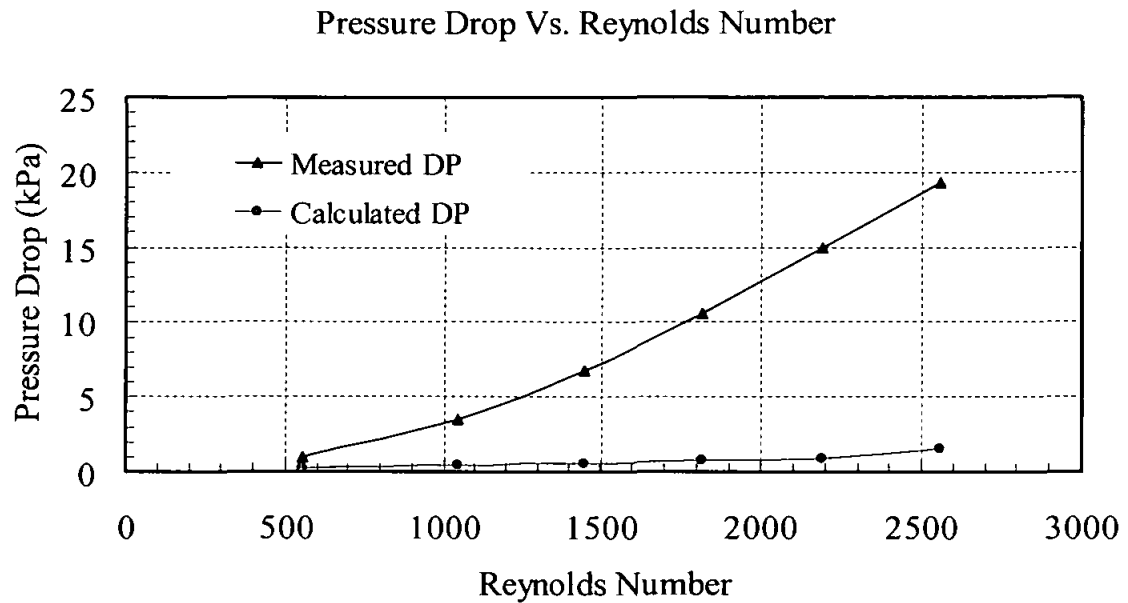


Figure 4.6: Measured and Calculated Pressure Drop Values in Laminar Flows at 50 °C.

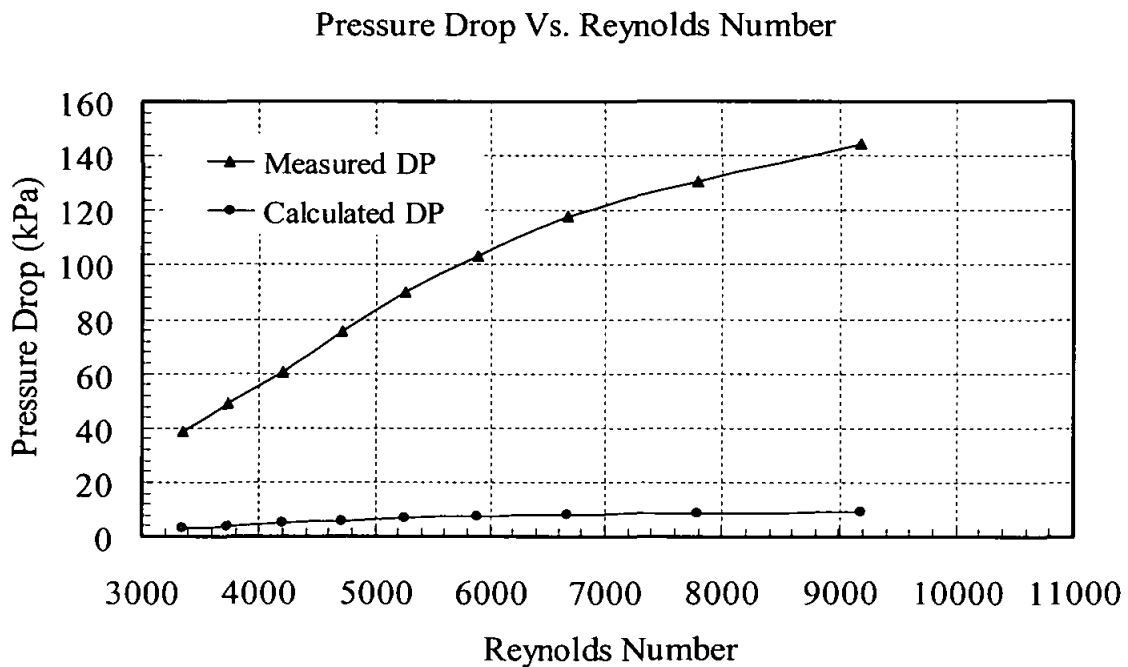


Figure 4.7: Measured and Calculated Pressure Drop Values in Turbulent Flows at 50 °C.



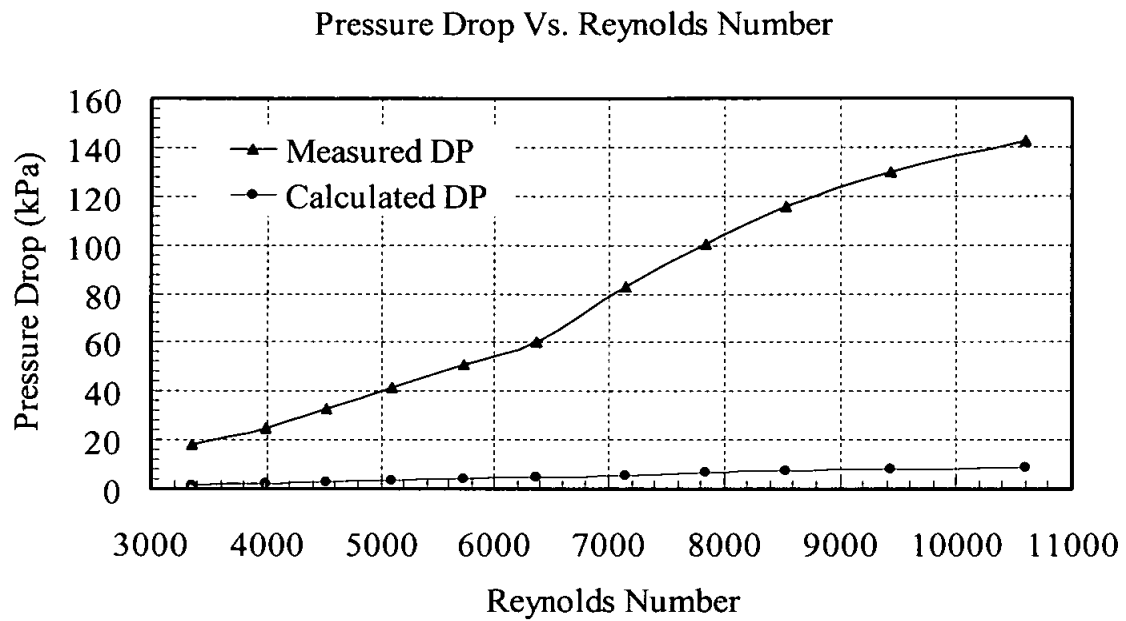


Figure 4.8: Measured and Calculated Pressure Drop Values in Turbulent Flows at 60 °C.

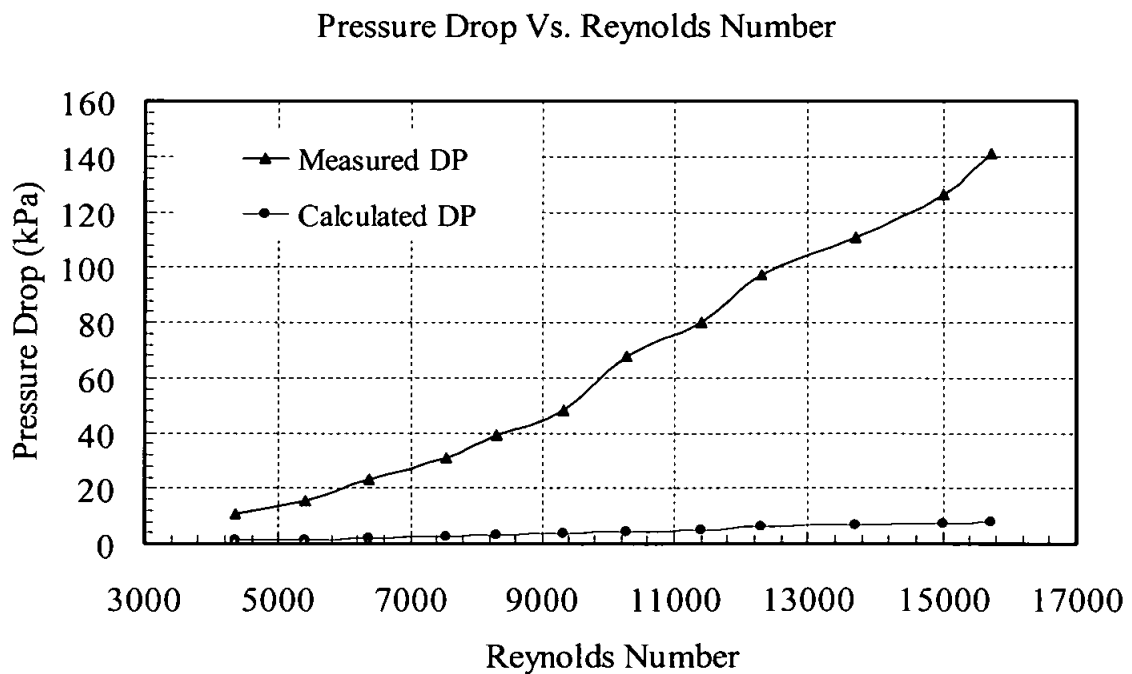


Figure 4.9: Measured and Calculated Pressure Drop Values in Turbulent Flows at 70 °C.

---

In spite of great differences between calculated and measured pressure drop illustrated in Figs. 4.7 - 4.9, good linear correlations between calculated and measured pressure drop are observed in Figures 4.10 - 4.12 for all cases (correlation coefficient  $R^2 > 0.98$ ). This indicates that the measurement error is of *systematic nature* and did not appear to be related to “independent” parameters (such as viscosity-density models or other factors).

Four possible explanations for poor (absolute values) matching are suggested:

1. Systematic errors in the flow rate indication (to be checked by comparing the measured power absorbed by the pump with the calculated value).
2. Systematic errors in the Differential Pressure Drop transmitter (DPT 03) measurement the DPT 03 has to be checked carefully (both taps fill with non-gelling liquid and calibrated in accordance with manufacturer instructions).
3. An improper estimation of the equivalent diameter replacing the conventional circular pipe diameter for an annular-concentric duct flow,
4. Strong influence of the fluid “entrance-exit” effects and of the “nozzle” effect at the transition from 2” pipe (ID = 49.25 *mm*) to DA – will be further discussed.

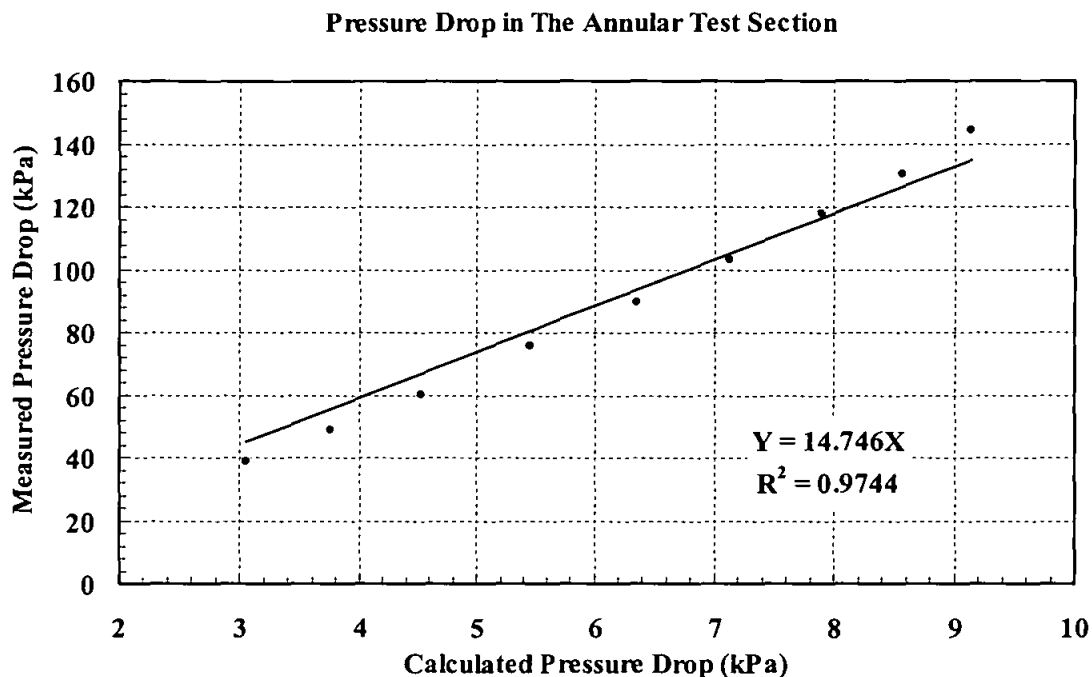


Figure 4.10: Measured Versus Calculated pressure drop across DA (laminar, transition and turbulent regime) for white oil recirculated at 50 °C.

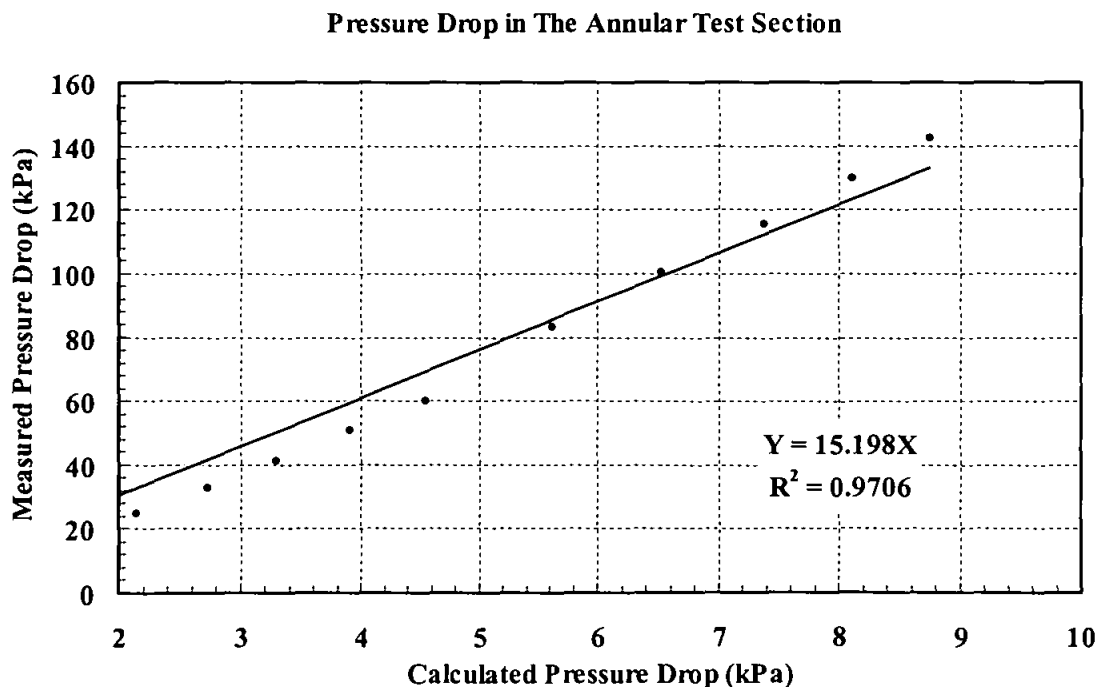


Figure 4.11: Measured Versus Calculated pressure drop across DA (laminar, transition and turbulent regime) for white oil recirculated at 60 °C.

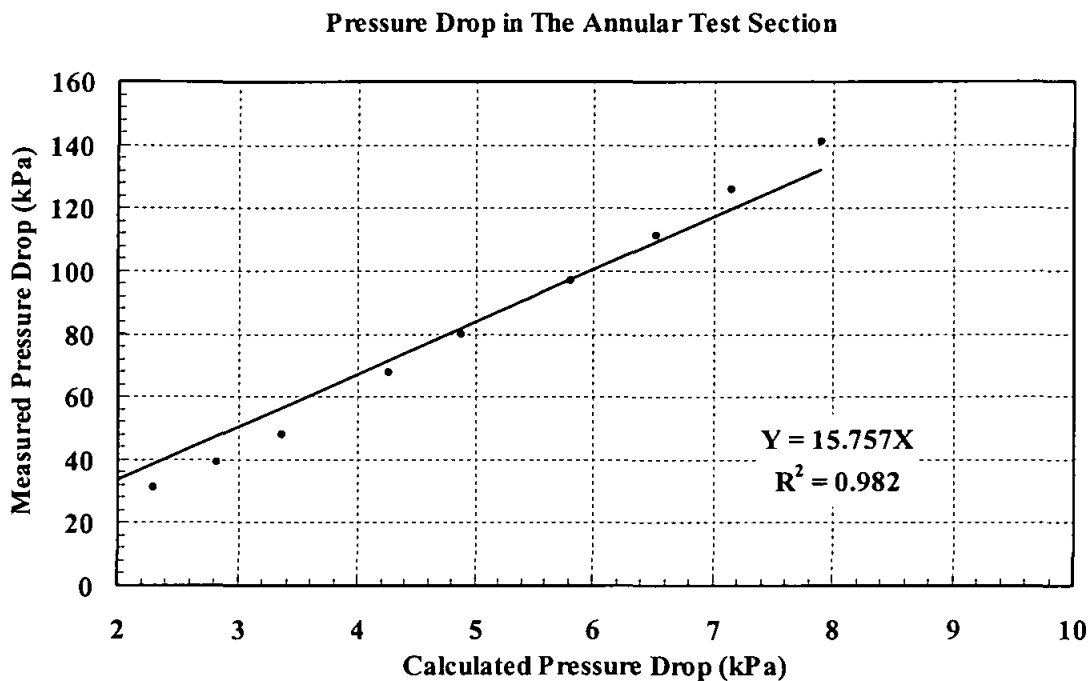


Figure 4.12: Measured Versus Calculated pressure drop across DA (laminar, transition and turbulent regime) for white oil recirculated at 70 °C.

## 4.6 PARAMETERIC ANALYSIS

### 4.6.1 THE FRICTION FACTOR

In addition using the Churchill equation, the Swamee-Jain and Haaland equations were also used to determine theoretical friction factors. The Swamee and Jain equation provides an explicit method to calculate the friction factors for turbulent flow (Hodge & Taylor, 1998).

$$f_M = \frac{0.25}{\left[ \log \left( \frac{\varepsilon}{3.7D} + \frac{5.74}{\text{Re}^{0.9}} \right) \right]^2} \quad (4.13)$$

The Haaland equation shown in Eq. 4.14 is valid for  $\varepsilon/D > 10^{-4}$  for turbulent flow, considering the Darcy friction factor (Hodge & Taylor, 1998).

$$f_M = \frac{0.3086}{\left[ \log \left( \frac{6.9}{\text{Re}} + \left( \frac{\varepsilon}{3.7D} \right)^{1.11} \right) \right]^2} \quad (4.14)$$

The friction factor formula for turbulent flow – Eq. 4.15 - developed by Paul H. R. Blasius is also used:

$$f_M = \frac{0.3164}{\text{Re}^{0.25}} \quad (4.15)$$

The results for the three equations are plotted together on Figure 4.13. The purpose was to justify the use of the Churchill and to determine its contribution on the error associated with calculated pressure drop values. By examining Figure 4.13 it was observed that the theoretical values obtained with the aid of the friction factor correlations (Churchill, Haaland, Swamee-Jain and Blasius) are agreed well within  $\pm 2\%$  error band. It appears from Fig. 4.13 that all the theoretical values of the four correlations studied, produced very similar results with data overlapping.

Likewise, the theoretical values of the four friction factor correlation are compared with experimental friction factor data obtained from the pressured drop measurements and fluid properties. An absolute average error of 93 % between the experimental and theoretical values is recorded for the four friction factor correlations with a standard deviation of 0.25.

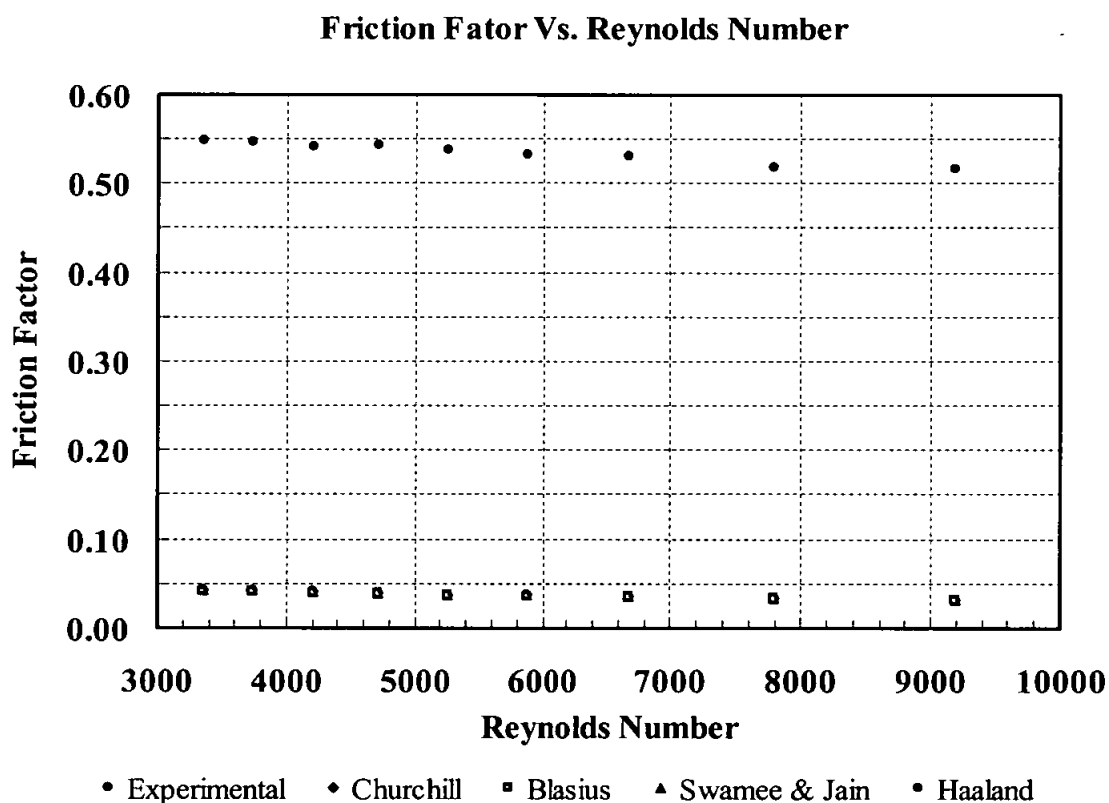


Figure 4.13: The effect of different friction factor correlations.

It is concluded that the theoretical values of the four friction factor examined is agreed well and the error between these values and the experimental data is consistent. This finding revealed that Churchill equations can be confidently used factoring the calculation routine, and it has no effect in the error associated with calculated pressure drop values.

#### 4.6.2 EQUIVALENT DIAMETER APPROXIMATION

In addition to the hydraulic diameter customarily given by Eq. 4.7, and accepted as “equivalent” diameter for the annular concentric ducts, there are many equivalent diameter correlations also suggested in the literature. These correlations have been checked against the hydraulic diameter to extend the criteria of the pressure drop characterization.

##### *The Petroleum Diameter Method*

One of the suggested ways of calculating the pressure drop of a non-circular, concentric-annular flow cross-section named “The Petroleum Engineering Method” uses Eq. 4.16 for evaluating an equivalent calculation diameter to replace the circular pipe diameter (Bertuzzi et. al., 1987).

$$d_e = \sqrt[5]{(d_2 + d_1)^2 \times (d_2 - d_1)^3} \quad (4.16)$$

##### *The Equivalent Area Diameter Method*

As suggested by Lamb, Eq. 4.17 – simply is assuming an equivalent, diameter of a circular pipe having the same flow area,. The “equivalent area” diameter is calculated as:

$$d_e = (d_2^2 - d_1^2)^{1/2} \quad (4.17)$$

##### *The Equivalent Geometry Diameter Method*

Another criterion used to obtain an equivalent circular radius from comparing the geometry in the pressure-loss equations for pipe flow and concentric annulus flow of Newtonian fluid terms is the geometry terms in the, is the “equivalent geometry” diameter given by:

$$d_e = \sqrt{d_2^2 + d_1^2 - \frac{d_2^2 - d_1^2}{\ln(d_2 / d_1)}} \quad (4.18)$$

In the previous three correlations,  $d_e$  is the equivalent diameter,  $d_1$  is the inner diameter of the annulus passage of the test section under the investigation and  $d_2$  is the outer diameter. The Dimensions of Deposition Apparatus (DA) test section and calculated values of equivalent diameters using different (literature) suggested models (Eqs. 4.16 – 4.18) are given in Table 4.2.

Table 4.2: Dimensions of Deposition Apparatus (DA) and calculated values of various equivalent diameter models

Deposition Apparatus dimensions ( $m$ )	
Inner Diameter ( $d_1$ )	0.0422
Outer Diameter ( $d_2$ )	0.0801
Circular Equivalent diameter ( $m$ )	
Hydraulic diameter Method	0.0379
Petroleum diameter Method	0.0605
Equivalent Area diameter Method	0.0681
Equivalent Geometry diameter Method	0.0310

Figure 4.14 compares the results of pressure drop obtained by using the various equivalent diameter models shown in Table 4.2.

The “base-line” comparisons of calculated and measured pressure drop (Figs. 4.7 through 4.9) are suggesting that the “hydraulic diameter” model used to assimilate an annular duct geometry with a simple, circular one, indicate a much lower calculated than measured value. Therefore a better model should be able to lead to a higher pressure drop value than the “hydraulic” model used as base-line.

The “Equivalent Geometry” model, indicates a pressure drop range slightly above the range calculated with the aid of hydraulic diameter model, therefore, slightly decreasing the discrepancy between calculated and measured pressure drop values. The “petroleum”



---

diameter model, and the “equivalent area” diameter model, is showing lower pressure drop values than the base-line values, therefore increasing the discrepancy between measured and calculated pressure drop values for turbulent flow regime.

Figure 4.14 shows the pressure drop variation with respect to  $Re$  values for the turbulent flow. Different trends of the pressure drop are observed for the each equivalent diameter. As it seen form the plot, the equivalent diameter has effect on the flow regime length. In case of the equivalent area method, which has the biggest values, the turbulent regime start early at the low flow rates Figure 4.14. The length of the turbulent flow regime decrease with the increase of the value of the equivalent diameter. For this point care must be taken in chose of the appropriate equivalent diameter which can give a good representation for the flow phenomenon in the annular passage.

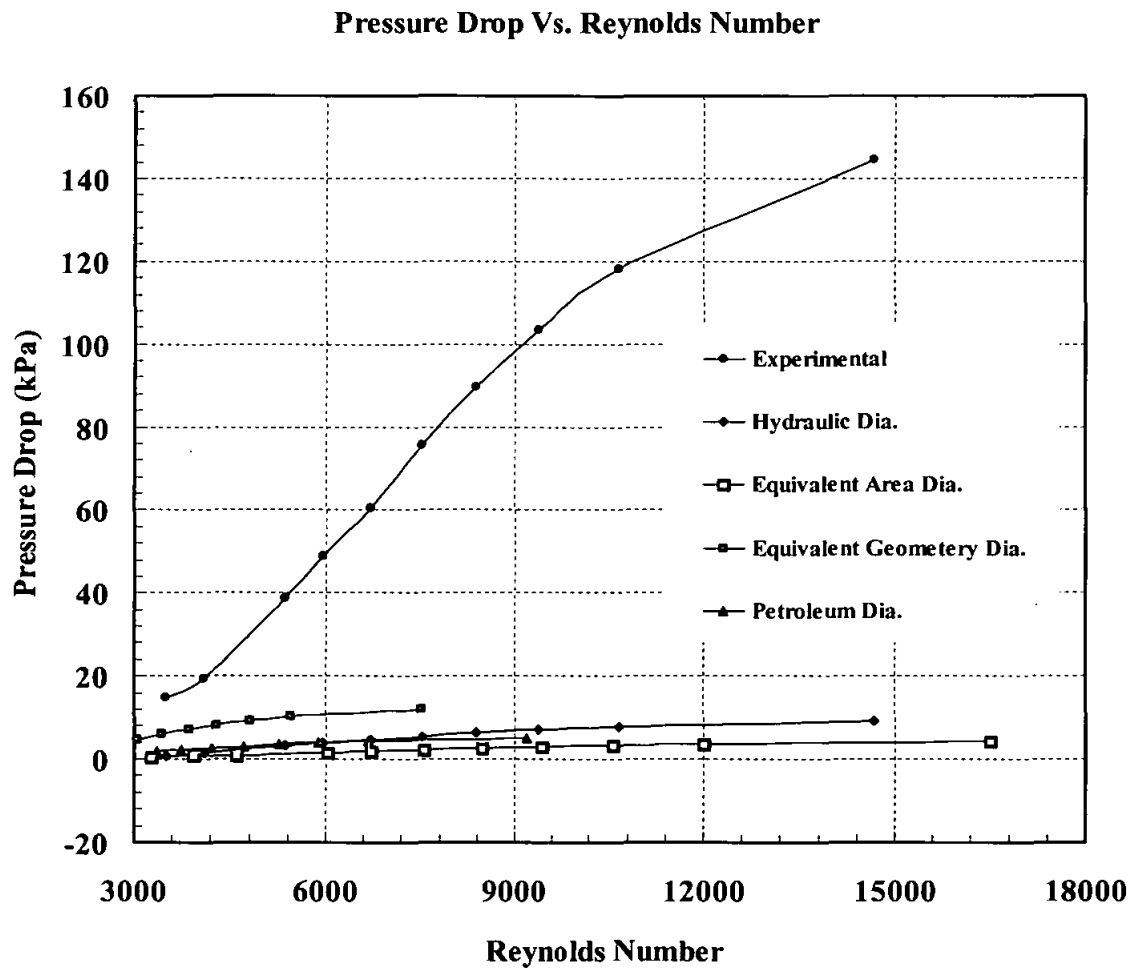


Figure 4.14: The effect of the various equivalent diameter models to the turbulent regime length.

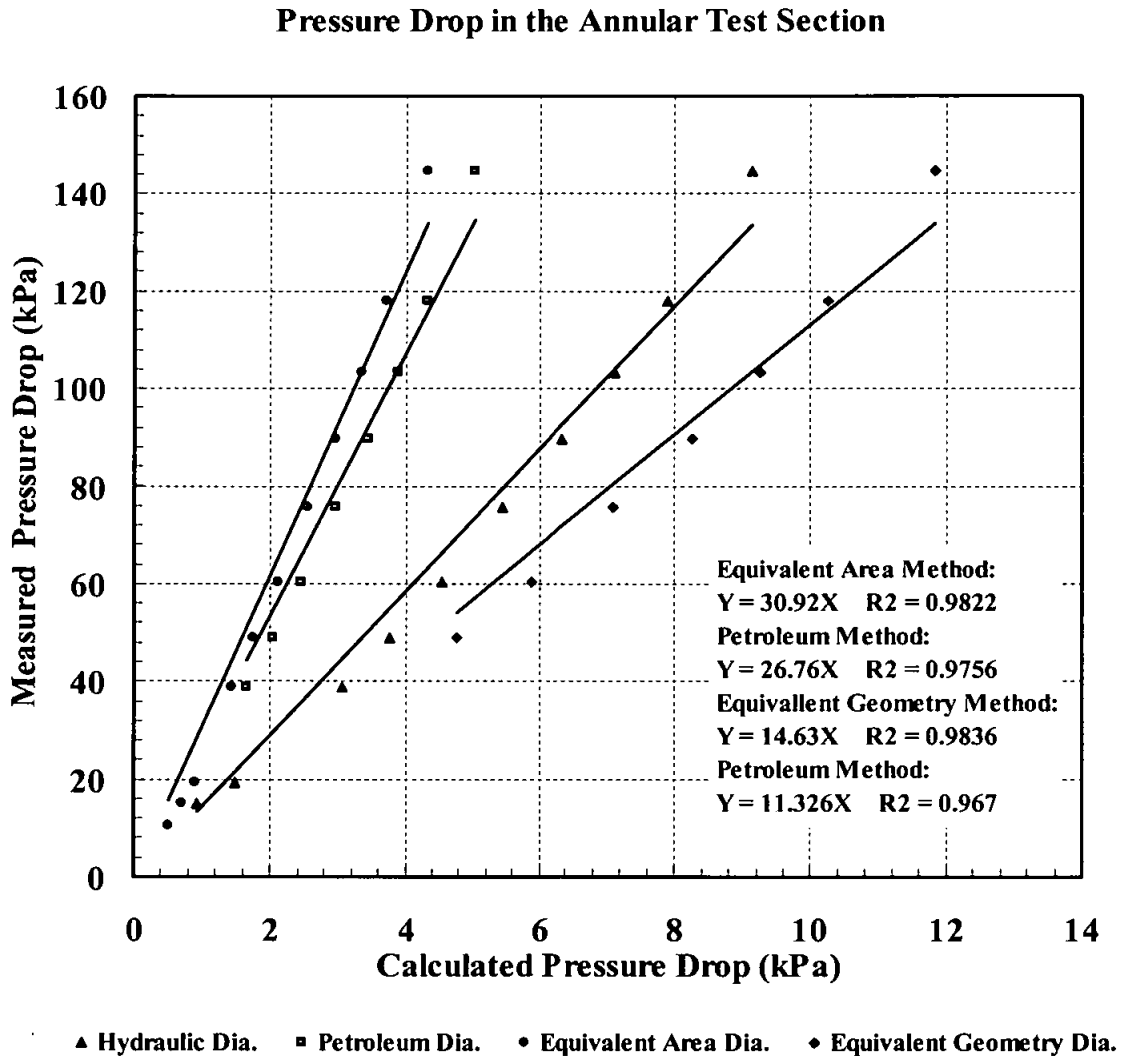


Figure 4.15: Calculated versus measured pressure drop and linear regressions; the effect of various equivalent diameter models used for the annular duct.

Figure 4.15 show the regression analysis for the calculated and measured pressure drop using different equivalent diameter models., The “Equivalent Area” model shows the biggest deviation of 96 % between the measured and calculated pressure drop, the measured pressure drop was 31 times the calculated values with standard error of 3.8, while “Equivalent Geometry” model showed the smallest deviation of 91 % and the measured pressure drop was 11 times the calculated pressure drop with standard error of 3.99.

---

Although the “Equivalent Geometry” model, used to calculate the equivalent diameter of the annular flow geometry (Eq. 4.18), slightly reduces the discrepancy between the measured and calculated pressure drop data as compared with other equivalent diameters illustrated in Figures 4.15; the hydraulic diameter will be used as standard for the calculations and further analysis; the following reasons are given:

- The hydraulic diameter is a convenient substitute for the characteristic physical dimension of a non circular duct, and it leads to fairly good correlation between turbulent fluid flow and heat transfer characteristic of circular and noncircular ducts. The hydraulic diameter is also used for ducts involving laminar flow to provide a consistent basis of comparison with turbulent flow results. However, for laminar flow itself this quantity does not lead to satisfactory correlations between circular and noncircular ducts (Kakac *et al.*, 1987).
- Using a general correlation for the equivalent length is not advised as it demonstrated that the equivalent length is not sufficient for accurate description of the observed behaviour, no existing correlation method has yet found general acceptance (Jones & Leung, 1981).
- Changing the diameter (to better fit the measured data) is also avoided due to envisaged problems, later, when the pressure drop increase related to the “jelly layer deposit” will create confusing effects (between real reduction and “arbitrary” reduction of flow area).

### 4.6.3 THE "CORRECTION FACTOR" MODEL

Another suggested methods for calculating the frictional pressure drop for flow in an annular (concentric) conduits (long pipe - stabilized flow assumption) suggests the use of a correction coefficient,  $k$ . this factor is to be separately evaluated for laminar and turbulent flow conditions and applied to the frictional pressure drop calculation with the aid of a circular pipe standard correlations (Eqs. 4.8 – 4.12) but having a diameter equal to the hydraulic diameter of annular conduit (Fried & Idelchik, 2003).

For a round annular tube the correction factor, which is a function of the diameter ratio can be found for ( $Re \leq 2000$ ) from:

$$k_{non-c,lam} = \frac{1 - (d_1/d_2)^2}{1 + (d_1/d_2)^2 + [1 - (d_1/d_2)^2]/\ln(d_1/d_2)^2} \quad (4.19)$$

In the case of turbulent flow  $k_{non-c}$  depends only slightly on the diameter ratio and lies in the range 1.0 – 1.07. The correction factor of such a tube can also be calculated from the following formula.

$$k_{non-c,turb} = f \left( \frac{0.02d_1}{d_2} + 0.98 \right) \left( \frac{1}{f} - 0.27 \frac{d_1}{d_2} + 0.1 \right) \quad (4.20)$$

where  $d_1$  and  $d_2$  are the inner and outer diameters of the annulus passage. For the deposition apparatus the correction factor for laminar flow,  $k_{non-c, lam}$ , according to Eq. 4.19 is equal to 1.49. The same value is obtained by using Eq. 4.21.

Eq. 4.21 is also proposed a use of correction factor for the laminar flow in the annular passage. It is obtained by Jones & Leung, 1981. Both Eq. 4.19 and 4.21 are not a function of Reynolds number (only of the diameters of the annular flow conduits).

$$\xi = \frac{(d_2 - d_1)^2 \cdot (d_2 - d_1)^2}{(d_2^4 - d_1^4) - (d_2^2 - d_1^2)^2 / \ln(d_1/d_2)} \quad (4.21)$$

For turbulent flow the correction coefficient,  $k_{non-c, turb}$ , is dependent on Re number. This dependency found to be weak as for  $Re = 2000 - 10000$ ,  $k_{non-c, turb} = 1.058 - 1.060$ .

Therefore, according to the handbook of Hydraulic Resistance, the actual frictional pressure drop in a stabilized (“long pipe assumption”) flow in an annular conduits should be calculated as a product of a correction coefficient and the frictional pressure drop calculated for the hydraulic diameter of the annular conduits.

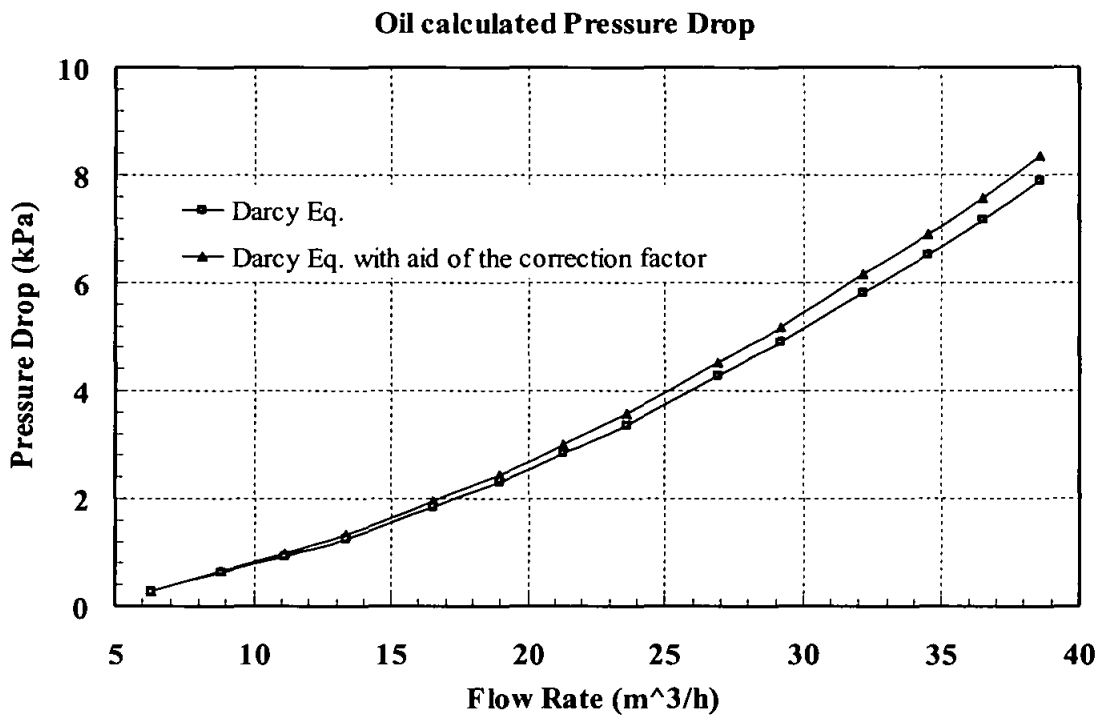


Figure 4.16: The effect of the correction factor on the calculation of the pressure drop

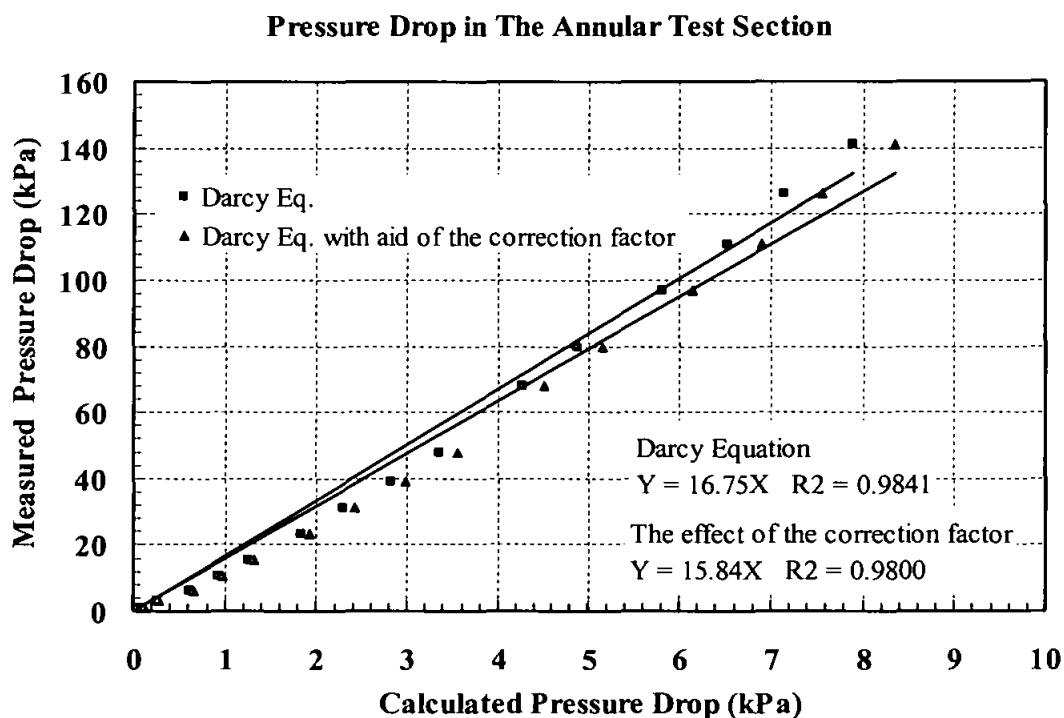


Figure 4.17: The effect of the correction factor on the calculated pressure drop (regression analysis).

Figures 4.16 and 4.17 illustrate the correction factor effect on the calculation of the pressure drop. As it can be seen from Fig. 4.17, the measured pressure drop is 17 times the calculated pressure drop (base-line), is reduced to 16 times when the Jones & Leung (J-L) correction factor is used. Also, the use of the J-L correction factor reduces the root mean square of the error between the measured and calculated values by 2%, while the standard deviation from the measured values remain the same about (44.33) with or without J-L correction. Therefore the correction factor produces insignificant (positive) effect for improving the calculation routine. However, the correction factor method should be considered for “polishing” calculation results when the hydraulic diameter approximation is used (Jones & Leung, 1981, White, 1999 and Fried & Idelchik, 2003).

---

The test of various models recommended in the literature for replacing the annular duct with an equivalent diameter, insignificantly reduced (or even increased) the gap between the measured and the calculated pressure drop values.

The consistency of measured and calculated deviations, at different scale, are in fact identical regardless of temperature and flowrate used. The significant difference between the two is suggesting that a rather important physical flow condition in the deposition apparatus design was not considered.



---

#### 4.7 DEVELOPMENT OF REALISTIC PRESSURE DROP CORRELATION

In such geometrical setting similar to the deposition test section, a complex fluid flow phenomenon exists. These phenomenon should be considered in order to accurately predict the pressure drop in the deposition test section.

***The effect of the changing direction:*** The fluid entering and exiting the test section (see Fig. 4.5) is forced to change direction. At the entrance, it will have to change direction from vertical to horizontal before entering the annular passage, and, again at the exit, from horizontal to vertical to flow back to the main tank. Even though the pressure transducer taps are located at the vertical inlet and outlet piping shortly before the fluid changes its direction through the annular passage and from where the fluid enters and exits, the change of flow direction nearby will significantly alter the readings. A stagnant pressure component is expected to influence the total pressure measurement and should be accounted for.

***The sudden contraction effect:*** The actual flow into the annular channel is quite complicated in nature and difficult to be accounted for. Complex fluid-wall interactions are taking place in the zone of fluid is entering into a larger area from a smaller one. The fluid sweeps-in and tries to fill-up the new volume. Eddies exist in the bottom corner of the space where the fluid is churned as it enters (White, 1998).

As the fluid enters the annular test section in the wax deposition flow loop, one might expect to see a similar occurrence. Although no photographs can be obtained of this phenomenon during actual testing, it was witnessed that as the fluid entered the annulus from the radial inflow section, the fluid became very churned up. This suggested that some local complex flow and mixing phenomenon occurred.

The sensitivity study of the parameters involved in the Darcy-Weisbach correlation, and the consistency of the error between the measured and calculated pressure drop values suggest that an additional frictional loss term is required to better represent the complex flow in the entrance-exit areas. This is expected to improve matching between the

measured and calculated pressure drop data. Since the annular deposition apparatus of the wax flow loop has a design feature of the double-pipe heat exchanger, Kay and London's expressions Eq. 4.22 (referenced by Hodge & Taylor, 1998) is valid for a situation such as the deposition apparatus under consideration and it can provide a better hydraulic performance assessment.

$$\Delta P = \underbrace{K_c \frac{v_1^2}{2g}}_{\text{entrance effect}} + \underbrace{\rho \frac{(v_2^2 - v_1^2)}{2}}_{\text{flow acceleration}} + \underbrace{f \frac{L}{d_h} \frac{\rho v_{ann}^2}{2g}}_{\text{core friction}} + \underbrace{K_e \frac{v_2^2}{2g}}_{\text{exit effect}} \quad (4.22)$$

In order to obtain better results of pressure drop calculation in the Deposition Apparatus an improved calculation method is suggested. The method uses the equivalent length ( $L_{eq}$ ) concept. In the proposed method, the pressure loss terms of the entrance, exit effect and the flow acceleration (Eq. 4.22) are simulated in form of a "conventional round pipe" of 1" (24.5 mm) diameter of a pre-determined, fixed length of  $L_{eq}$ . The total pressure drop in the deposition apparatus is expressed by Eq. 4.23 as a sum of two terms; the first term represents the core frictional pressure drop using the hydraulic diameter approximation, and the second term (replacing the actual entrance-exit hydraulic effects) modeled in a format similar to Darcy equation used for linear flow frictional pressure drop:

$$\Delta P_{DA} = \underbrace{f_M \frac{L}{d_h} \frac{\rho v^2}{2}}_{\text{oil annular passage}} + \underbrace{f_M \frac{L_{eq}}{D} \frac{\rho v^2}{2}}_{\text{circular pipe}} \quad (4.23)$$

---

#### 4.7.1 THE CALCULATIONS STEPS

Calculation routine of the total pressure drop in the DA with the proposed method is to be as following:

1. The total pressure drop in the Deposition Apparatus (Eq. 4.23) is calculated using the laboratory-measured fluid properties in two steps:
  - i. The calculations of the frictional pressure drop in the annular passage (first term in Eq. 4.23) is performed with the aid of the hydraulic diameter approximation (model) and the average velocity is calculated from the volumetric flow rate using and the annular flow cross-sectional area.
  - ii. The entrance, exit and acceleration flow effects (the second terms in Eq. 4.23) are accounted in the suggested calculation scheme using the equivalent frictional pressure drop of a virtual pipe with diameter of 1" (ID = 24.3 mm) and a certain length  $L_{eq}$ . The average velocity is obtained from the volumetric flow rate divided by the cross-sectional area of the flow. The equivalent length,  $L_{eq}$ , of the virtual pipe is determined by minimizing the sum of the square error between the measured and calculated pressure drop.
2. The calculation of the length of the "virtual pipe" uses the *Solver Parameters* tool (spreadsheet add-in feature) Figure 4.21, the equivalent length is obtained such as measured and calculated pressure drop are producing a near-perfect match. This was achievable by adjusting the initial value of the equivalent length to the optimum value by statistically minimizing the sum of root mean square (RMS) of the errors between the measured and calculated pressure drop values.
3. The validity of the suggested "virtual pipe" calculation method is verified by comparing the length of the "virtual pipe" required to match calculated-measured groups of values for different experiments (performed at various temperature conditions).
4. Approximately, same equivalent lengths were obtained with various experiments performed with different fluid properties.

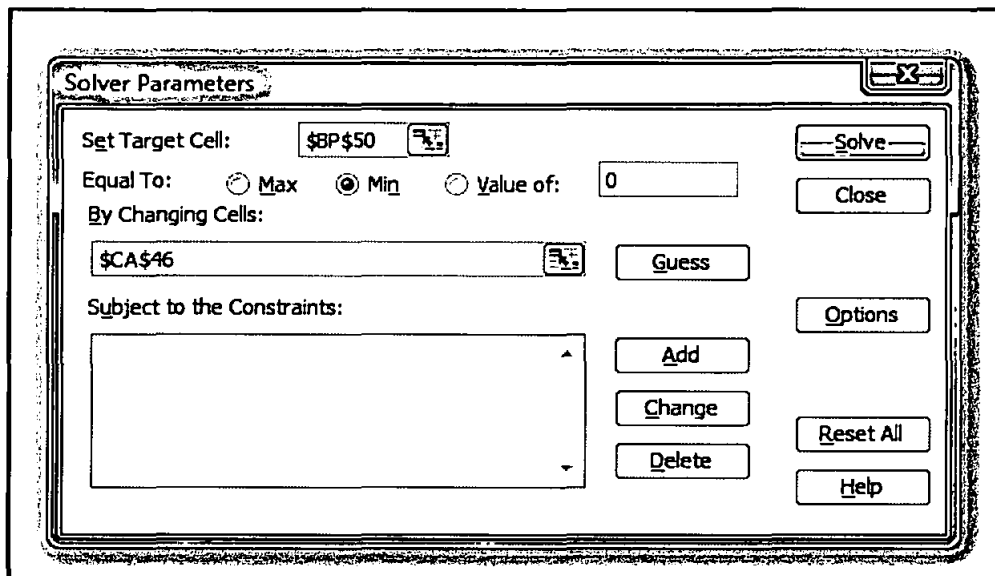


Figure 4.18: solver parameter window.

The goodness of the developed calculation procedure defined as (Figures 4.19 – 4.24)

$\Delta P_{\text{calculated}} = a \times \Delta P_{\text{measured}}$ , using the following criterion:

- i. Value of coefficient “a” (should be close to 1.0).
- ii. Coefficient of correlation  $R^2$  (close to unity).
- iii. Grouping of all experimental data around the median  $45^\circ$  line – measured by normalized standard deviation between measured and calculated values. Good grouping can be also evaluated visually from graph in Figures 4.19 – 4.24.

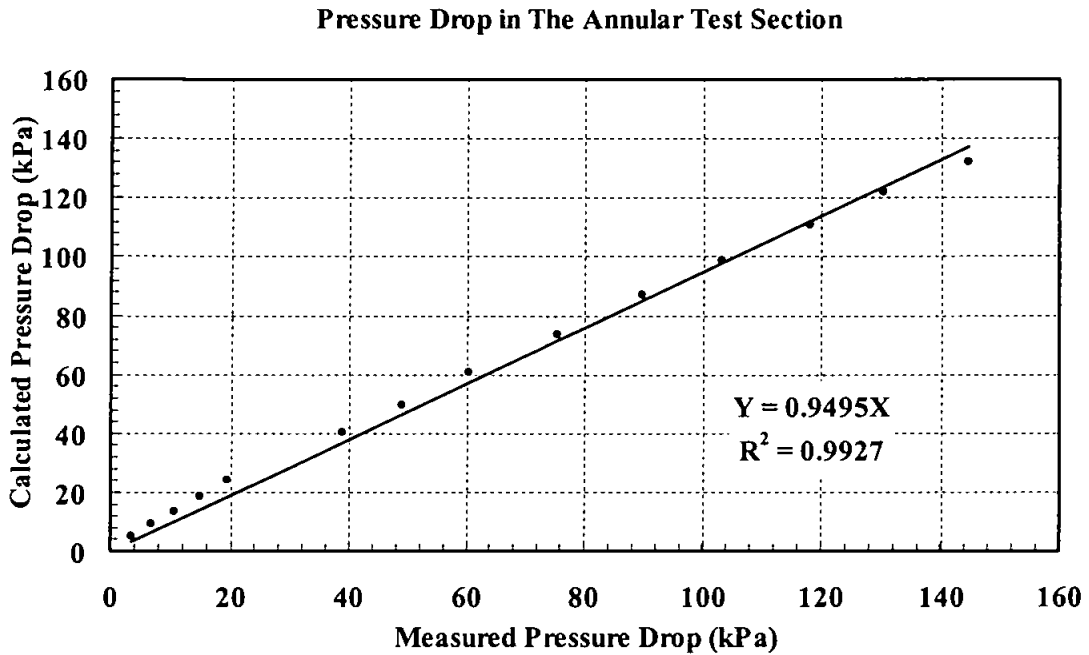


Figure 4.19: Measured Versus Calculated pressure drop across DA (laminar, transition and turbulent regime) for white oil recirculated at 50 °C.

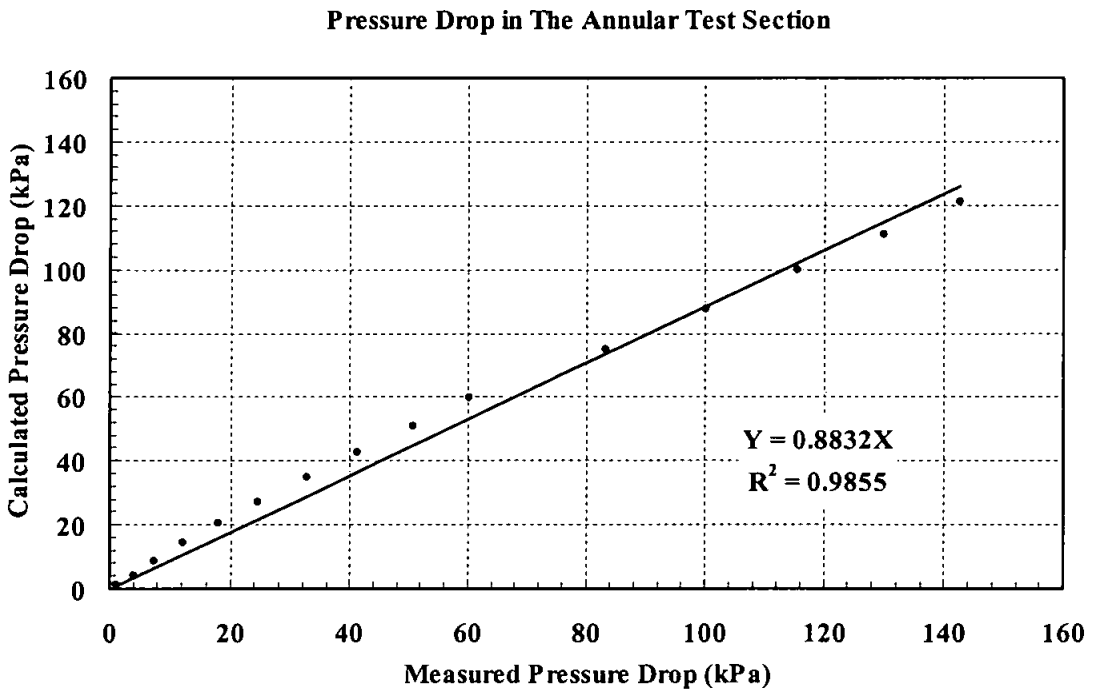


Figure 4.20: Measured Versus Calculated pressure drop across DA (laminar, transition and turbulent regime) for white oil recirculated at 60 °C

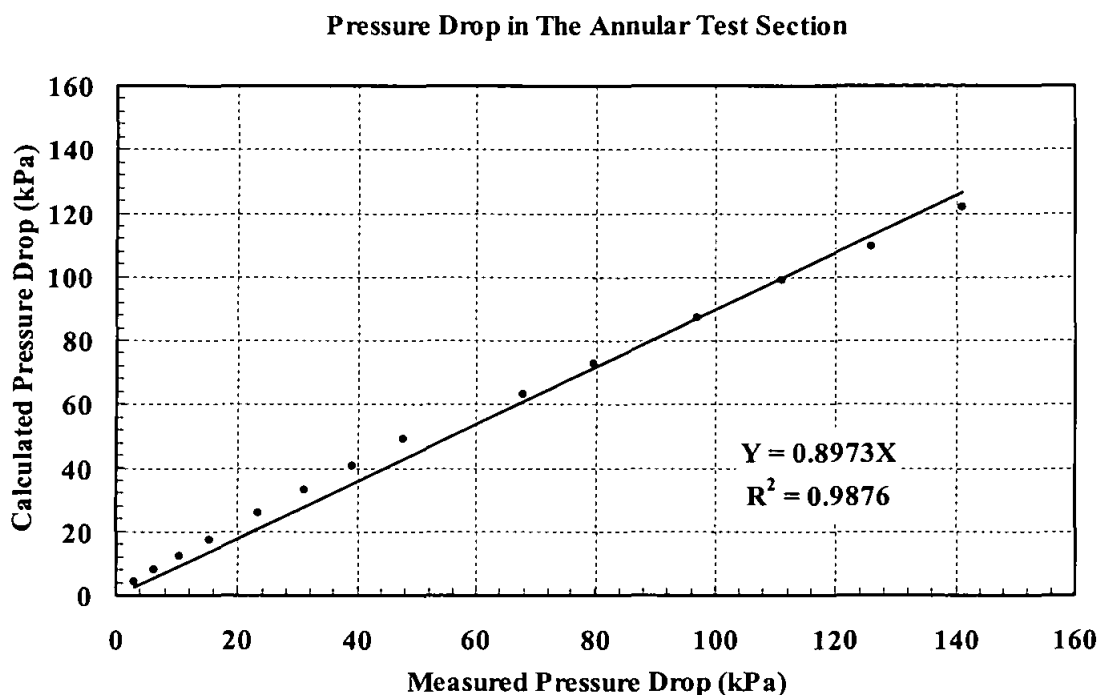


Figure 4.21: Measured Versus Calculated pressure drop across DA (laminar, transition and turbulent regime) for white oil recirculated at 70 °C

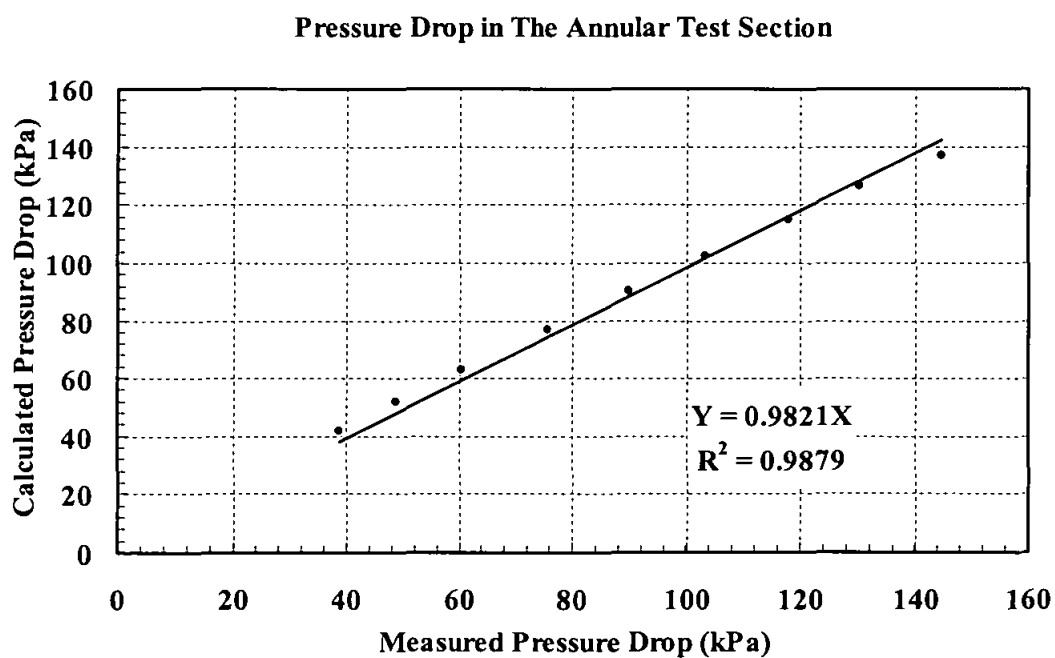


Figure 4.22: Measured Versus Calculated pressure drop across DA (turbulent regime) for white oil recirculated at 50 °C

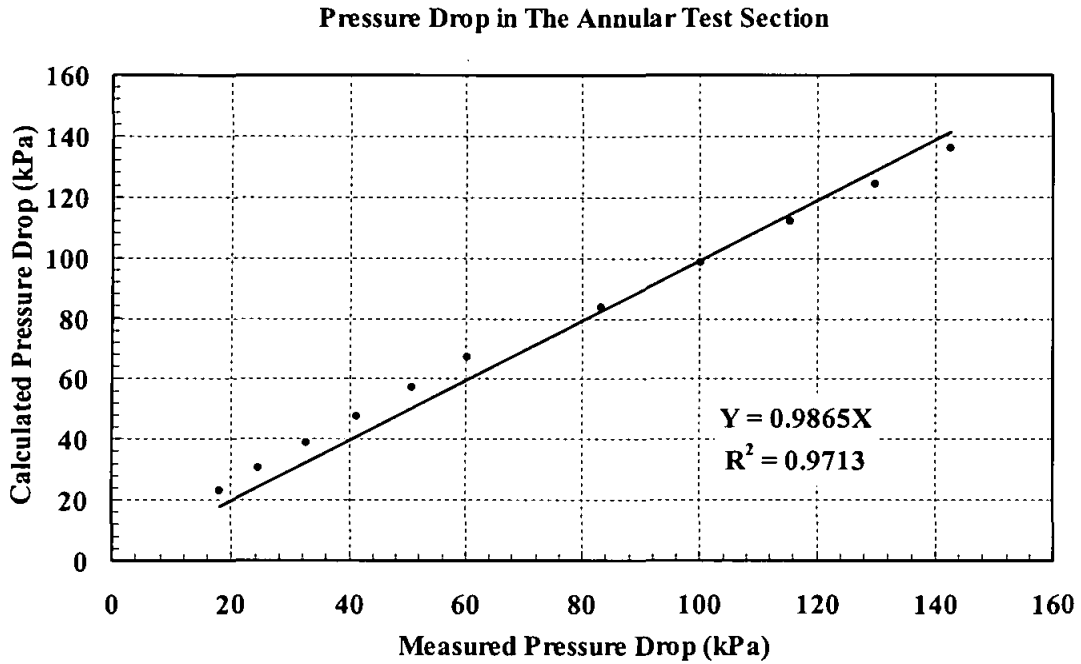


Figure 4.23: Measured Versus Calculated pressure drop across DA (turbulent regime) for white oil recirculated at 60 °C.

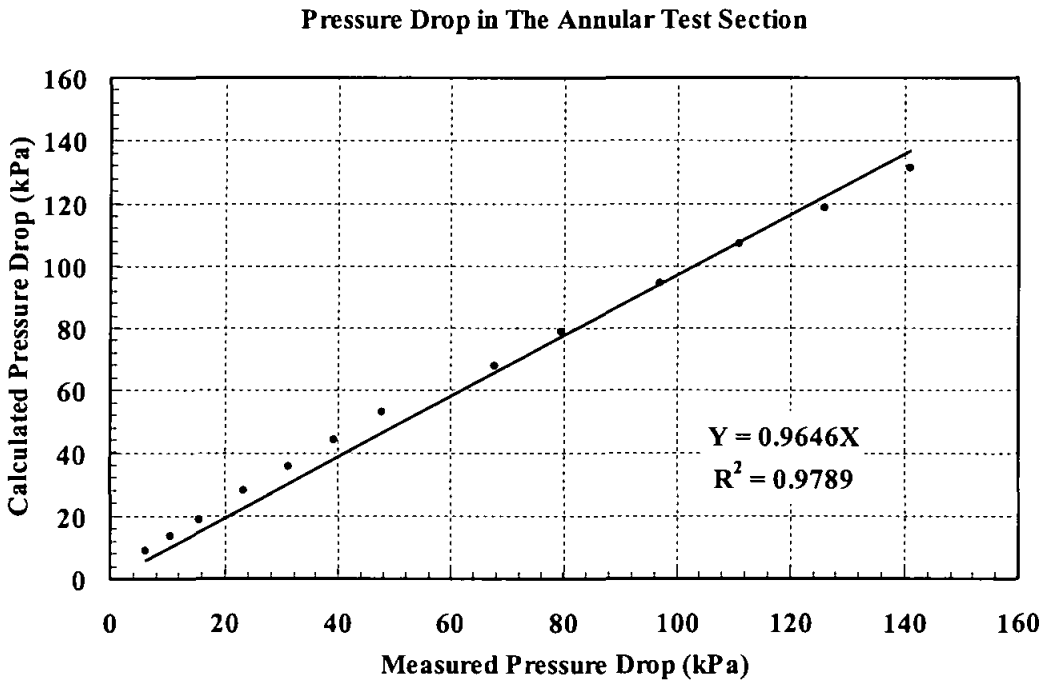


Figure 4.24: Measured Versus Calculated pressure drop across DA (turbulent regime) for white oil recirculated at 70 °C

#### 4.7.2 STATISTICAL ERROR ANALYSIS

This error analysis is utilized to check the accuracy of the new calculation method. The statistical parameters used in the present work are: average percent relative error ( $E_r$ ), average absolute percent error ( $E_a$ ), minimum and maximum absolute percent error ( $E_{min}$ ,  $E_{max}$ ), root mean square error (RMSE), standard deviation of error (STD), and the correction coefficient ( $R^2$ ), equations for these parameters are given in appendix E.

Table 4.3: Statistical Error Analysis (all statistical error analysis values is expressed in percentage (%))

Trail No.	$L_{eq}$ (m)	$E_r$	$E_a$	$E_{min}$	$E_{max}$	RMSE	$R^2$	STD
Trail 1	0.573	- 08.42	21.04	00.00	44.80	45.87	0.993	45.87
Trail 2	0.539	00.43	12.17	00.00	28.16	34.89	0.986	42.58
Trail 3	0.578	- 01.04	14.80	00.00	51.63	38.47	0.988	42.63
Trail 4	0.597	- 00.40	03.70	00.00	13.20	19.24	0.988	33.39
Trail 5	0.609	- 02.79	07.80	00.00	23.48	27.93	0.971	34.97
Trail 6	0.627	- 00.23	08.92	00.00	22.40	29.87	0.979	39.10

Figure 4.19 through Figure 4.24 present crossplot of calculated pressure drop (total pressure drop) versus measured pressure drop of the deposition apparatus. In this graphical based technique, all calculated values are plotted against the measured value and thus a crossplot is formed. A 45° straight line between the calculated versus measured data points is drawn on the crossplot, which denotes a perfect correlation line, the tighter the cluster a bout the unity slope, the better the agreement between calculated and measured values.

Figures 4.19, 4.20 and 4.21, show the result of developed correlation for three runs performed with a mineral oil re-circulated at different temperature conditions 50, 60 and 70 °C, respectively. In these figures, the calculation performed when the entire regime (laminar, transition and turbulent) is considered, while in the next three Figures 4.22, 4.23 and 4.23 the calculation carried out for the same condition but for the turbulent flow regime only.



---

An equal  $L_{eq}$  of almost 0.60 m is obtained for different flow condition with very close standard deviation. This justifies the finding of the systematic nature of the error that is found between the experimental and calculated values. The developed method is correlated the experimental data and the calculated values for turbulent regime much better than that one when the entire regime is considered. An error reduction from absolute average percent error (AAPE) of 92 % to less than 15 % for the entire regime and less than 8 % for the turbulent regime is achieved. This improvement is depicted in Figure 4.26 and tabled in Table 4.4.

The goodness of the turbulent regime correlation also can be observed from the crossplot Figures (Figs. 4.19 – 4.24). By checking the values of the slope of the line correlating the calculated and measured values such that  $\Delta P_{calculated} = a \times \Delta P_{measured}$ , the values of “a” for the turbulent regime is closer to the unity than for the entire regime consideration.

Table 4.4: Experimental-measured data Average Absolute Percent Error (AAPE).

	Test Condition #1	Test Condition #2	Test Condition #3
Initial Data	91 %	92 %	93 %
Entire Regime Modification	14 %	11 %	13 %
Turbulent Regime Modification	4 %	7 %	8 %

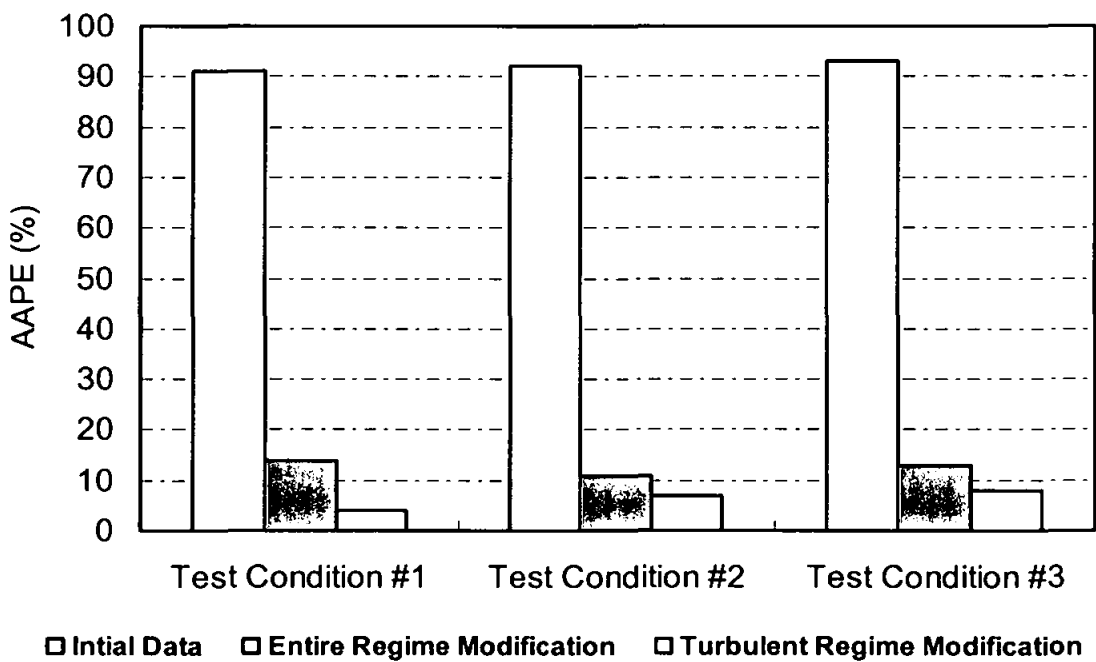


Figure 4.25: Experimental-measured data error reduction in terms of the AAPE.

### 4.7.3 ISOTHERMAL PRESSURE DROP

A pressure drop run trail termed “*Isothermal Pressure Drop*” was performed to double-check the accuracy of the developed method used to interpret and manage the discrepancy between the measured and calculated pressured drop data in the test section. In this run all the flowing fluid in the test section (cold pipe, annular passage and the heat jacket) are kept at same temperature of 50 °C. the purpose was to account for the effects of the temperature-dependent properties (viscosity and density).

The pressure drop calculation performed with the isothermal run data showed that the same order of discrepancy between measured and calculated pressure drop data occurred with diabatic pressure drop data.

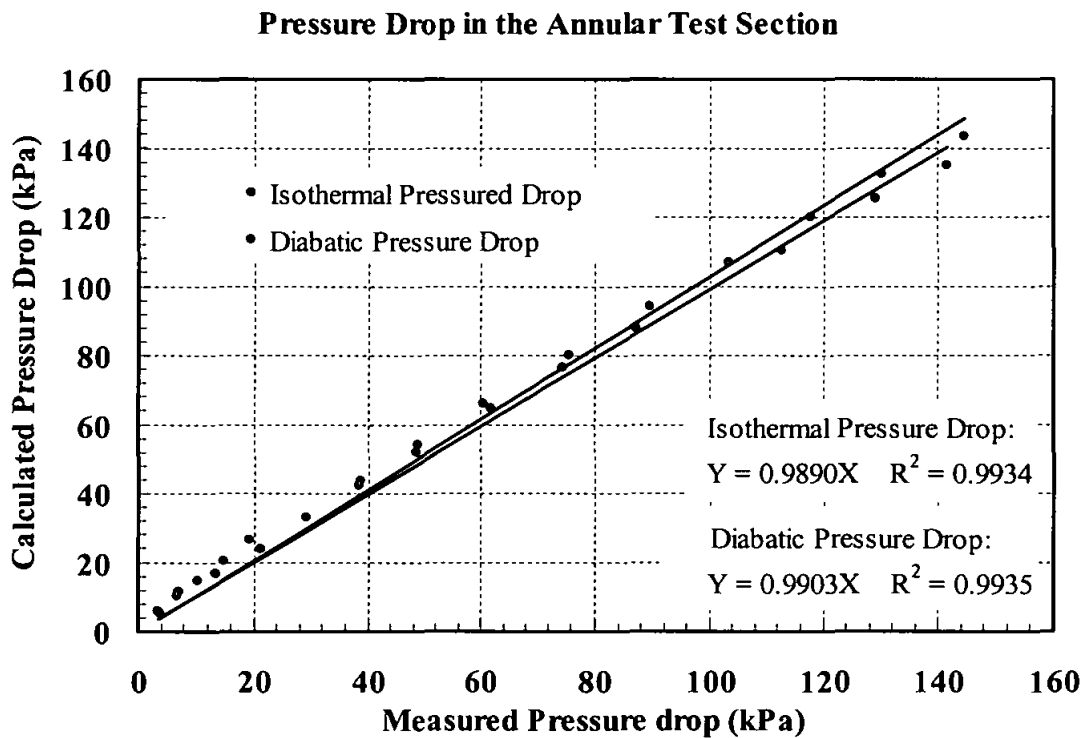


Figure 4.26: Isothermal and diabatic pressure drop data comparison (turbulent, transition and laminar regime) – using the equivalent length of 0.60 m.

Figure 4.27 show the developed calculation method comparison for isothermal and diabatic pressure drop data. Both the isothermal and the diabatic pressure drop data yield the same statistical analysis data which insured the reliability of the developed method and indicates that within the test temperature range, there is no temperature-dependent or viscosity effect on the calculations of the pressure drop.

---

## CHAPTER V

### HEAT TRANSFER EXPERIMENTAL INVESTIGATIONS

This chapter deals with the heat transfer aspects in the test facility (HT/HPMPWDF). Many models governing the heat transfer process have been analysed and compared with the experimental data. Recommendations are made based on the minimum AAPE error.

#### 5.1 INTRODUCTION

The main scope of this work is to prove the equipment “scalability” in order to transfer laboratory data of heat transfer to pipeline and wells transporting waxy crude. The laboratory-field transfer tool is an improved calculation model capable to represent and calculate the effect of paraffin deposition.

This experimental work is essential to:

- Investigate the possibility to use HT/HPMPWDF equipment for validating heat transfer models suitable for calculating waxy crude cooling without deposition, at  $T > WAT$ .
- Investigate the operation mode of HT/HPMPWDF and equipment accuracy to a level required for further validation tests of waxy crude deposition conditions.
- Determine optimal operation conditions and limitations leading to maximum accuracy and confidence.

This part of the work aims, therefore, to demonstrate the quality of HT/HPMPWDF equipment for developing and adapting calculation models for assessing waxy crude transportation using velocity (flow)-temperature conditions similar to field but in the absence of deposition. Simulated “white mineral oil” is used in lieu of waxy crude.

By minimizing (in comparison with the amount of heat transferred to the cold glycol/central pipe zone) the amount of heat transferred from waxy crude to environment

(here assimilated through the hot glycol zone), the main target of this experimental stage is to be able to prove (or closely compare) the heat rate transferred between the annular hot oil zone and the cold glycol, central pipe zone and further to compare the measured heat rate with the heat transferred calculated with the aid of existing “internal flow/pipe forced convection” models.

Main assumptions:

$$Q_{hot\ glycol} \ll Q_{cold\ glycol}$$

$$Q_{oil} \ll Q_{cold\ glycol}$$

Proper adjustment of measuring techniques and accuracy, and, to select a suitable model has to be implemented in order to achieve the proposed target of:

$$Q_{cold\ glycol} \approx Q_{oil} \approx Q_{calculated}$$

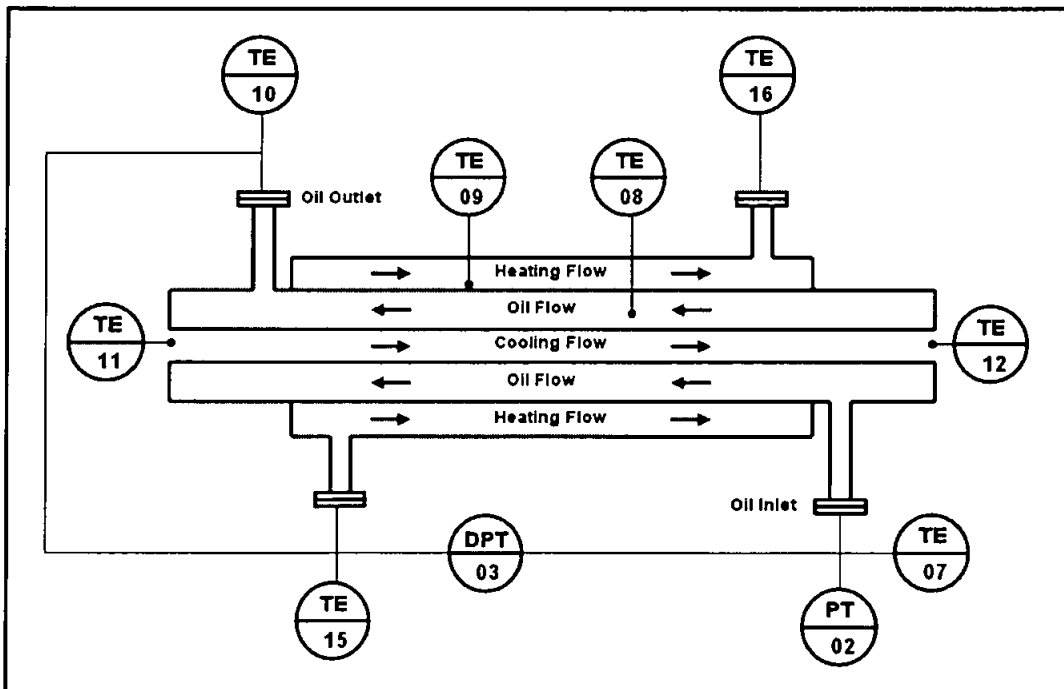


Figure 5.1: Schematic of the test section with temperature and pressure drop measurement

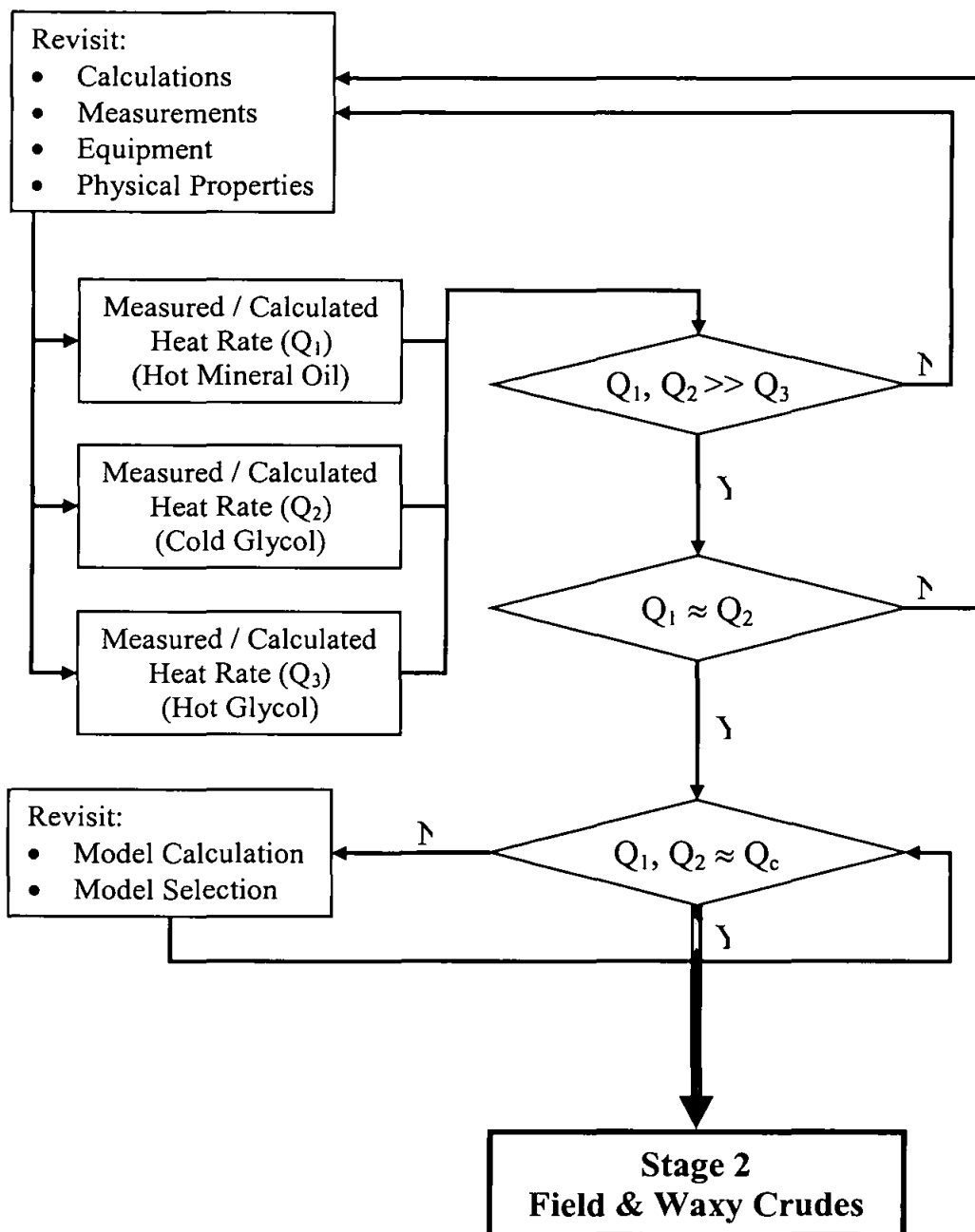


Figure 5.2: The information flux adopted for the thermal experimental stage using simulated crude (white oil)

---

## 5.2 EXPERIMENTAL PROCEDURE

### 5.5.1 Thermocouple details

A number of 31 type-T (copper-constantan) thermocouple probes (Omega Engineering Inc.) were installed along the test facility for the temperature measurements. The data acquisition card is automatically recalibrated each time the computer is turned-on using internal standards, therefore no extra calibration were required after the installation calibration (determined to be accurate to  $\pm 0.05$  °C).

Eight of these thermocouples were installed along the annular deposition test section to measure the temperatures at the inlets and outlets of the test section as well as the mid-stream and wall of the oil passage. These Thermocouples were selected and tested in pairs to ensure that the same temperate bias is measured to provide better accuracy. Temperature differences were determined to be measurable to within  $\pm 0.1$  °C.

### 5.5.2 Temperatures and flow-rates measurements

Inlet Temperature measurements of white mineral are illustrated in Figs. 5.3 and 5.4 for the cold glycol. Fig. 5.3 shows typical temperature-flow behaviour for three run trails #1, #2 and #3 performed at 50, 60 and 70 °C respectively. The best temperature control achieved is with trail#3 when the mineral oil re-circulated at 70 °C and a good temperature-flow data grouping is observed with a standard deviation of 0.38 as minimum value compare to standard deviation of 2.83 for the trail2 and standard deviation of 1.01 for the trail1.

At high flow rates the pump acted as additional heat source, when the heat converted from the pressure energy at the high flow-rate, it increase the heat content of the flowing oil. The pump effect can be seen from Fig. 5.3 for trail1, mineral oil re-circulated at 50 °C. The temperature at the high flow-rates (above 500 LPM) started to increase out of control. This increase reported within 12 °C. With the increase of the oil temperature as in trail#2 and trail#3, the effect of the pump started to terminate.



---

Figure 5.4 shows the measurement of the cold glycol temperature. The cold glycol flow rate is kept constant all the time of the test run. As it can be seen from the figure a good temperature control is achieved with different oil's flow rates and temperatures. At relatively high oil temperature and flow rate the glycol temperature start to increase slightly out of control (as in case of trail3 Fig. 5.3). This is because of more heat given up by the oil to the cold glycol. this will lead to the rate of the heat exchanging in the primary cycle of the cooling system to be higher than the rate of cooling in secondary system.

Small temperature differences, of average of 0.86, 0.95 and 1.22 °C between inlet-outlet temperatures of oil recirculated at 50, 60 and 70 °C respectively, are recorded. These small differences suggests that the heat transfer may be considered as a “constant temperature” (instead of constant heat flux) situation, it also indicate a good temperature control throughout the experiment. However, significant temperature difference between cold glycol (approximately 15 °C) and white oil (approximately 70 °C) may create problems such as:

- Important differences between bulk and wall temperatures.
- Errors in measurement (note, if a sheath conduction error is not avoided).

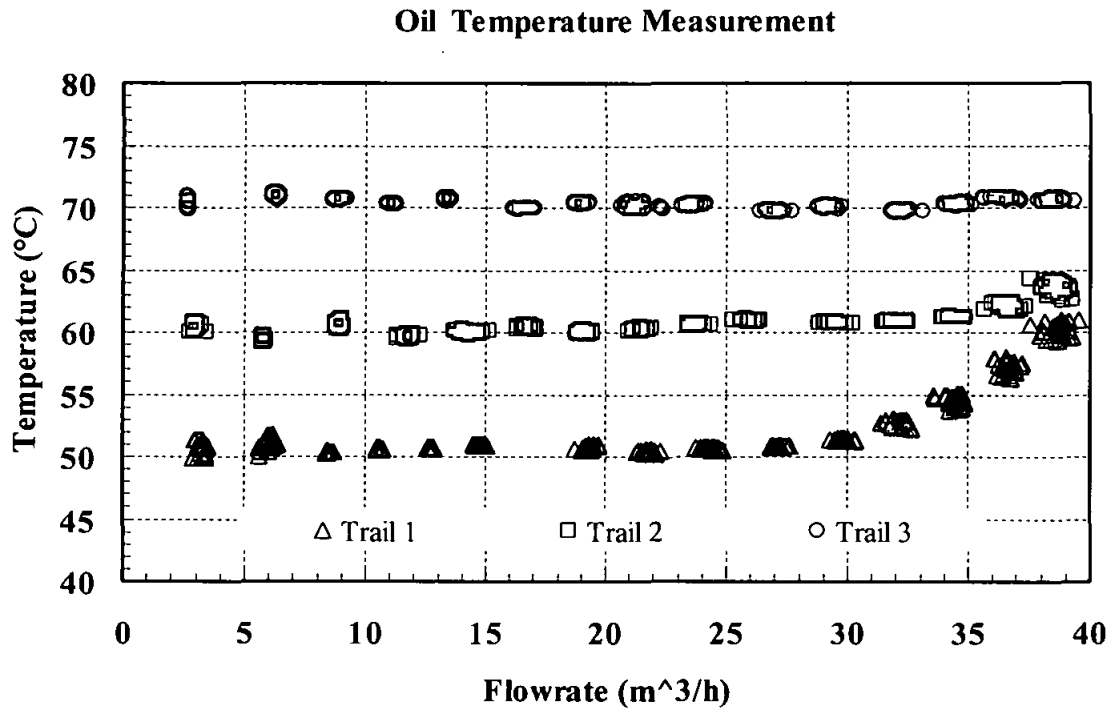


Figure 5.3: Mineral oil temperature measurement

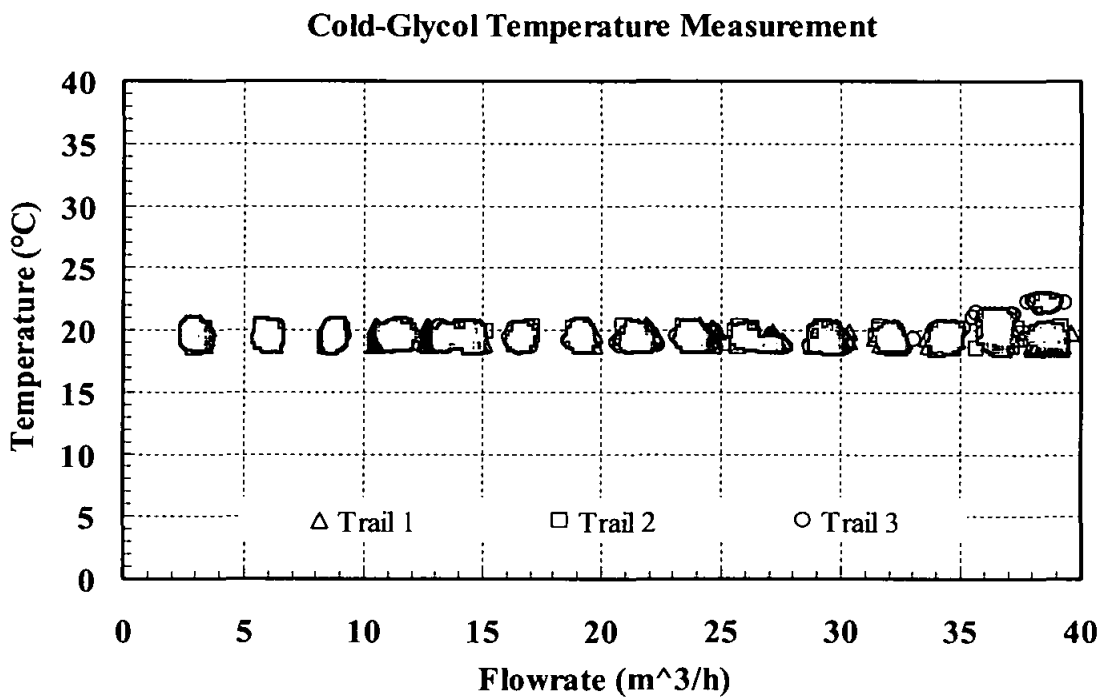


Figure 5.4: Cold glycol temperature measurement

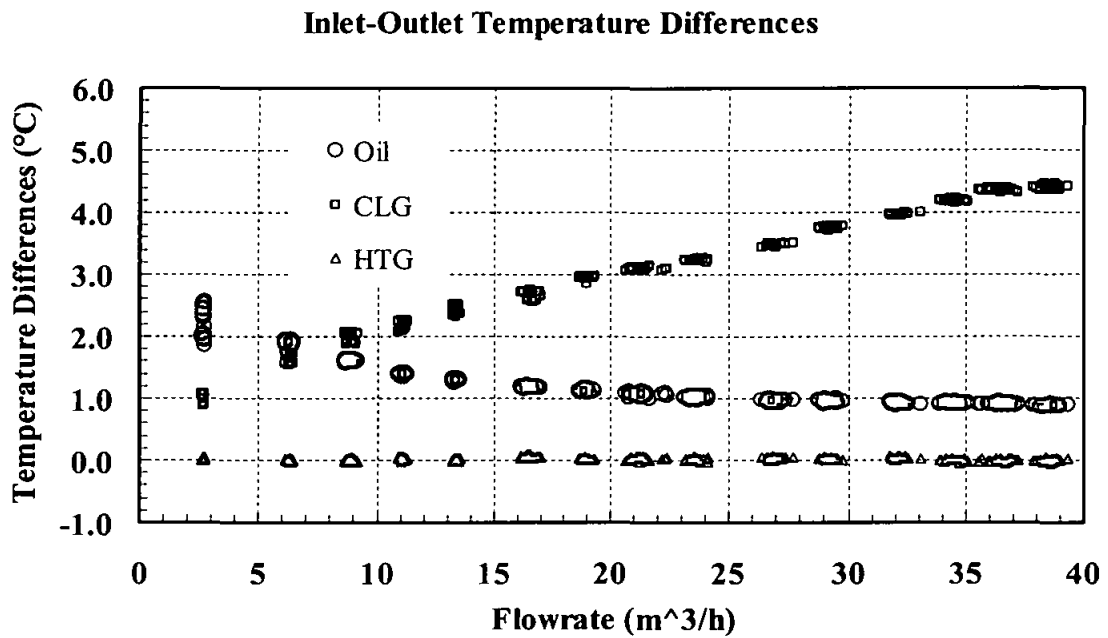


Figure 5.5: Working fluids inlet-outlet temperature differences

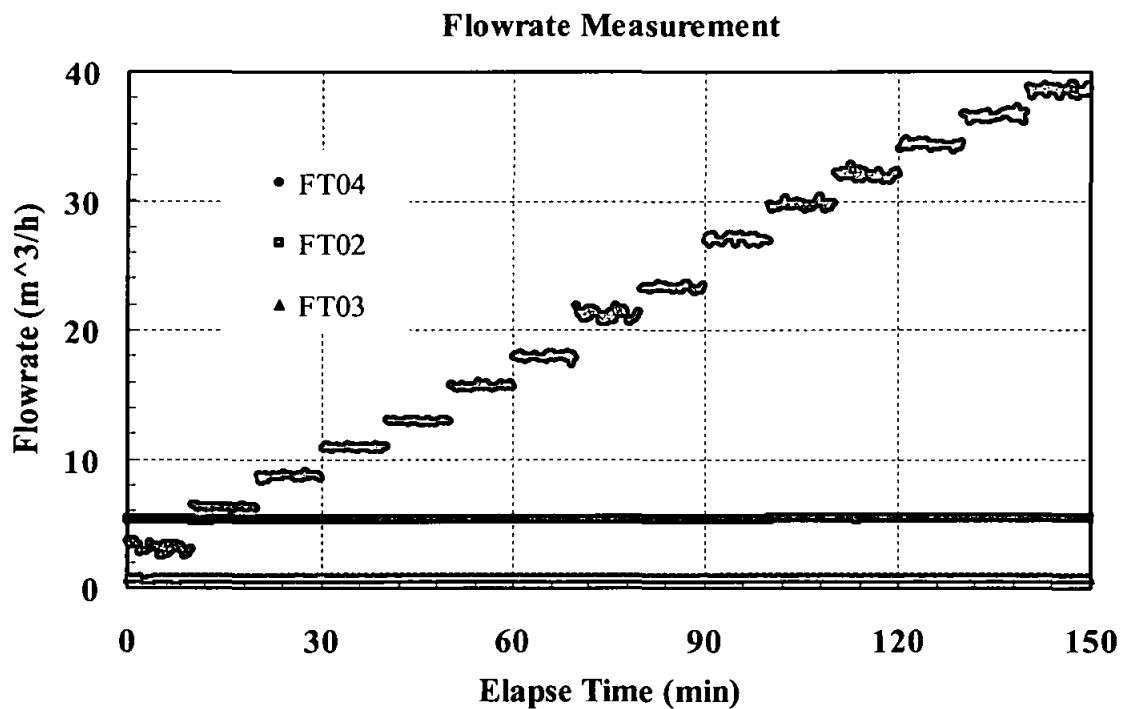


Figure 5.6: Mineral oil (FT04), cold glycol mixture (FT02) and hot glycol mixture (FT03) flow rate measurements

Figure 5.6 shows the measurements of flow rates of the process fluids (mineral oil, cold and hot glycol mixture). The flow rate of the cold glycol (flowing in central pipe) and the hot glycol (flowing in the heat jacket) are kept unchanged during the experiment time while the mineral oil (flowing in annulus) is changed by stepwise increments. A good flow rate control for all the process fluid is observed.

### 5.3 THEORETICAL ANALYSIS

In the present study, the test section is treated as double-pipe heat exchanger or annulus heat exchanger. As shown in Fig. 5.1 in this arrangement one fluid (cold glycol) flows through the centre pipe, while another (mineral oil) flows in the annulus. The whole test section is heat jacketed.

The first method developed for heat exchanger design, and still widely used for the analysis of the heat exchanger performance, is the *Log Mean Temperature difference (LMTD)* method. A relatively recent method is the Number of Transfer Units (NTU) approach. For general-purpose use, analysis or design, both methods will yield the same result for a given problem.

#### *Log Mean Temperature Difference (LMTD)*

The heat transfer between two fluids separated by a surface is (Hodge & Taylor, 1998):

$$q = UA(T_h - T_c) = UA\Delta\bar{T} \quad (5.1)$$

Where  $U$  is the overall heat transfer coefficient and  $A$  is area on which  $U$  is based.

The problem in applying Equation 5.1 in the heat exchanging process is what  $\Delta\bar{T}$  to be used.  $\Delta\bar{T}$  is seldom constant for any heat exchanger configuration and for any increment of area  $dA$  of an exchanger the  $dq$  expressed as (Hodge & Taylor, 1998):

$$dq = U\Delta T dA = U dA(T_h - T_c) \quad (5.2)$$

Where  $\Delta T$  is the temperature difference at a given area. Heat balance on the hot and cold fluid for a counter flow yield, with  $dT_c$  and  $dT_h$  negative.

$$\left. \begin{aligned} -dq &= \dot{m}_c C_{p_c} dT_c = C_c dT_c \\ -dq &= \dot{m}_h C_{p_h} dT_h = C_h dT_h \end{aligned} \right\} \quad (5.3)$$

$$d(\Delta T) = dT_h - dT_c = \frac{dq}{C_c} - \frac{dq}{C_h} \quad (5.4)$$

Equating the integrated energy balance expressions given by Equation 5.3 gives:

$$C_h (T_{h,in} - T_{h,out}) = C_c (T_{c,out} - T_{c,in}) \quad (5.5)$$

From it which follow that:

$$d(\Delta T) = \frac{-dq}{C_h} \left( 1 - \frac{T_{c,out} - T_{c,in}}{T_{h,in} - T_{h,out}} \right) \quad (5.6)$$

Substituting Equation 5.2 for  $dq$  and integrating gives:

$$\int_{\Delta T_1}^{\Delta T_2} \frac{d(\Delta T)}{\Delta T} = \frac{UA}{q} (\Delta T_2 - \Delta T_1)$$

Where  $\Delta T_2 = (T_{h,in} - T_{h,out})$  and  $\Delta T_1 = (T_{c,out} - T_{c,in})$  so:

$$\ln \frac{\Delta T_2}{\Delta T_1} = \frac{UA}{q} (\Delta T_2 - \Delta T_1)$$

$$q = UA \frac{\Delta T_2 - \Delta T_1}{\ln(\Delta T_2/\Delta T_1)}$$

$$\Delta \bar{T} = \frac{\Delta T_2 - \Delta T_1}{\ln(\Delta T_2/\Delta T_1)} \quad (5.7)$$

#### 5.4 EXPERIMENTAL ANALYSIS

The primary measurements consist of the flowrates of each fluid stream, and their inlet outlet temperatures ( $T_i$  and  $T_{out}$ ), in the test section.

First, the overall energy balance between the oil and cold glycol mixture is achieved by the following equations (Hodge & Taylor, 1998):

$$\left. \begin{aligned} Q_H &= [\dot{m}C_p(T_i - T_o)]_{oil} \\ Q_C &= [\dot{m}C_p(T_i - T_o)]_{cold\_glycol} \end{aligned} \right\} \quad (5.8)$$

The energy balance between the heat given up by the hot oil ( $Q_H$ ) and the heat gained by the cold glycol mixture ( $Q_C$ ) is maintained within  $\pm 5.8\%$  after accounting for to environmental heat losses, and the average of  $Q_{oil}$  and  $Q_{cold\ glycol}$  are taken as total heat load.

Again, The rate of heat transfer for the mineral oil to cold glycol is calculated as a product of the overall coefficient of heat transfer ( $U$ ), the area ( $A$ ) of interface between hot oil and cold glycol measured at the  $\frac{1}{2}$  of cold pipe thickness and the “logarithmic mean temperature difference - LMTD” as:

$$Q_{LMTD} = UA(LMTD) \quad (5.9)$$

Where, the  $LMTD$  between the oil and cold glycol which describes the average temperature difference between the temperatures of the oil and cold glycol mixture throughout the test section is obtained considering the counter-current flow arrangement as:

$$\Delta\bar{T} = \frac{[(T_{h,i} - T_{c,o}) - (T_{h,o} - T_{c,i})]}{\ln\left[\frac{(T_{h,i} - T_{c,o})}{(T_{h,o} - T_{c,i})}\right]} \quad (5.10)$$

The overall heat transfer coefficient  $U$  (Eq. 5.11), which describes the rate of heat transfer as function of “glycol-film heat transfer coefficient” ( $h_f$ ) and “oil-film heat

transfer coefficient" ( $h_2$ ) and the conductivity ( $k$ ) of the central pipe separating the cold glycol and hot oil zones,

$$U = \left[ \frac{r_o}{r_i h_1} + \frac{r_o}{k} \ln \left( \frac{r_o}{r_i} \right) + \frac{1}{h_2} \right]^{-1} \quad (5.11)$$

The heat transfer coefficient depends on: shape and dimensions of the surface, roughness of the surface, direction and velocity of the flow, the temperature of the surface and the fluid and the flow properties ( $\rho$ ,  $\mu$ ,  $C_p$  and  $k$ ). The heat transfer coefficients of the hot oil ( $h_1$ ) and cold glycol ( $h_2$ ), were determined from the equation of *Petukhov* (1970) for turbulent flows inside pipes. For the present situation this equation is written as:

$$Nu = \frac{(f/8)RePr}{1.07 + 12.7(f/8)^{1/2}(Pr^{2/3} - 1)} \quad (5.12)$$

Where  $Nu$  is the average Nusselt number of the fluid (mineral oil/cold glycol),  $D_h$  is the hydraulic diameter of the annular passage (or internal diameter of the inner circular tube) of the test section,  $k$  is the fluid thermal conductivity,  $Re$  and  $Pr$  are the Reynolds number and Prandtl number of the fluid (mineral oil/cold glycol), respectively. These dimensionless parameters are given by:

$$Re = \frac{\rho v D_h}{\mu} \quad (5.13)$$

$$Pr = \frac{\mu C_p}{k} \quad (5.14)$$

In Eqs. (5.13) and (5.14),  $\rho$  is the density,  $\mu$  is the dynamic viscosity and  $C_p$  is the specific heat at constant pressure. All physical and thermal fluid properties are calculated at the mean average temperature along the conduit that is given by:

$$T_{av} = \frac{(T_i + T_o)}{2} \quad (5.15)$$

In all the test runs the hot oil flow rates were maintained such that  $\dot{m}_{oil} > \dot{m}_{cold\_glycol}$  to ensure that the process of the heat transfer from the hot oil (annular zone) to the cold glycol (deposition zone) provided the dominant thermal resistance. The steady-state energy balance on the hot oil and cooling fluid repeated, this time in addition to the basic heat transfer Equations 5.8. A third basic Equation 5.9 which incorporates the aid of the forced convection model (Eq. 5.12), is used. The steady-state energy balance expressed as:

$$\left. \begin{aligned} Q &= Q_{oil} = Q_{cold\ glycol} = Q_{LMTD} \\ Q &= [\dot{m}C_p (T_i - T_o)]_{oil} = [\dot{m}C_p (T_i - T_o)]_{cold\_glycol} = UA(LMTD) \end{aligned} \right\} \quad (5.16)$$

after accounting for all heat loss, the energy balance between the  $Q_{oil}$  and  $Q_{LMTD}$  is maintained within  $\pm 6.90\%$  and within  $1.80\%$  between  $Q_{cold\ glycol}$  and  $Q_{LMTD}$ , and as mentioned early in this paragraph, the average of  $Q_{oil}$  and  $Q_{cold\ glycol}$  as well as  $Q_{LMTD}$  are taken as total heat load.



---

## 5.5 ENERGY BALANCE INVESTIGATIONS

### 5.5.1 *The balancing by released-gained heat transfer criteria*

Figures 5.7 through 5.11 show the trends of the heat transfer rates for the mineral oil and cold glycol with the change of the mineral oil flow rate. The heat transfer rates calculated using Equation 5.8 and steady-state energy balance is made. The specific heat, flow rate and the temperature differences were the deriving factors in the energy balance. Due to insignificant oil temperature variations during the experiment (good temperature control) the oil and glycol specific heat remain almost unchanged throughout the test run. The glycol flow rate was constant throughout the test run while the mineral oil flow rate was changed from 3 up to 40 m<sup>3</sup>/h in stepwise manner.

The steady-state energy balance between the mineral oil and the cold glycol is achieved in two steps. First, the cold glycol flow rate kept at 1 m<sup>3</sup>/h and inlet temperature of 15 °C and the oil inlet temperature was 50 °C. At this condition a big discrepancy between the two heat transfer rates is observed as it can be seen from Fig. 5.7. This discrepancy starts to slightly decrease with the increments of oil inlet temperature. Fig. 5.8 and 5.9 shows the trends of the heat transfer rates with oil inlet temperature of 60 and 70 °C respectively, and the balance is still not yet close.

Secondly, the flow rate of the cold glycol is increased from 1 to 3 m<sup>3</sup>/h. a remarkable improvement in the energy balance is observed (Fig. 10). The best energy balance of 5.8 % error discrepancy is achieved with cold glycol flow rate of 5 m<sup>3</sup>/h, and the inlet temperatures of the cold glycol and mineral oil were 15 and 70 °C, respectively. This is highlighted that the flow rate of the cold glycol should be selected carefully, as appeared in the investigation results show that low flow rate led to big discrepancy. When the cold glycol flow became turbulent same to the oil flowing counter currently in the annulus space, the temperature differences (inlet-outlet) of the each fluid reduced, increasing the flow rate of the cold glycol compensated the temperature differences reduction and increase the heat transfer rate significantly.

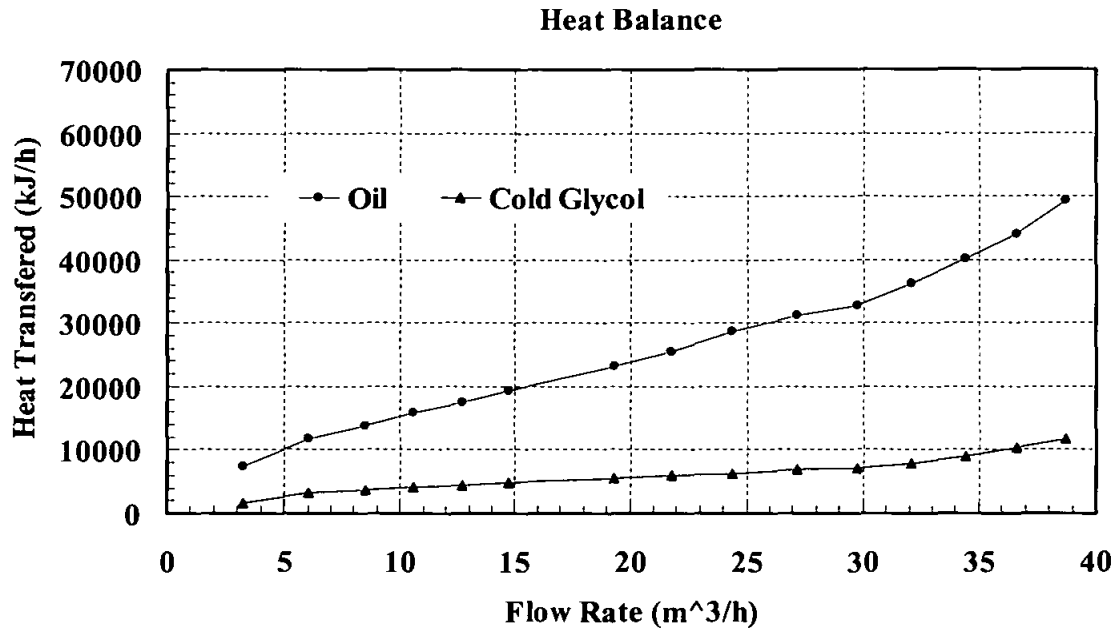


Figure 5.7: Comparison of heat transfer rate, oil inlet temperature at 50 °C, glycol inlet temperature 15 °C and 1 m<sup>3</sup>/h flow rate.

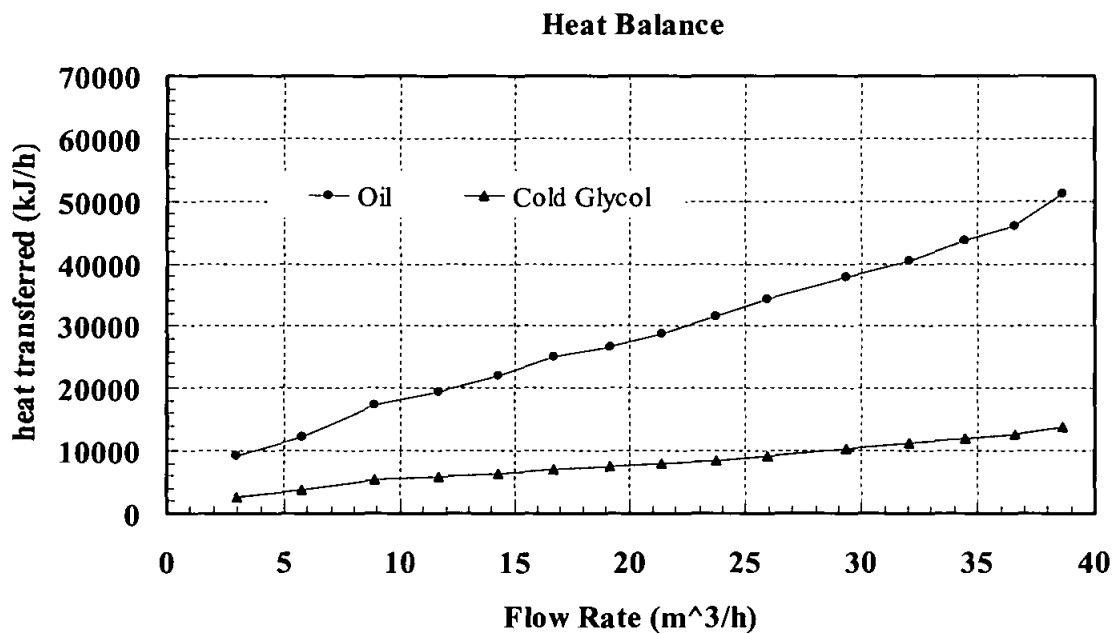


Figure 5.8: Comparison of heat transfer rate, oil inlet temperature at 60 °C, glycol inlet temperature 15 °C and 1 m<sup>3</sup>/h flow rate.

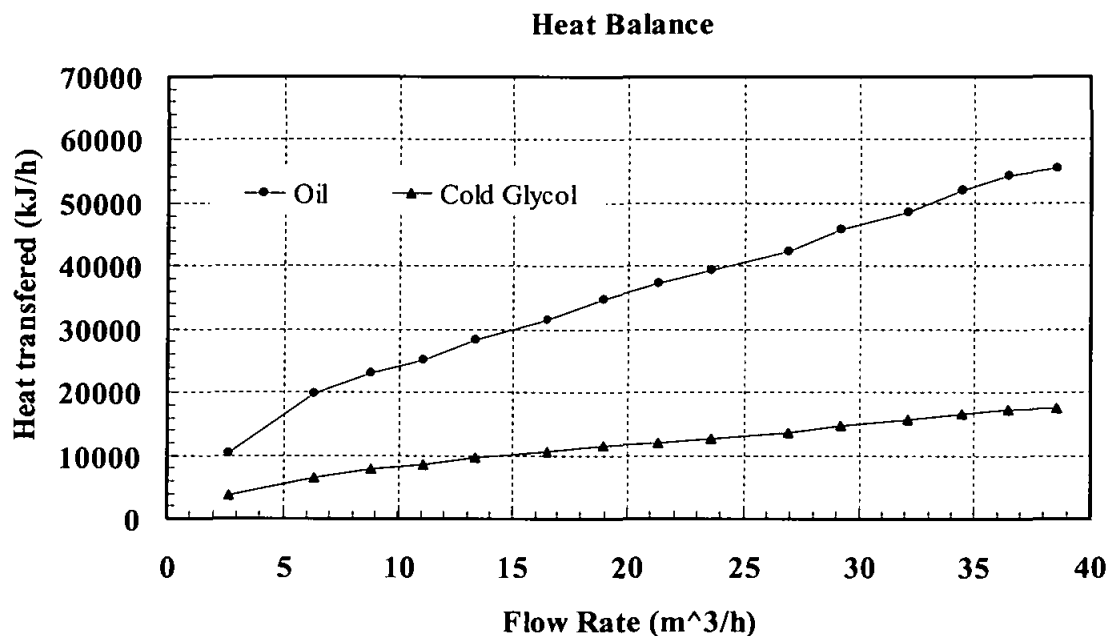


Figure 5.9: Comparison of heat transfer rate, oil inlet temperature at 70 °C, glycol inlet temperature 15 °C and 1 m<sup>3</sup>/h flow rate.

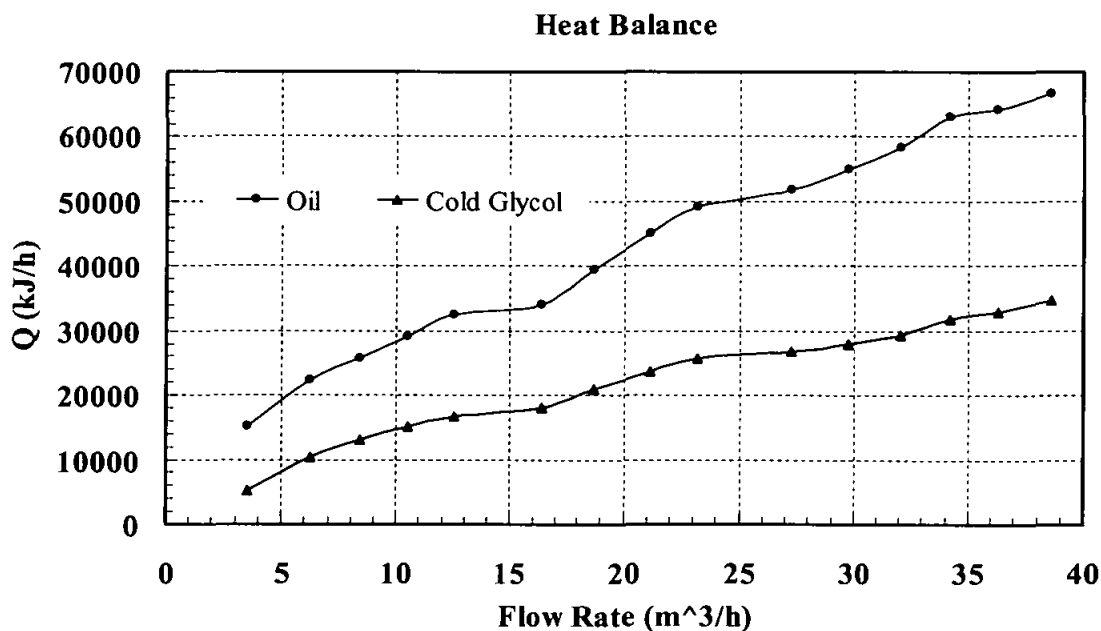


Figure 5.10: Comparison of heat transfer rate, oil inlet temperature at 70 °C, glycol inlet temperature 15 °C and 3 m<sup>3</sup>/h flow rate.

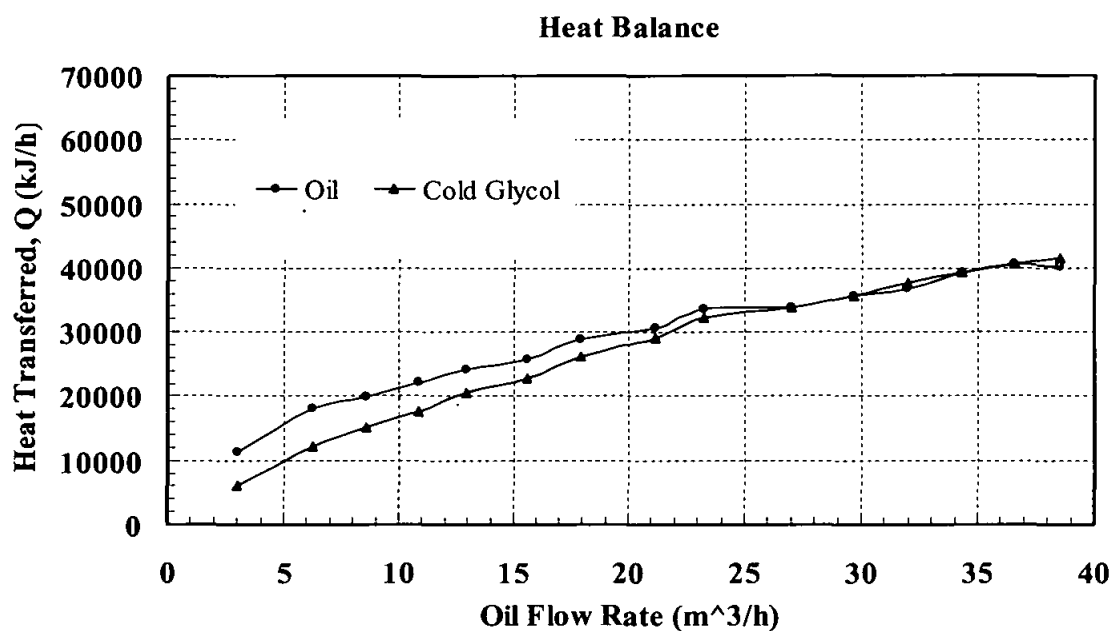


Figure 5.11: Comparison of heat transfer rate, oil inlet temperature at 70 °C, glycol inlet temperature 15 °C and 5 m<sup>3</sup>/h flow rate.

### 5.5.2 The balancing based on LMTD criteria:

In these criteria, the LMTD is evaluated and used for the calculation of the rate of heat transfer with the aid of the turbulent *Petukhov* model of the convective heat transfer (Eq. 5.12). Figures 5.12 and 5.13 depict the trends of the heat released by the oil, the heat gained by glycol and the heat transferred – across the deposition wall - from the oil to glycol. From these figures it is observed that; for the turbulent flow regime of oil  $Re < 3200$ , the calculated heat transfer compares the heat released by the oil which is in turn, gained by the cold glycol satisfactorily.

For the laminar flow,  $Re < 3200$ , the laminar convective heat transfer model used is:

$$\left. \begin{array}{l} Nu_T = 3.66 \\ Nu_H = 4.36 \end{array} \right\} \quad (5.17)$$

The result presented in Fig. 5.12 and 5.13 show unsatisfactorily heat transfer rate balance for the laminar regime. This may due to the independent of the inertia parameter in the laminar convective model, i. e. independent of  $Re$ , while the measured values (hot oil or cold glycol) appears to be  $Re$  dependant (even for laminar flow regime). This can be corrected by using a different MODEL for laminar regime.

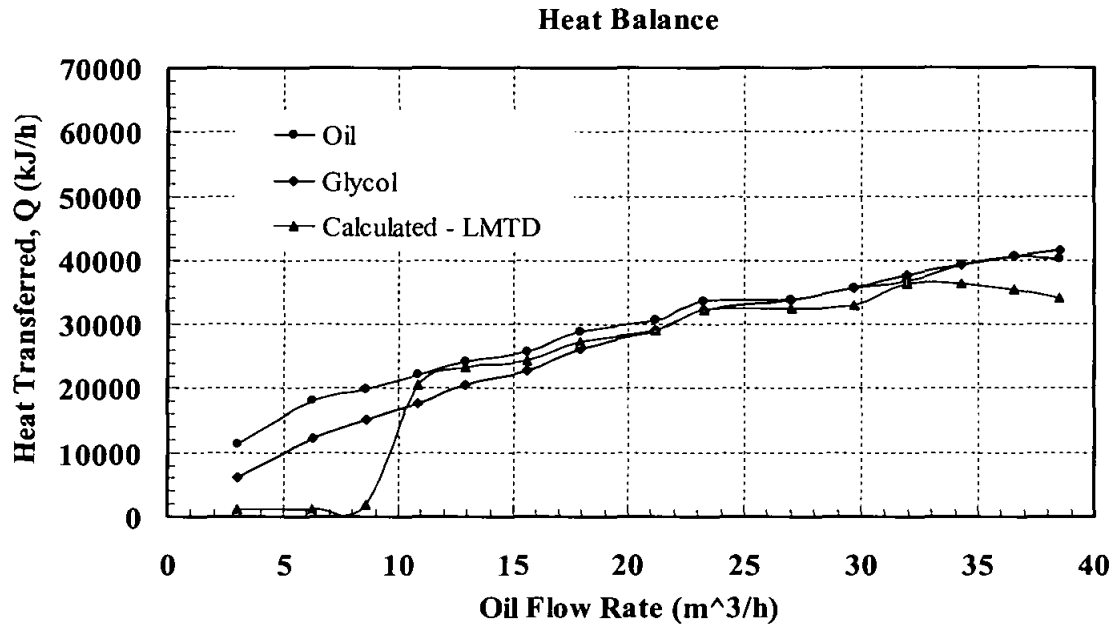


Figure 5.12: Comparison of measured heat rates (mineral oil - cold glycol) and calculated heat rate, oil inlet temperature at 70 °C, glycol inlet temperature 15 °C and 5 m<sup>3</sup>/h flow rate.

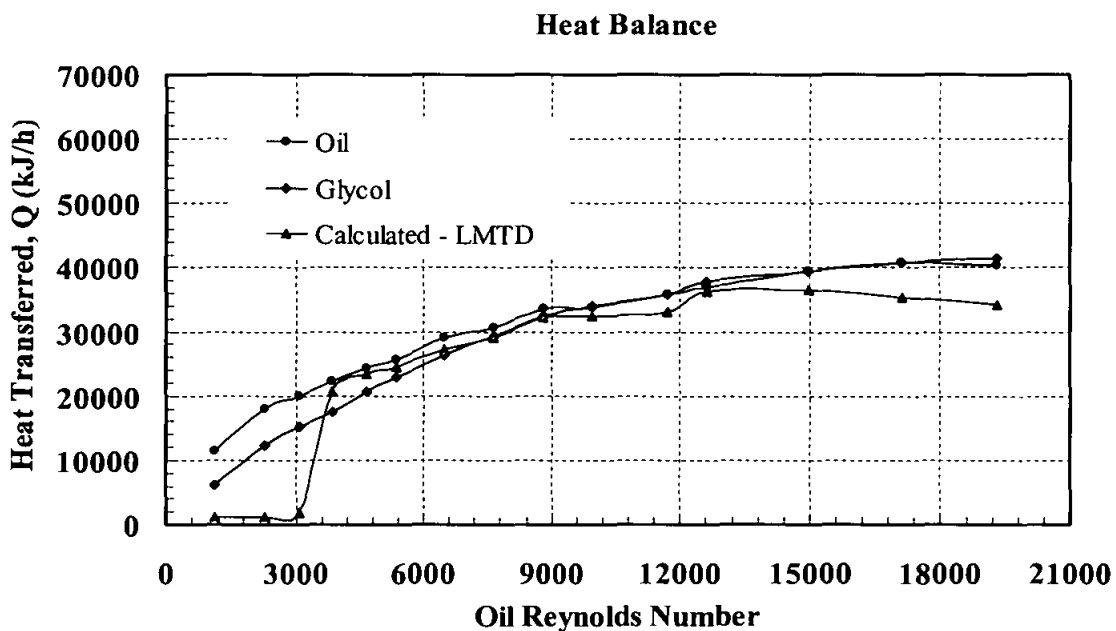


Figure 5.13: Comparison of measured heat rates (mineral oil - cold glycol) and calculated heat rate, oil inlet temperature at 70 °C, glycol inlet temperature 15 °C and 5 m<sup>3</sup>/h flow rate.

---

## 5.6 HEAT TRANSFER CORRELATION INVESTIGATIONS

In the test facility, under study, the wax deposition scenario has been described as a non-isothermal flowing system that appears to be driven by heat flux. Consequently, the success in predicting wax deposition rates in this test facility depends on how heat transfer characteristics are evaluated. These include the forced convective film heat transfer coefficient, bulk and wall temperatures and local heat flux across the pipe wall. Numerous heat transfer correlations and experimental data for forced convective heat transfer have been published over the past 40 years. Finding the most suitable correlation is one of the objectives of this experimental study.

The principal difference between laminar and turbulent flow, as far as heat transfer is concerned, is that an additional mechanism of heat transfer in the radial and azimuthal directions becomes available in turbulent flow. This is commonly termed “eddy transport” and is intense, providing much better transfer of energy across the flow at a given axial position than in laminar flow. Another difference worthwhile noting is the extent of the “thermal entrance region” in which the transverse temperature distribution becomes “fully developed.” This region is relatively short in turbulent flow, whereas, it tends to be long in laminar flow. Heat transfer correlations, based on experimental results, are typically divided into those applicable in the thermal entrance region, and those that apply in the “fully developed” region. In the case of laminar flow, it is important to be aware of this distinction, and normally a laminar flow heat exchanger is designed to be short, to take advantage of relatively high heat transfer rates that are achievable in the thermal entrance region. In the case of turbulent flow, the thermal entrance region is short, as noted earlier, and typically heat transfer occurs mostly in the “fully developed” region. Therefore, turbulent heat transfer correlations are commonly provided for the latter region (Hinze, 1975).

Table 5.1 provide the most common and widely-used fully-developed convective heat transfer correlation. These correlations are usually expressed in terms of Nusselt number. The limitations and conditions required for these correlations to be applicable are also provided in Table 5.1.

---

Two types of correlations can be found in the existing literature (Kakac *et. al.*, 1987, Hodge & Taylor, 1998):

- a. All physical parameters are calculated for the average temperatures, bulk fluid conditions.
- b. A correction coefficient taking into account the respective wall temperature is introduced.



Table 5.1: Fully-Developed Turbulent Convective Heat Transfer Correlations

Investigator	Correlation	Remark
Dittus and Boelter (1930)	$Nu = \begin{cases} 0.023 Re^{0.8} Pr^{0.4} & \text{for heating} \\ 0.023 Re^{0.8} Pr^{0.3} & \text{for cooling} \end{cases}$	<p>These classical correlations has confirmed experimentally for the following range of condition: <math>0.7 \leq Pr \leq 120</math>, <math>2500 \leq Re \leq 1.24 \times 10^5</math> and <math>L/D \geq 10</math> where L is the length from the inlet of the tube. These correlations may be used for moderate temperature differences with fluid evaluated at the bulk fluid temperature. The objective of providing different correlations for heating and cooling was to account for variation of the fluid properties with temperature</p>
Sieder and Tate (1936)	$Nu = 0.027 Re^{0.8} Pr^{1/3} \left( \frac{\mu_{bulk}}{\mu_{wall}} \right)^{0.14}$	<p>Recommended the following expression for applications with large property variations from the bulk flow to the wall temperature. For: <math>0.7 \leq Pr \leq 16000</math>, <math>Re \geq 10000</math> and <math>L/D \geq 10</math>.</p>
Petukhov (1970)	$Nu = \frac{(f/8)RePr}{1.07 + 12.7(f/8)^{1/2}(Pr^{2/3} - 1)}$	<p>Recommended For more accurate calculations in fully developed turbulent flow (to within about <math>\pm 10\%</math>), it is valid for <math>0.5 \leq Pr \leq 2000</math>, <math>10^4 \leq Re \leq 5 \times 10^6</math>. Where the friction factor can be obtained from Moody diagram or</p>

from Petukhov's friction factor correlation for smooth tubes valid for:  $3000 \geq Re \geq 5 \times 10^6$

$$f = (1.58 \ln Re - 3.28)^{-2}$$

Webb

$$Nu = \frac{(f/8)RePr}{1.07 + 9(f/8)^{1/2}(Pr-1)Pr^{1/4}}$$

For  $0.5 \leq Pr \leq 100$  and  $10^4 \leq Re \leq 5 \times 10^6$ , the predictions are within + 10.4 % and - 7.3 % of Gnielinski correlation.

Bernado and  
McAdams

$$Nu = 0.048 Re^{0.73} Pr^{0.4}$$

For  $0.5 \leq Pr \leq 2000$  and  $10^4 \leq Re \leq 10^5$ , the predictions are within + 19.2 % and - 20.5 % of Gnielinski correlation.

Gnielinski  
(1976)

$$Nu = \frac{(f/8)(Re-1000)Pr}{1 + 12.7(f/8)^{1/2}(Pr^{2/3}-1)}$$

It is a modified version of Petukhov correlation extending it to the  $2300 \leq Re \leq 5 \times 10^4$  range.

For  $0.5 \leq Pr \leq 2000$  and  $2300 \leq Re \leq 5 \times 10^4$  it is in overall accord with the experimental data; it agrees with the Petukhov correlation within -2% and +7.8%.

Sandal *et al.*

$$Nu = \frac{\sqrt{f/8} Re Pr}{12.5 Pr^{2/3} - 7.9 Pr^{1/3} + 3.6 \ln Pr + c}$$

$$c = 5.8 + 2.78 \ln(\sqrt{f/8} Re / 45)$$

For  $0.5 \leq Pr \leq 2000$  and  $10^4 \leq Re \leq 5 \times 10^6$ , the predictions are within + 6.6 % and - 4 % of the Gnielinski correlation.

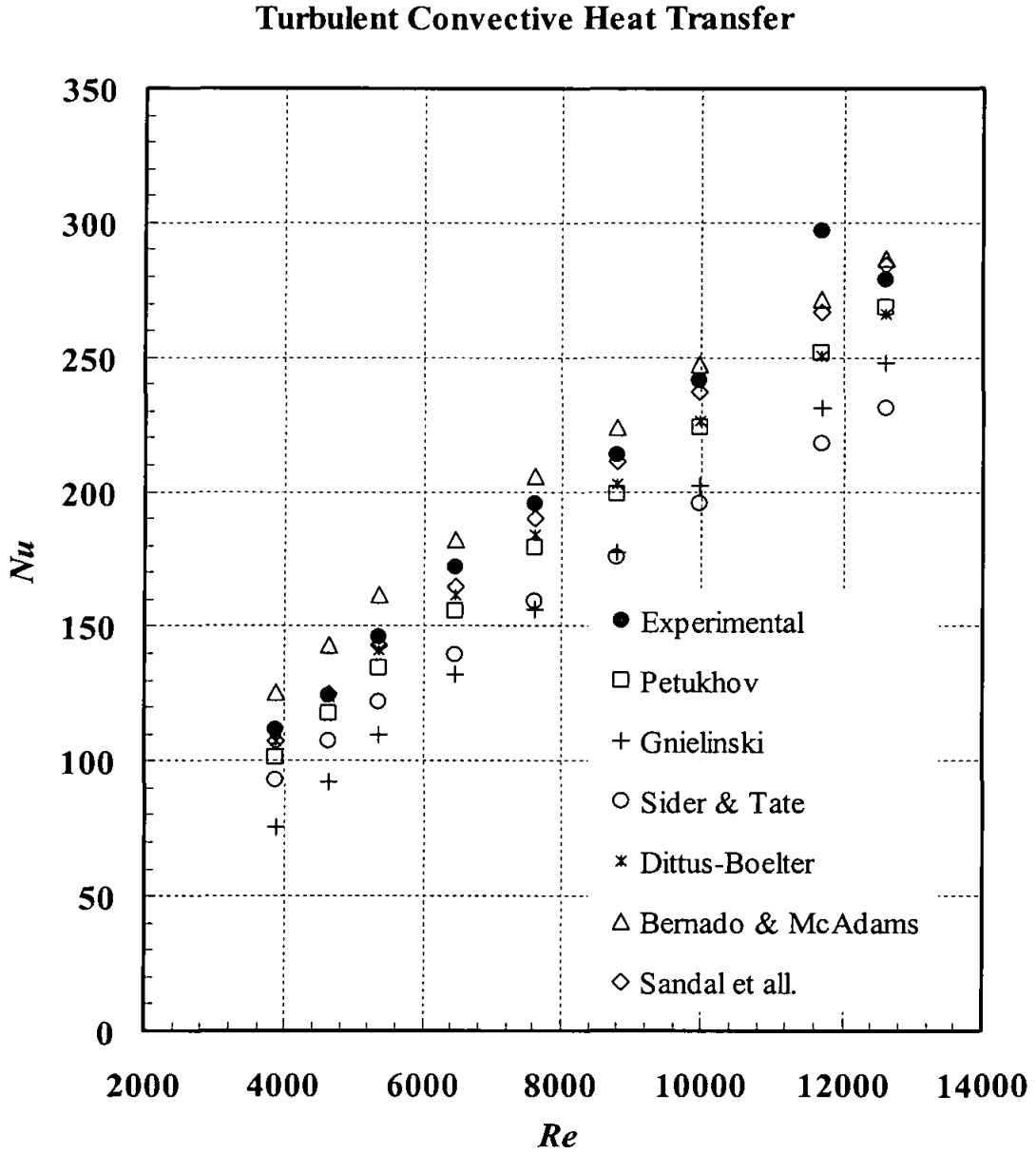


Figure 5.14: Experimental and theoretical turbulent Nusselt Number data

---

Figure 5.14 shows a dimensionless representation of different convective heat transfer correlations (discussed in Table 5.1) in terms of  $Nu$  and  $Re$ . These correlations are further compared with the experimental  $Nu$  data obtained from the thermal energy balance (Eq. 5.8) over the test section. Likewise, the overall heat transfer coefficient is obtained and compared with the theoretical value. In the calculation procedure, the thermal properties of the working fluids, such as specific heat ( $C_p$ ), thermal conductivity ( $k$ ) and Prandtl number ( $Pr$ ) values are remain almost unchanged throughout the test run. This is fairly reasonable due to insignificant temperature variations during the experiment.

A good agreement between the experimental and theoretical data is observed and it will be discussed in statistical detailed analysis in the coming paragraph.

The mineral oil used in the experimental program of this study can be classified as high Prandtl number fluid (particularly, in this study the  $Pr$  almost equal to 100) sine it is essentially and fluid  $Pr > 10$  can be considered to have high Prandtl number. Because of that the effect of the variable-property which is expressed in the Sieder-Tate correlation by the term  $\frac{\mu_{bulk}}{\mu_{wall}}$ , is cancelled out (the ratio of the bulk to wall viscosity set to be 1 in the calculation). The reason is that in the turbulent flow with high Prandtl number, the increase in  $Re$  is to decrease the thickness of the sublayer and increase the eddy diffusivity in the outer region, both of which lead to “square” temperature profile (Kays et. al., 2005). The major part of the thermal resistance appears closer and closer to the surface (the region where the temperature changes from its surface value to its centreline value is very close to the surface). For Prandtl numbers greater than 10, almost the entire temperature profile is inside the sublayer.

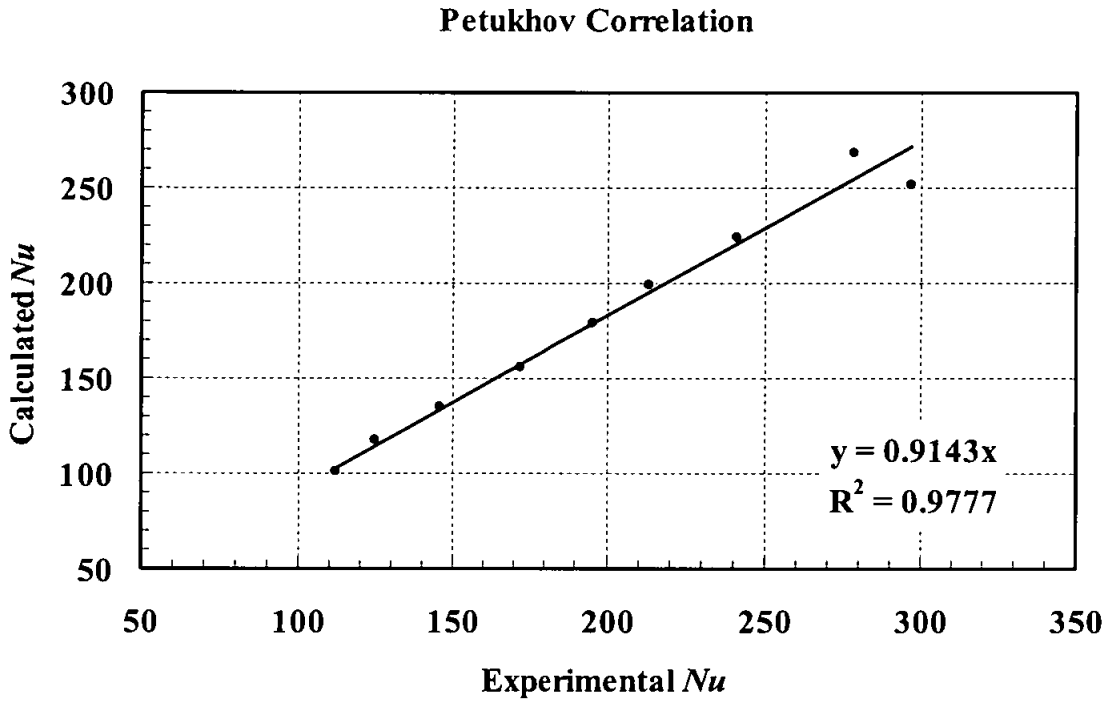


Figure 5.15: Experimental vs. Calculated Nusselt Number for Petukhov Correlation

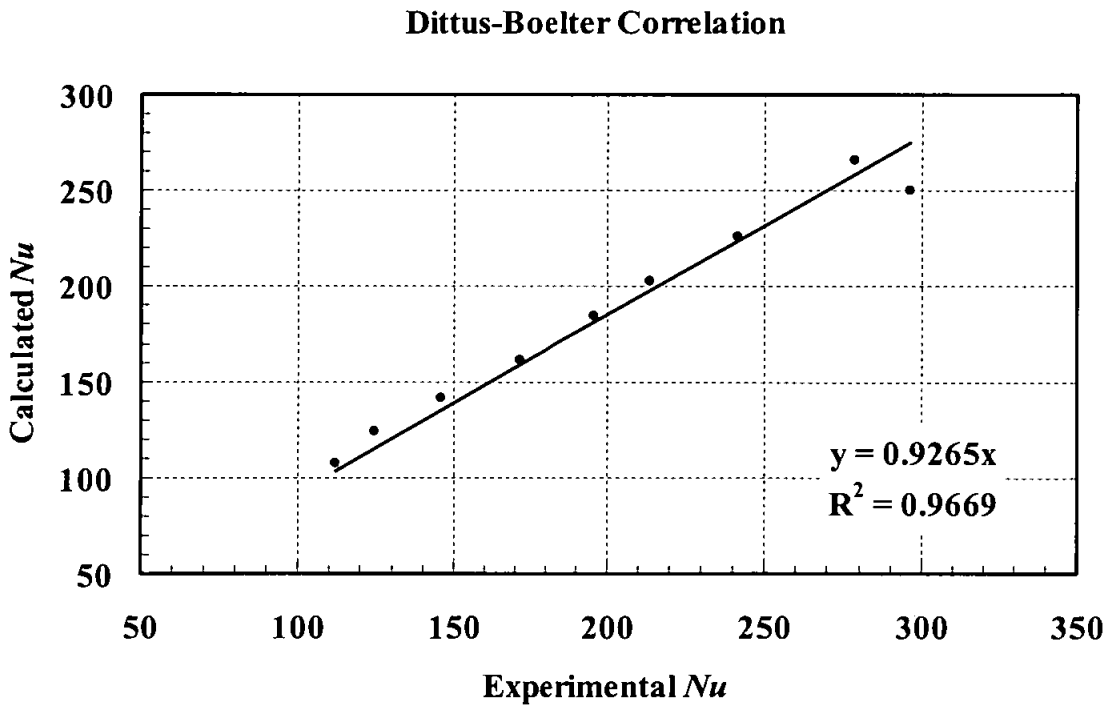


Figure 5.16: Experimental vs. Calculated Nusselt Number for Dittus-Boelter Correlation

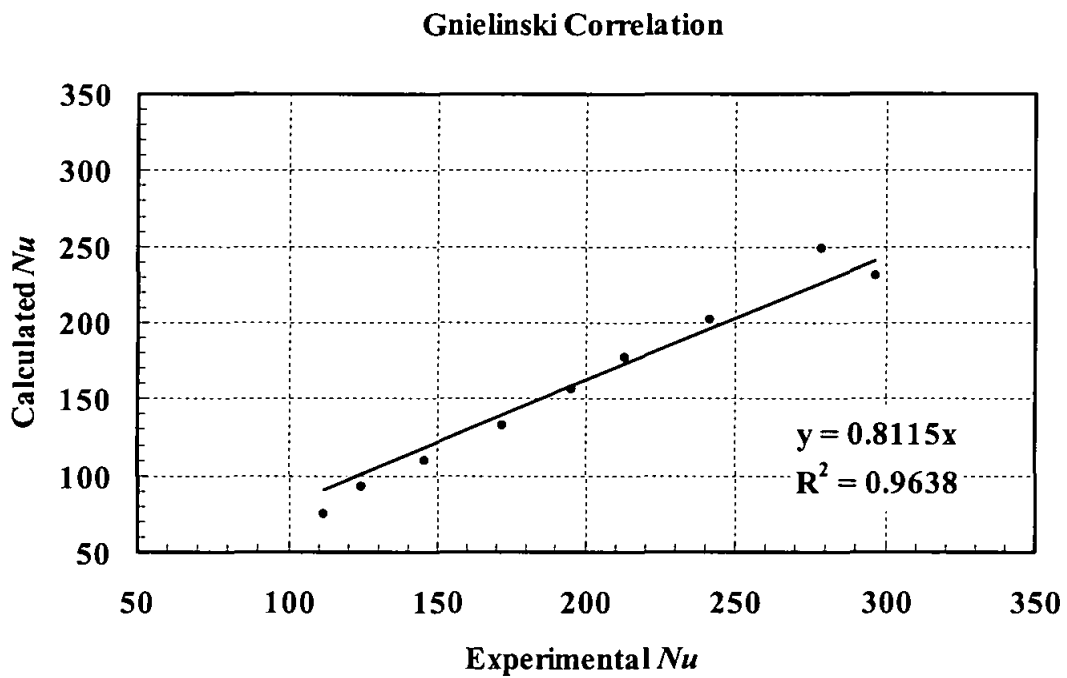


Figure 5.17: Experimental vs. Calculated Nusselt Number for Gnielinski Correlation

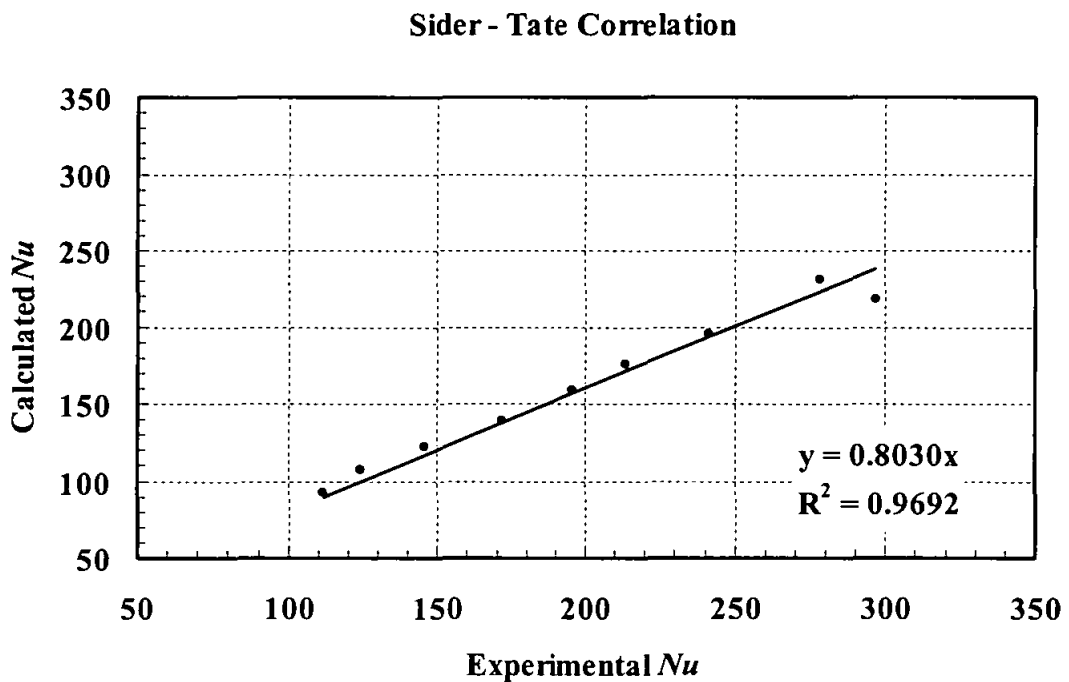


Figure 5.18: Experimental vs. Calculated Nusselt Number for Sider and Tate Correlation

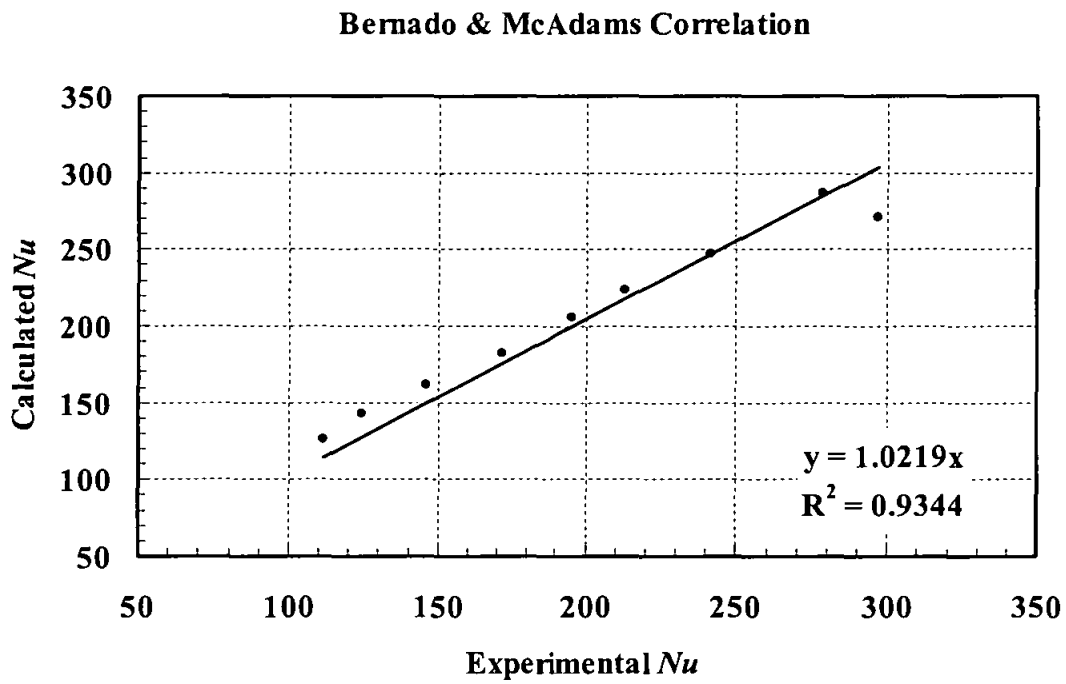


Figure 5.19: Experimental vs. Calculated Nusselt Number for Bernado and McAdams Correlation

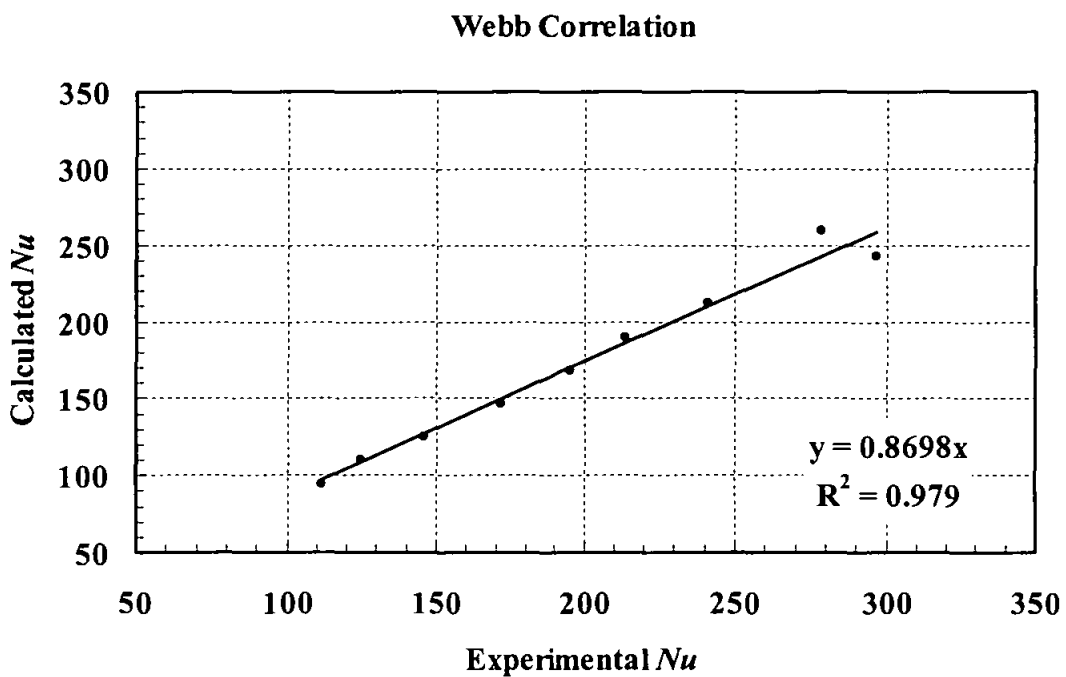


Figure 5.20: Experimental vs. Calculated Nusselt Number for Webb Correlation

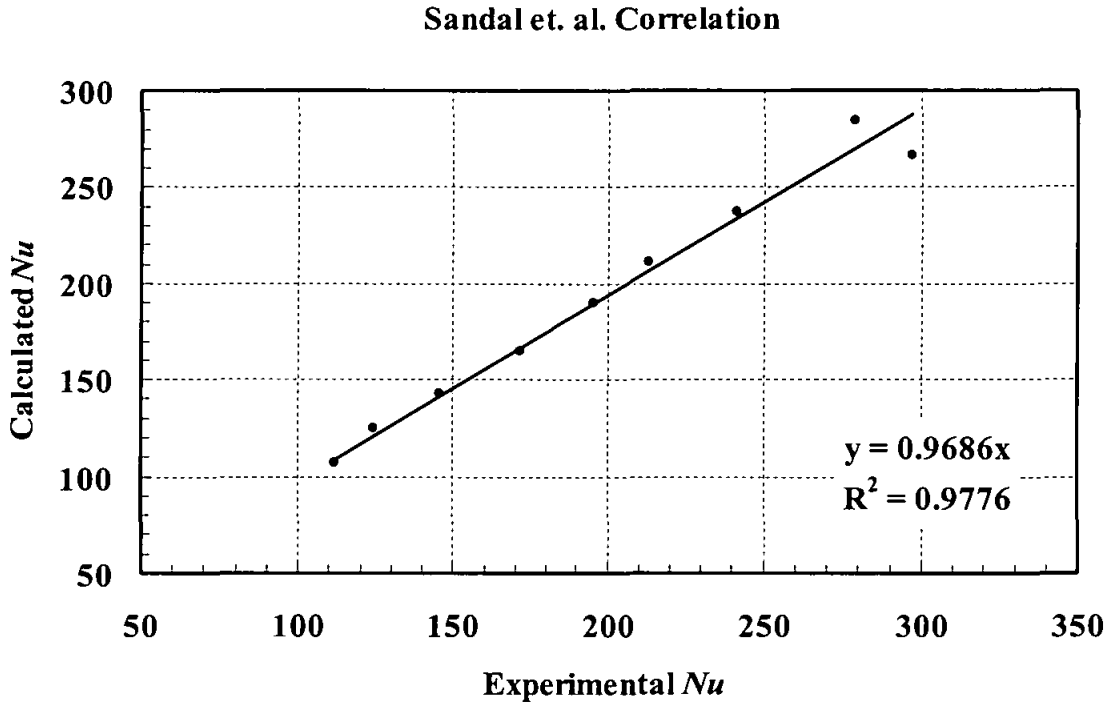


Figure 5.21: Experimental vs. Calculated Nusselt Number for Sandal et. al. Correlation

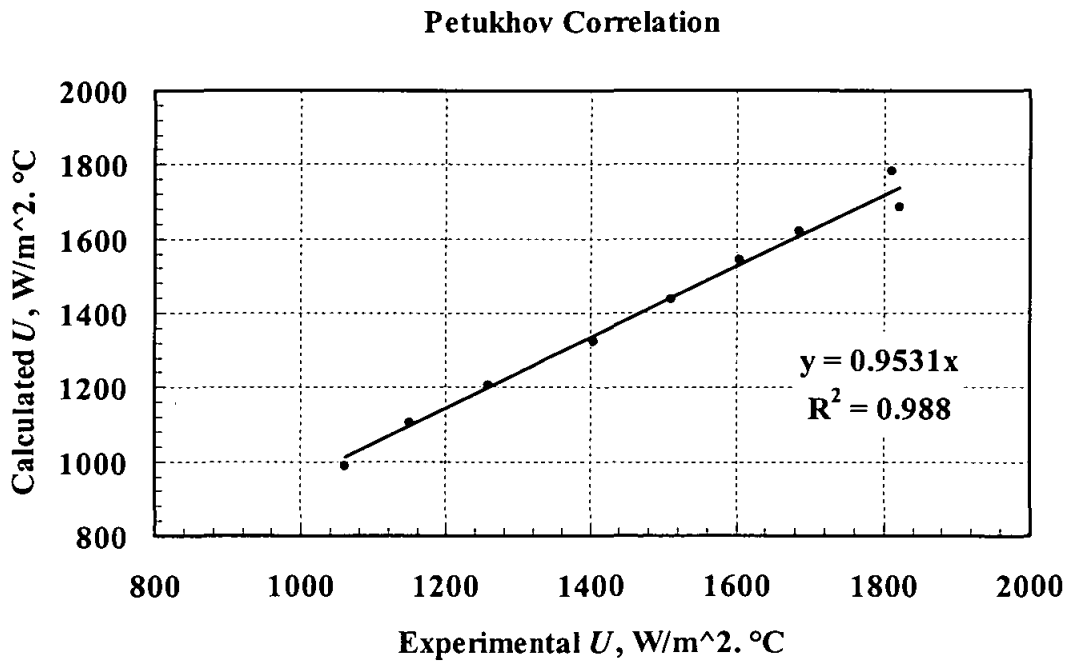


Figure 5.22: Experimental vs. Calculated Overall Heat Transfer Coefficient for Petukhov Correlation



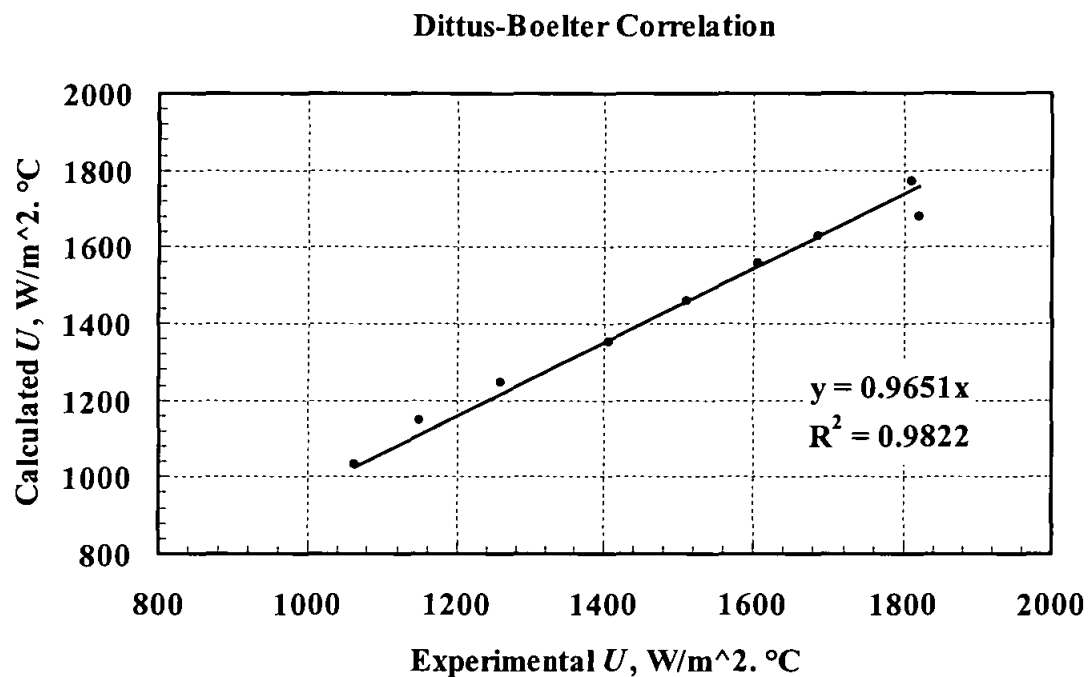


Figure 5.23: Experimental vs. Calculated Overall Heat Transfer Coefficient for Dittus-Boelter Correlation

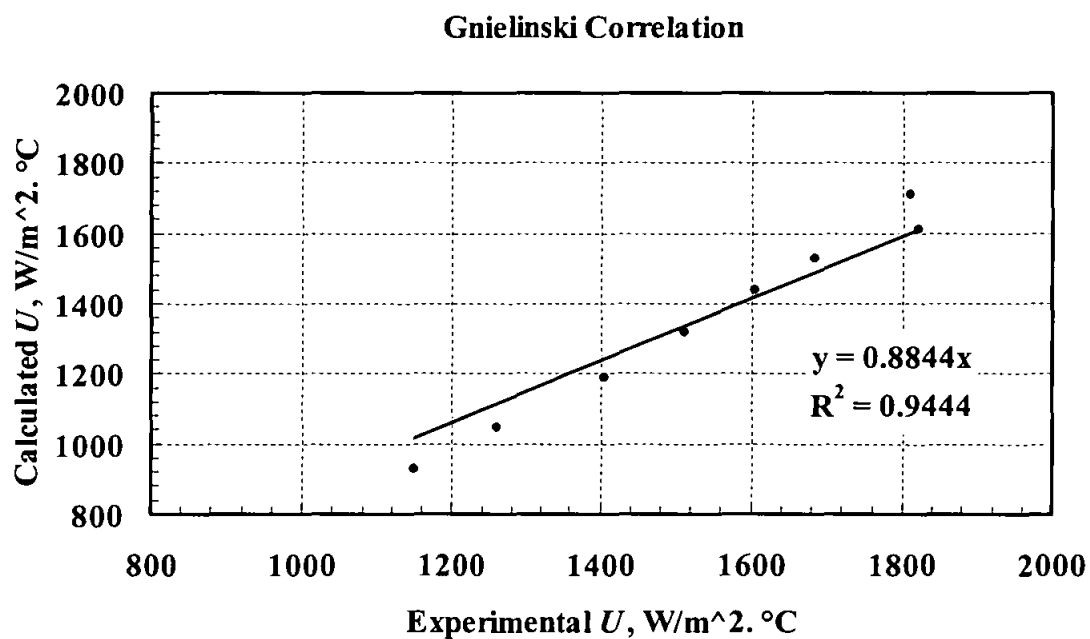


Figure 5.24: Experimental vs. Calculated Overall Heat Transfer Coefficient for Gnielinski Correlation

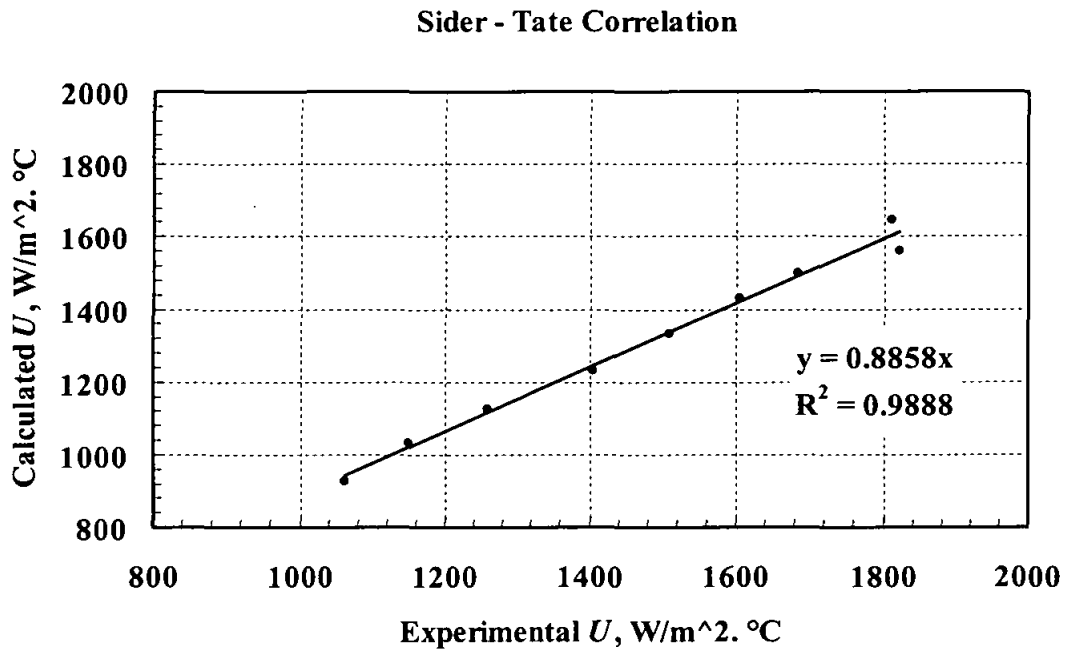


Figure 5.25: Experimental vs. Calculated Overall Heat Transfer Coefficient for Sider and Tate Correlation

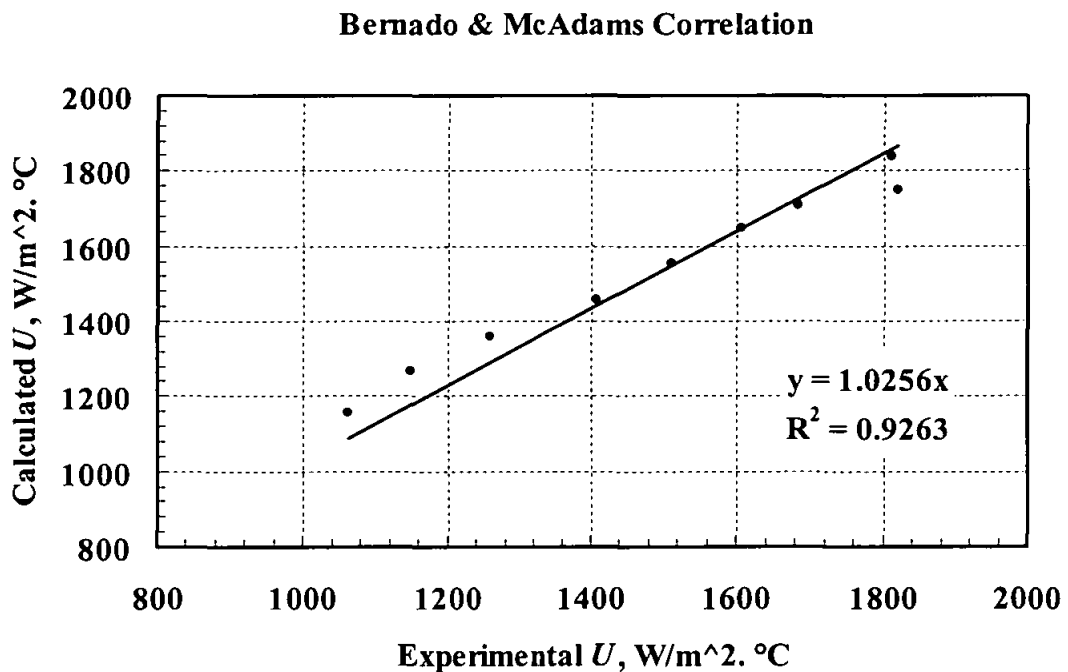


Figure 5.26: Experimental vs. Calculated Overall Heat Transfer Coefficient for Bernado and McAdams Correlation

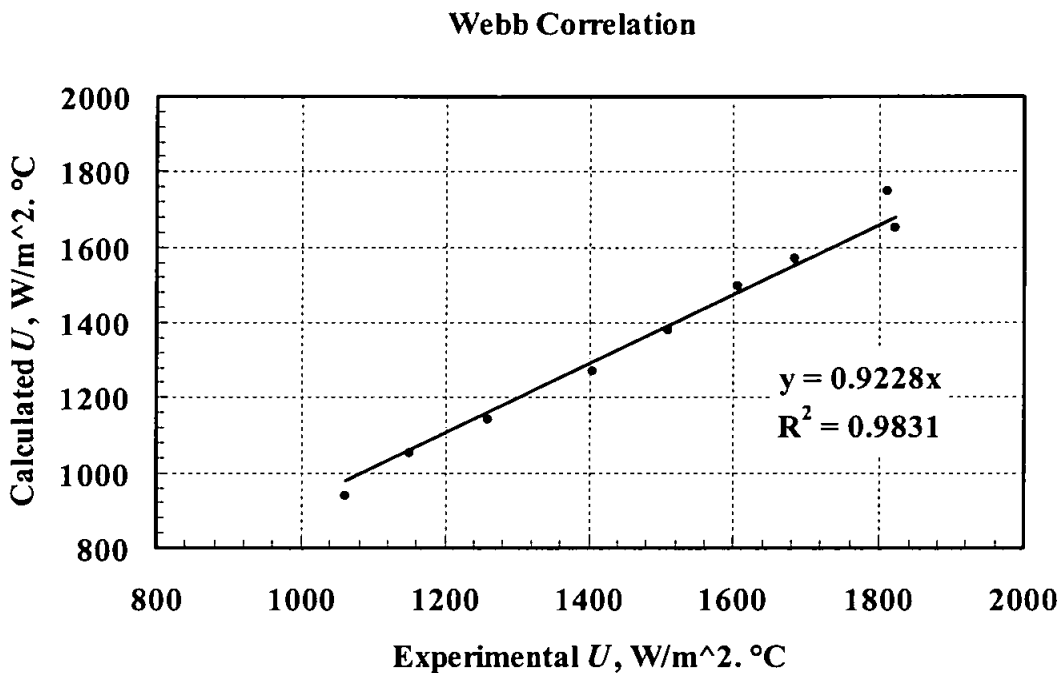


Figure 5.27: Experimental vs. Calculated Overall Heat Transfer Coefficient for Webb Correlation

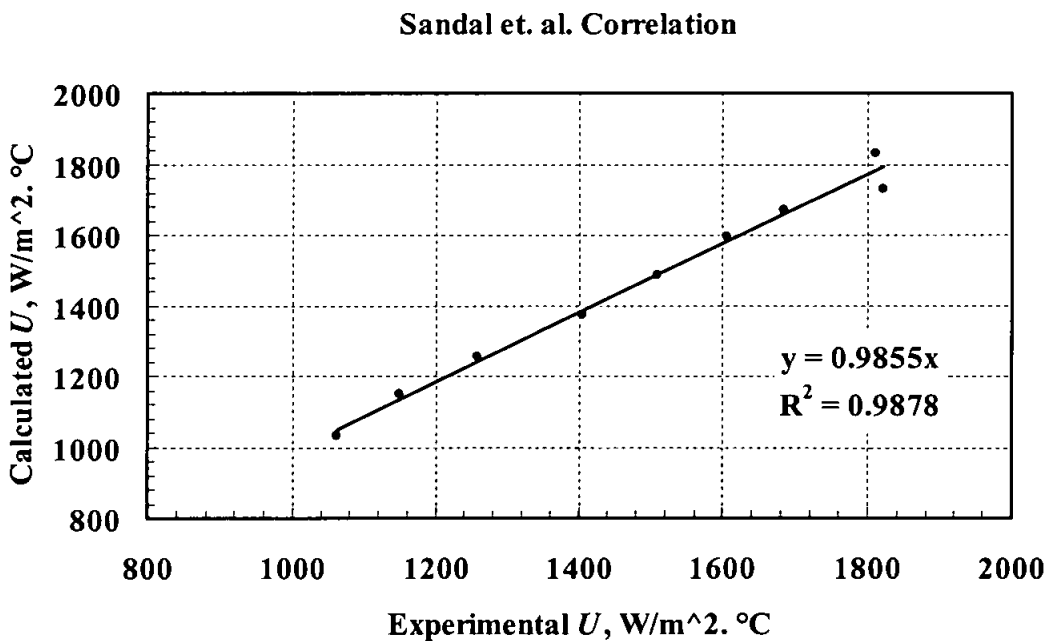


Figure 5.28: Experimental vs. Calculated Overall Heat Transfer Coefficient for Sandal et. al. Correlation

Figure 5.15 through 5.21 show the comparisons between the theoretical Nusselt number predicted with aid of the convective heat transfer correlations, and the experimental data for turbulent flow regime. The best agreement between the theoretical and the experimental data achieved with *Sandal et. al.* correlations which yielded a average absolute Percent relative error (AAPE) of 3.85 %, while the largest AAPE of 21.4% is occurred with Gnielinski correlation. Table 5.2 presents the statistical error analysis for the different heat transfer correlations consisting of the AAPE of Nu and the overall heat transfer coefficient.

Table 5. 2: Theoretical-Experimental error analysis of the convective heat transfer correlations.

Heat Transfer Correlation	AAPE (%)	
	Nusselt Number, $Nu$	Overall heat transfer coefficient, $U$
Petukhov	08.04	04.88
Gnielinski	21.40	14.30
Dittus & Boelter	05.61	03.22
Sider & Tate	18.08	11.42
Bernado & McAdams	08.28	05.03
Webb	13.18	08.30
Sandal et. al.	03.85	02.20

Figure 5.22 through 5.28 show the comparisons between the overall heat transfer coefficient calculated with the aid of the heat transfer correlations and experimental one obtained from the heat transfer data. All the theoretical and experimental data for all correlation agreed well within 15%. Within this error band, Petukhov, Dittus & Boelter, Bernado & McAdams and Sandal *et. al.* correlations were more better, since their deviations is of 5% in AAPE value.

Comparison between average absolute percent errors for all heat transfer correlations for Nusselt Number is provided in Figure 5.29 and for the overall heat transfer coefficient in Figure 5.30.

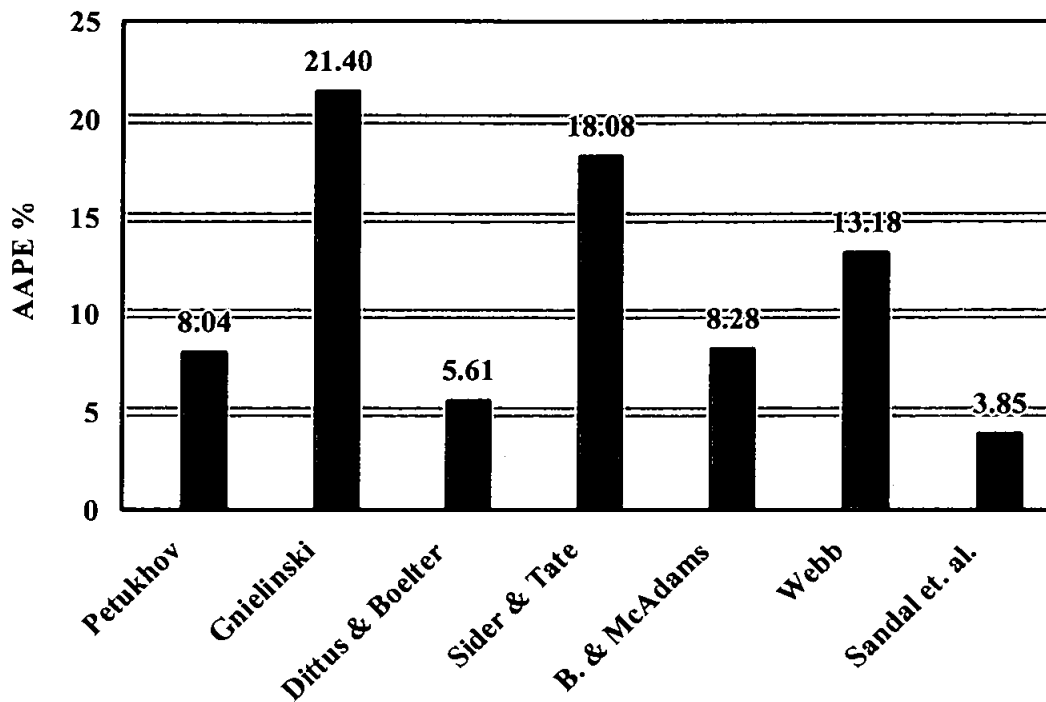


Figure 5.29: Comparison of AAPE of the Convective Heat Transfer Correlations for obtaining Nusselt Number

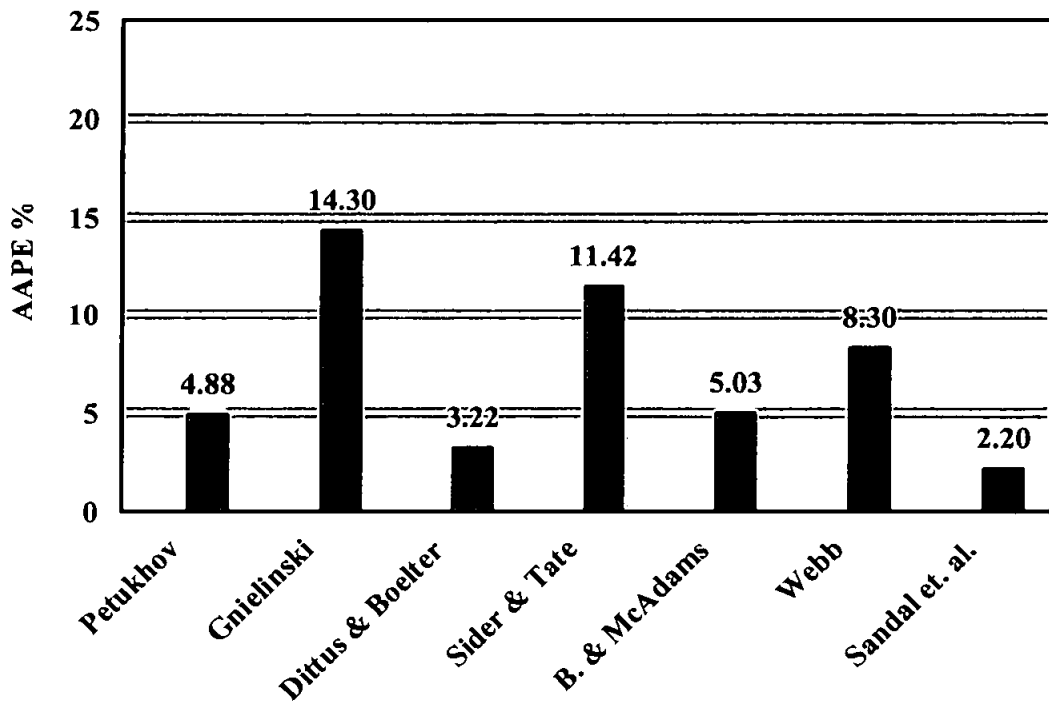


Figure 5.30: Comparison of AAPE of the Convective Heat Transfer Correlations for obtaining the Overall Heat Transfer Coefficient

---

As a conclusion, comparisons of the calculated Nusselt number for different heat transfer correlations and the experimental data are quite scattered. As the AAPE % is a significant sign of the accuracy, it is used as base in the accuracy judgement of this study. Examining Figure 5.29, *Sandal et. al.* correlation outperforms other correlations in terms of lowest average absolute percent error of 3.85 %. Accordingly, it can be judged that *Sandal et. al.* correlation is the best correlation that can be used to model and to characteristics the heat transfer process within the test section of the HT/HPMPWDF. In spite of the goodness of the *Sandall et. al.* correlation, still Petukhov, Dittus-Boelter and Bernado-McAdams correlations are quite acceptable, since its fall within 8% average absolute percent error, and it can give good heat transfer characterisation for the test section.

The highest average absolute percent error of 21.40 % is accomplished by Gnielinski correlation. Accordingly, some contradiction between the literature findings and the experimental result of this study arose. Kakac, shah and Aung, pointed out (quoted by Kays *et. al.*, 2005) that they have examined great many correlation for fully developed turbulent flow in circular tube, and concluded that Gnielinski correlation (Table 5.1), correlates the available data somewhat better than any other over the range  $0.5 < Pr < 2000$  and  $2300 < Re < 5 \times 10^6$ . In the present study this contradiction can be justified by the flow geometry test section. Entirely different phenomenon between the flow and heat transfer in tube and annulus can be responsible for such error like the one reported in this study. It can be due to the approximation of the equivalent diameter for correlation between turbulent fluid flow and heat transfer characteristic of circular and noncircular ducts.

---

## CHAPTER VI

### CONCLUSIONS AND RECOMMENDATIONS

#### 6.1 CONCLUSION

Experimental and analytical approaches have been adopted to investigate the pressure drop and heat transfer in the test section of the HT/HPMPWDF, which has annular geometry feature. The pressure drop throughout the test section of the HT/HPMPWDF has been investigated and realistic pressure drop correlation is developed. The heat transfer based on the *Re-Nu* characterization has been analyzed. The convective heat transfer correlations represent the thermal performance of the apparatus have been justified.

The properties of the fluid used in this study are measured via standard laboratory tests analysis (ASTM 4052 – 96” for density and “ASTM D 445 – 06” for kinematic viscosity). The velocity of the flow is determined from the flow rate of the oil and the dimensions of the cross section flow area. The tests are carried out for mineral oil at 50, 60, 70 °C. These temperatures are selected 10 – 15 °C above the WAT proposed for the real test.

Based on the experimental and analytical analysis, the following can be concluded:

#### *The Pressure Drop Investigations*

The goal was to develop a calculation routine to characterize the pressure drop in the deposition test section with good accuracy level and acceptable confidence limitation. Comparisons between measured and correlated results are carried out.

A pressure drop calculation routine is developed using Darcy-Weisbach equation. Churchill friction factor is used to express the friction factor in the pressure drop

---

equation. Among four geometry approximation criteria, the hydraulic diameter approximation is used to express the dimensions of the test section.

Reynolds number-pressure drop plot is constructed for both the calculated and the experimental results. A cross-plot with a regression line is constructed to compare the calculated values with the experimental results. The experimental results are found to being larger about fifteen times the calculated values, with an absolute average percent error of 93 % and standard deviation of 43.4.

To ensure the consistency of the calculation routine and whether it has a contribution on the error reported, a parametric analysis is performed. Three different equations were used to plot the theoretical friction factor values against the experimental friction factor. From these results, it is concluded that any one of the friction factor equations can be used to compare the experimental values if only turbulent regime is considered. The Churchill friction factor can be used confidently for the entire flow regime.

Another suggested methods for calculating the frictional pressure drop for flow in annular (concentric) conduits suggests the use of a correction coefficient. The correction factor is separately evaluated for laminar and turbulent flow, and applied to the frictional pressure drop calculation with the aid the Churchill friction factor expression and the hydraulic diameter approximation. Using the correction factor, the calculated friction factor is corrected by 2 % absolute average percent error.

The type of flow in the test section is very complex and there are many factors that must be considered to determine the friction factor accurately. These factors are: direction changing, the effect of the sudden contraction, entrance-exit effects and the acceleration effects. A realistic pressure drop correlation is developed to accommodate these factors in the calculation routine. All these factors are simulated into 1 inch round pipe with the same properties of the flowing fluid. The error between the theoretical and experimental results is compensated by the equivalent length of the round tube. An optimum equivalent length obtained by statistically minimizing the sum of root mean square of the errors



---

between the measured and calculated pressure drop values. A solver parameter technique is used. The developed correlation achieved an error reduction down from 93 % to 11 %, which is fairly good to insure the adequacy of the experimental procedure. The best accuracy achieved with the turbulent flow regime with an absolute average error of 4 %, which is fairly good to ensure the accuracy and the confidence for predicting the growth of the deposited layer, normally measured in micrometers.

From the overall evaluation of the pressure drop, it is concluded that the wax deposition can be modeled accurately for the turbulent regime, which is encountered in the real field practice and has to be modeled in laboratory to satisfy the physical similarity.

### ***The Heat Transfer Investigations***

Three different oil temperatures are maintained while the flowrate is changed in stepwise manner. Temperature 60 and 70 °C showed good thermal stabilization throughout the test of 15 flowrate steps. While, for 50 °C the temperature measurements showed some unstabilization for the high flow rate. The oil flow temperature started to increase out-of-control with the flowrate increments. From these results, it is concluded that a stable temperature control can be achieved and measurement can be conducted.

In which concern the heat exchanging process between the hot oil and the cold glycol flowing counter currently to each other, a steady state heat transfer balance is established. The balance is made between three heat transfer rate terms; the heat released by the oil flow, the heat gain by the cold glycol flow and the heat transfer from the oil to the cold glycol across the deposition wall. The latter quantity is calculated with the aid of the *LMTD* and the overall heat transfer coefficient. Large variation between the heat released by the oil and the heat gained by the cold glycol is observed. After investigating the measuring device and the parameters involved in the calculation the flowrate of the cold glycol is found to be the source of the variations and need to be maintained some high to achieve the balance. The turbulent *Petukhov* model of the convective heat transfer is used to calculate the film heat transfer coefficients for both the oil and the cold glycol. For the

---

laminar regime of the oil, the convective heat transfer evaluated from  $Nu = 3.66$ . This showed unsatisfactorily results due to its velocity and/or Re independency nature, while the measured values appears to be inertia force dependant. Incorporating the three heat transfer terms, the energy balance of the annular deposition test section was satisfied to within 5.8 %, attesting to the good quality of the thermal insulation.

The *Sandal et. al.* model yield the most satisfactory result among the other correlations within 4 % AAPE for Nusselt number and within 2 % APPE for the overall heat transfer coefficient. In spite of that, its use as the best for the deposition modeling is not yet to be confirmed by this study, since some of other correlations yield satisfactory results as well. More investigation with real petroleum fluid is required to address the effect of the thermal properties and the composition variations.

---

## 6.2 RECOMMENDATIONS

In order to improve the test program of the test facility, some recommendations are made as follows:

1. The velocity in the annulus was not directly measured. The mean velocity is being calculated from the flow rate measured at the flow meter on the pipe line downstream the oil pump immediately. If swirling and eddies effects are introduced in the annulus section, the mean velocity calculated will not be the actual velocity in the annulus. Accordingly, a velocity measurement in the test section is recommended and it will be more beneficial if it traverse the annular.
2. Further temperature monitoring in the oil section is required to measure the effect of the pressure dissipation to thermal energy in the oil flow passage at the high flow rates.
3. The number and quality of temperature measurement instruments must be improved. This may include reliable instruments for measuring the deposition wall temperature, as the thermocouple installed currently was not able to provide accurate reading because of its improper configuration. As this thermocouple installed across the flowing oil, the wall temperature measurement taken by the end of thermocouple adhere to the wall, will affected by bulk oil flowing over the probe of the thermocouple, the same case happened with the thermocouple installed at the mid stream temperature. Also some thermocouples required to be installed equidistance along the 3 m length of the test section. This way, temperature measurements along the axial path of the annulus will be obtained.
4. The cooling system of the test section needs to be redesigned to obtain better cold glycol temperature control particularly at the high flow rates and high oil temperatures. This can be achieved either by increasing the cooling rate of the chiller

---

or by installing a heat exchanging unit to trim the temperature of glycol mixture after exchanging heat with the oil and before it introduced to the cooling system again.

5. Additional or re-configuration of the flowmeter of the cooling system is required to meter the flow stream in the test section, because the current flowmeter is installed in the main outlet port of the cooling system and if more than one outlet port branched from the main is used, metering the flow rate will be unachievable, then the calculation of the heat transfer can not be performed.

---

## REFERENCES

- Peter Toma, John Ivory, Gerard Korpany, Mario deRocco, Chris Goss, Larry Holloway, Jamal Ibrahim and Ismail Omar, "A Two-Layer Paraffin Deposition Structure Observed and Used to Explain the Removal and Aging of Paraffin Deposits in Wells and Pipelines", *Journal of Energy Resources Technology*, ASME Transaction, 128 (2006), 49-59.
- Kristofer G. Paso (2005), "Paraffin Gelation Kinetics", (Ph.D. thesis, University of Michigan).
- Kays W. M., M. E. Crawford and Bernhard Weigand (2005), "Convective Heat and Mass Transfer" Fourth Edition, New York, Mc-Graw Hill Companies Inc.
- Cem Sarica, Michael Volk, "Paraffin Deposition Research and Model Development", Final Technical Report, Paraffin Deposition Projects, Tulsa University (2004).
- Ramachandran Venkatesan (2004), "The Deposition and Rheology of Organic Gels", (Ph.D. thesis, University of Michigan).
- Idelchik I. E., Steinberg M. O., Malyavskaya Greta R. and Martynenko oleg G. (2003), "Handbook of Hydraulic Resistance", Third Edition, Mumbai, Jaico Publishing House.
- Coelho P.M. and Pinho F.T., "Fully-Developed Heat Transfer in Annuli with Viscous Dissipation" *International Journal of Heat and Mass Transfer*, 49 (2006) 3349–3359.

- 
- Masayuki Kaneda, Bo Yu, Hiroyuki Ozoë and S. W. Churchill, "The Characteristics of Turbulent Flow and Convection in Concentric Annuli. Part I: Flow", *International Journal of Heat and Mass Transfer*, 46 (2003) 5045-5057.
- Mansoori G. Ali, Barnes H. Lindsey and Webster Glen M. "Petroleum Waxes", Chapter 19 in "Fuels and Lubricants Handbook", ASTM International, West Conshohocken, PA, (2003) 525-556.
- Dirker Jaco and Meyer Josua P., "Heat Transfer Coefficients in Concentric Annuli", *Journal of Heat Transfer, Transactions of ASME*, 124 (2002) 1200-1203.
- James G. Speight (2001), Thermal Properties, Chapter 5 in "Handbook of Petroleum Analysis", John Wiley & Sons Inc., Canada.
- Holman J. P. (2001), "Experimental Methods for Engineers", Seventh Edition, New York, Mc-Graw Hill Companies Inc.
- Solaimany Nazar R., Dabir B. and Islam M. R., "Measurement and Modeling of Wax Deposition in Crude Oil Pipelines", SPE 69425, (2001).
- Mustafa Versan Kok and Onder Saracoglu, "Mathematical Modeling of Wax Deposition in Crude Oil Pipeline Systems", SPE 64514, (2000).
- Sadeghazad, Ayoub, Christiansen, Richard L., Sobhi, Ali G., and Edalat M., "The Prediction of Cloud Point Temperature: In Wax Deposition", society of petroleum engineering, SPE 64519, (2000).
- White Frank M. (1999), "Fluid Mechanics", fourth edition, New York, Mc-Graw Hill Companies Inc.

- 
- Hodge B. k. and Taylor Robert P. (1998), "Analysis and Design of Energy System", Third Edition, New Jersey, Prentice Hall.
- Gerard Korpany, Kerry Scott, Linda Coates, Mario DeRocco and Peter Toma, "ARC/PETRONAS High Temperature/High Pressure Model Pipeline and Wax Deposition Facility Safe Operating Procedures and Manual", Alberta Research Council, Energy Group, Edmonton, 1998.
- Churchill Stuart W., "New Simplified Models and Formulations for Turbulent Flow and Convection", American Institute of Chemical Engineering Journal, 43 (5) (1997) 1125-1140.
- Hamouda A. A. and Davidsen S., "An Approach for Simulation of Paraffin Deposition in Pipelines as a Function of Flow Characteristics with a Reference to Teesside Oil Pipeline", Society of Petroleum Engineers, SPE28966, (1995).
- Hsu J.J.C. and Brubaker J.P., "Wax Deposition Measurement and Scale-Up Modeling for Waxy Live Crudes under Turbulent Flow Conditions", Society of Petroleum Engineers, SPE 29976, (1995) 241-250.
- Sadik Kakac and Yaman Yener (1995), "Convective Heat Transfer", Second Edition, Florida, CRC press Inc.
- Hsu J.J.C., Santamaria M. M., and Brubaker J.P., "Wax Deposition Waxy Live Crudes under Turbulent Flow Conditions", Society of Petroleum Engineers, SPE 28480, (1994) 179-192.
- Sanjay Misra, Simanta Baruah and Kulwant Singh, "Paraffin Problems in Crude Oil Production and Transportation: A Review", Society of Petroleum Engineers, SPE 28181, (1994).

- 
- Brown T.S., Niesen V.G., and Erickson D. D., "Measurement and Prediction of the Kinetics of Paraffin Deposition", Society of Petroleum Engineers, SPE 26548, (1993).
- Ajienka J.A., "The Effect of Temperature on the Rheology of Waxy Crude oils", Society of Petroleum Engineers, SPE 23605, (1991).
- Shigechi T., Kawae N. and Lee Y., "Turbulent Fluid Flow and Heat Transfer in Concentric Annuli with Moving Cores", International Journal of Heat and Mass Transfer, 33 (9) (1990) 2029-2037.
- Weingarten J. S. and Euchner J. A., "Methods For Predicting Wax Precipitation And Deposition", Society Of Petroleum Engineering, SPE15654, (1988) 121-126.
- Sadic Kakac, Ramesh K. Shah and Win Aung (1987), "Handbook of Single Phase Convective Heat Transfer", First Edition, New York, John Wiley & sons.
- A. F. Bertuzzi, M.J. Fetkovich, Fred H. Poettmann and L.K. Thomas (1987), Wellbore Hydraulics, Chapter 34 in "Petroleum Engineering Handbook", Third Printing, Society of Petroleum Engineers, Richardson, TX, U.S.A.
- Jones O. C. and Leung J. C., "An Improvement in the Calculation of Turbulent Friction in Smooth Concentric Annuli", Journal of fluid engineering, 103 (1981) 61-623.
- Burger E. D., Perkins T.K., and Striegler J. H., "Studies of Wax Deposition in the Trans Alaska Pipeline", J. Pet. Technol., June, 1075 (1981).
- Hinze J. O. (1975), "Turbulence", Second Edition, New York, Mc-Graw Hill Companies Inc.



- 
- Hanjalić K., "Prediction of Turbulent Flow in Annular Ducts with Differential Transport Model of Turbulent" *Wärme-und Stoffübertragung*, Bd 7 (1974) 71-78.
- Lawn C. J. and Elliott C. J., "Fully Developed Turbulent Flow through Concentric Annuli", *Journal Mechanical Engineering Science*, 14 (3) (1972) 195-204.
- Lee Y. and Park S. D., "Developing Turbulent Flow in Concentric Annuli: An Analytical and Experimental Study", *Wärme-und Stoffübertragung*, 7 (1971) 156-166.
- Roy D. N. and Gangopadhyay U., "Turbulent Friction Factor and Velocity Profile in Smooth Annuli", *Applied Science Research*, March 1971.
- Crookston R. B., Rothfus R. R. and Kermode R. I., "Turbulent Heat Transfer in Annuli with Small Cores", *International Journal of Heat and Mass Transfer*, 11 (1968) 415-426.
- Quarnby A., "An Analysis of Turbulent Flow in Concentric Annuli", *applied science research*, 19 (1968) 250-273.
- Lee Y., "Turbulent Heat Transfer from the Core Tube in the Thermal Entrance Regions of Concentric Annuli", *International Journal of Heat and Mass Transfer*, 11 (9) (1968) 509-522.
- Roberts A., "A Comment on the Turbulent Flow Velocity Profile in A concentric Annuli", *International Journal of Heat and Mass Transfer*, 10 (1967) 709-712.
- Barrow H., Lee Y. and Roberts A., "the similarity hypothesis applied to turbulent flow in an annulus", *International Journal of Heat and Mass Transfer*, 8 (1965) 1499-1505.

- 
- Brighton, J.A., and Jones, J.B., Fully Developed Turbulent Flow in Annuli, *Journal of Basic Engineering*, 86 (1964), 835-844.
- Kays W. M. and Leung E. Y., "Heat Transfer in Annular Passages- Hydrodynamically Developed Turbulent Flow with Arbitrarily Prescribed Heat Flux", *International Journal of Heat and Mass Transfer*, 6 (1963) 537-557.
- Stein Ralph p. and William Begell, "Heat Transfer to Water in Turbulent Flow in Internally Heated Annuli", *American Institute of Chemical Engineering Journal*, 4 (2) (1958) 127-131.
- Rothfus R. R., Monrad C. C., Sikchi K. G. and Heideger W. J., "Isothermal Skin Friction in Flow through Annular Sections", *Industrial Engineering Chemistry*, 47 (5) (1955) 913-918.
- Deissler R. G., Cleveland and Ohio, "Turbulent Heat Transfer and Friction in the Entrance Region of Smooth Passage" *Journal of Heat Transfer, Transactions of ASME*, 124 (1955) 1221-1233.
- Reistle C. E., "Summary of Existing Information on Handling Congealing Oils and Paraffin", U. S. Bureau of Mines, (1927).

---

## **APPENDIX A: Main Observations Resulting From Experiments Performed With HT/HPMPWDF**

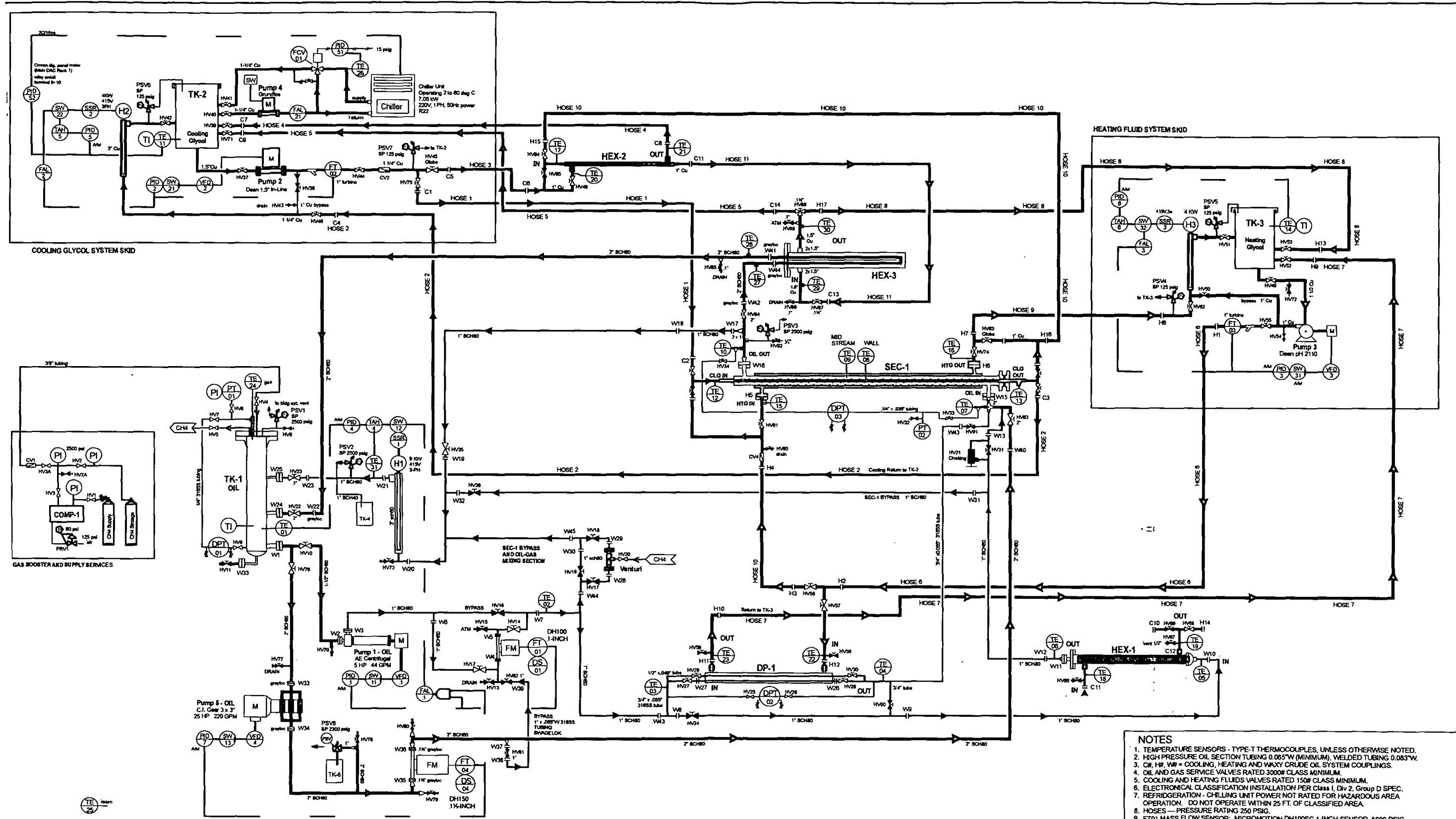
1. Proper assessment of paraffin deposition rate during land and offshore transportation of waxy crude is essential to the pipeline and pumping operation design as well as for estimating all flow assurance strategies (additives, pigging, insulations, re-starting etc) required to maximize the production of oil and gas. The lack of knowledge in this essential area results in excessive operation and capital expenditures and sometimes in improper assessment of field situations,
2. Direct observations and proper sampling of wax deposited on a cold pipe, during laminar and turbulent (bulk) flow of waxy crude, was made possible with a new design of a paraffin deposition loop. Major observations made are indicating that:
  - a) two layers are usually found in any deposit: a thin well attached to cold pipe and relatively hard layer and a gel-like layer; the aspect of the “gel” outer layer is rapidly changing (it hardens) after the flow of warm waxy crude stops;
  - b) a high concentration of alkanes ( $C>20$ ) is found in the thin, attached layer, while the alkane concentration of the “gel” layer is only slightly higher than concentration found in the re-circulated bulk oil;
  - c) the outer layer apparent structure is rapidly changing from a gel-like to a non-flow structure (a well-known “porous” structure formed by an alkane, solid skeleton filled with oil results a few minutes after circulation is stopped),
  - d) a precise measurement of the deposition depth is difficult and not reliable; however, precise sampling and measurement of C-composition – if made within a short time from stopping the flow - offers a good picture of the deposition rate and process.
3. Conventional deposition models are using a well accepted diffusion-dispersion coefficient to calculate the rate of (radial) transportation of wax, the deposit thickness and the “available” flow area are adjusted to better represent the mechanism of partial

---

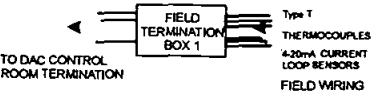
removal and shearing of alkanes back into the core flow. An axial description is customarily used for profiling the deposit. This description is far from the actual deposition-removal and flow of a Newtonian core and of a non-Newtonian (gel-like) layers and cannot explain at all the aging process observed in the laboratory and field through shifting of the C-composition of the deposited wax towards higher C-values with time, essential for establishing the pigging frequency.

4. A mechanistic model has been first time suggested and tested against existing laboratory data; it is able to assess the aging mechanism as a selective removal of alkane crystals floating in the “gel - (sub) layer” The proposed model uses the following salient (removal) features:
- a) a broad-spectrum of alkane crystals are nucleating and growing in the gel-layer,
  - b) if the core-flowing is laminar the gel-layer will grow and soon will be saturated with alkanes, the layer apparent viscosity will considerably increase and its axial transport decrease to reach a stationary (almost) condition;
  - c) if the core-flowing is turbulent a selective removal of growing crystals from the gel layer is balancing a diffusion transport of alkanes from core to gel layer;
  - d) the turbulent removal mechanism is featured following the “burst-removal” mechanism suggested by Cleaver and Yates (1973) and, for the size domain of alkane crystals (0-30  $\mu\text{m}$ ) the larger crystals will be first removed (Philips, 1980 - note: Philips’ size domain is totally different from ”Shield’s domain where  $d > 50 \mu\text{m}$ );
  - e) the process of nucleation and grows uses two main parameters to define the sub-cooling temperature (difference between wall temperature and C-specific solidification temperature);
  - f) If all of the above are considered, the model allow for selective removal—larger crystals formed from higher C-components will be predominantly removed.

5. Final: an axial (local bulk temperature-concentration only) calculation of the deposition is not possible; a radial distribution of temperature and C-concentrations (of alkanes) is a must and the mechanistic model described allows it.



- NOTES**
1. TEMPERATURE SENSORS - TYPE-T THERMOCOUPLES, UNLESS OTHERWISE NOTED.
  2. HIGH PRESSURE OIL SECTION TUBING 0.065" W (MINIMUM), WELDED TUBING 0.083" W.
  3. CH, H, W = COOLING, HEATING AND WAXY CRUDE OIL SYSTEM COUPLINGS.
  4. OIL AND GAS SERVICE VALVES RATED 3000# CLASS MINIMUM.
  5. COOLING AND HEATING FLUIDS VALVES RATED 150# CLASS MINIMUM.
  6. ELECTRICAL CLASSIFICATION INSTALLATION PER Class 1, Div 2, Group D SPEC.
  7. REFRIGERATION - CHILLING UNIT POWER NOT RATED FOR HAZARDOUS AREA OPERATION. DO NOT OPERATE WITHIN 25 FT. OF CLASSIFIED AREA.
  8. HOSES - PRESSURE RATING 250 PSIG.
  9. FT01 MASS FLOW SENSOR: MICROMOTION DH100SC 1-INCH SENSOR, 5600 PSIG 204°C RATING, CONNECTIONS GRAYLOC 1.5-INCH HUB SIZE GR11, SEAL RING SIZE 11, CLAMP SIZE 1.5
  10. FT05 MASS FLOW SENSOR: MICROMOTION DH150SC 1.5-INCH SENSOR, 5600 PSIG, 204°C RATING, CONNECTIONS GRAYLOC HUB SIZE 1.5 GR14, SEAL RING SIZE 14, CLAMP SIZE 1.5



Drawing File (Autobatch): PRSS HPDEPOS D-HOOS-F-0270 REV3.S4F

Location			Stamp	
PLMD, J, GLK	GLK	JUN1003	3701000	PTNS2002
Design	Drawn	Date	Checked	Approved
Work Order		File		

Title		PRSS DEPOSITION LOOP FACILITY P&ID	
Scale	Dwg No.	D-HOOS-F-0270	Rev.
N.T.S.			3



---

## APPENDIX B: Mechanical and Instrumentation Components

### Identification of the HT/HPMPWDF

Item	Tag	Identification
1.	SEC1	Main deposition test section
2.	DP-1	D.P. test section
3.	HEX1	Oil temp. trim HEX
4.	HEX2	Glycol temp trim HEX
5.	TK-1	main oil supply tank
6.	TK-2	glycol cooling bath tank
7.	TK-3	oil trim HEX bath glycol tank
8.	Pump1	main oil circulation, tank 1
9.	Pump2	cooling bath, tank 2
10.	Pump3	heating bath, tank 3
11.	Pump4	chiller recirculation pump
12.	M1	electric motor - pump 1
13.	M2	electric motor - pump 2
14.	M3	electric motor - pump 3
15.	M4	electric motor - pump 4
16.	VFD1	adj. frequency drive - pump 1 motor
17.	VFD2	adj. frequency drive - pump 2 motor
18.	VFD3	adj. frequency drive - pump 3 motor
19.	CV1	Gas inj. flow check valve to tank 1
20.	CV2	discharge flow check valve - Pump 3
21.	CV3	discharge flow check valve - Pump 4
22.	CV4	discharge flow check valve - Pump 5
23.	PRV1	Gas booster air supply pressure reg.
24.	PSV1	pressure safety valve
25.	PSV2	pressure safety valve

---

26.	PSV3	pressure safety valve
27.	PSV4	pressure safety valve
28.	PSV5	pressure safety valve
29.	PSV6	pressure safety valve
30.	PSV7	pressure safety valve
31.	FT01	mass flow meter
32.	FT02	turbine flow meter
33.	FT03	turbine flow meter
34.	DS01	density sensor
35.	PT-01	pressure transmitter
36.	PT-02	pressure transmitter
37.	DPT-01	differential pressure transmitter
38.	DPT-02	differential pressure transmitter
39.	DPT-03	differential pressure transmitter
40.	PID-P1	Pump 1 speed control / flow rate
41.	PID-P2	Pump 2 speed control / flow rate
42.	PID-P3	Pump 3 speed control / flow rate
43.	PID-H1	heater 1 control
44.	PID-H2	heater 2 control
45.	PID-H3	heater 3 control
46.	PID-C1	Tank 2 chiller control
47.	PID-C2	Tank 2 chiller control
48.	SSR1	solid state relay - power controller
49.	SSR2	solid state relay - power controller
50.	SSR3	solid state relay - power controller
51.	HTR1	Tank 1 fluid heater
52.	HTR2	Tank 2 fluid heater
53.	HTR3	Tank 3 fluid heater
54.	TE1	Tank 1 temp
55.	TE2	Oil temp, outlet of pump
56.	TE3	Oil temp, DP SEC inlet

---



---

57.	TE4	Oil temp, DP SEC outlet
58.	TE5	Oil temp, HEX1 inlet
59.	TE6	Oil temp, HEX1 outlet
60.	TE7	Oil temp, SEC1 inlet
61.	TE8	Oil temp 1 inside
62.	TE9	Oil temp 2 inside
63.	TE10	Oil temp, SEC1 outlet
64.	TE11	Tank 2 temp
65.	TE12	SEC1 CLG inlet
66.	TE13	SEC1 CLG outlet
67.	TE14	Tank 3 temp
68.	TE15	SEC1 HTG inlet
69.	TE16	SEC1 HTG outlet
70.	TE17	HEX2 inlet
71.	TE18	HEX1 jacket inlet
72.	TE19	HEX1 jacket outlet
73.	TE20	HEX2 jacket inlet
74.	TE21	HEX2 jacket outlet
75.	TE22	DP SEC jacket inlet
76.	TE23	DP SEC jacket outlet
77.	TE24	TK-1 Gas temp
78.	TE25	Room temp

---

## **APPENDIX C: Operating and Maintaining Procedures of the HT/HPMPWDF**

This section outlines the safe operating procedures (SOP) for the operation of the HT/HPMPWDF. The test unit is placed in a flow loop, in which waxy crude oil flows. The flow loop will be operated at a maximum temperature under 160°C and at pressures of up to a maximum of 2500 psig. The system will be pressurized using nitrogen or methane.

### **1.0 Experimental Operation**

The completion of a pressure drop/heat transfer test will involve the following stages:

- (a) Start-up of process control equipment,
- (b) Filling and preparation of process fluids,
- (c) Heating and pressurization,
- (d) Shutdown.

### **2.0 Start-Up of Process Control Equipment — Stage “a”**

#### **2.1 Energize Equipment**

Energize, switching power on to the following components:

##### **2.1.1 Within the process control room**

- The UPS power supply, which will energize the process computer, monitor, and instrument cabinet.
- At the DAC cabinet rear termination panel:
  - The 24V DC power supply which is mounted behind the panel, and  
The National Instruments SCXI-1001 chassis power.

- 
- Ensure that the parallel port cable linking the SCXI chassis to the process computer is firmly attached at both ends.
  - Energize each of the adjustable frequency drives for the process pumps: the three Baldor units for Pumps 1, 2, and 3; and the WEG drive for oil Pump5. When powered on the units enter into the “Remote” mode, waiting for the PC controller via an SCXI channel to send a 4-20mA analog speed control signal. By pressing the keypad button “Local” on the VFD unit the “Remote” mode is toggled to “Local” and back again.

The adjustable speed drives for each process pump have local start/stop switches mounted near the pump and on the DAC cabinet front panel (Fig. 3.9). Normal mode of operation is with the button “Out”. When either button is pushed in, the VFD will stop; and if pulled out again, the VFD will continue at the specified controlling frequency.

#### 2.1.2 At the depositions loop:

- Oil mass flow meter FT01 (DH100)
- Oil mass flow meter FT04 (DH150)

#### 2.2 Immersion Heater Disconnects

Ensure that all power to the immersion heaters is disconnected at this time:

- Press IN the red disconnect SHUTOFF buttons for the SSR power controllers serving the immersion heaters. These buttons are located at the front panel of the power controller box mounted in the control room.

#### 2.3 LabVIEW Data Acquisition Software

2.3.1 Once the PC controller operating system has booted and is ready, disable any active desktop screensaver.

2.3.2 LabVIEW executable programs have the .vi extension. Activate LabVIEW by double-clicking its desktop icon and open the process control program “DEPLOG-rev6.vi”.

- 
- Press “Open VI” on the LabVIEW main screen menu\
  - Select the path to the folder \LabVIEW\Loop DAC
  - Select DEPLOY-REV6.vi
  - Click on OPEN.
  - The front panel of the DAC program is displayed (Fig. 3.11).
  - The VI will run automatically when opened.
  - A sub-vi for data file creation will open and display a pop-up window prompting you to input a header for the scope of the test data to be logged. The path of the data file will be: C:\DEPLOY RunData\. Click on [OK].
  - In the opened file path window, select the above Rundata path folder location and input a filename with a “.txt” extension. Long filenames are acceptable. At the end of the test period and when the VI is stopped the text file can easily be opened into an Excel spreadsheet and processed.
  - On the lower right of the front panel a control box indicates the logging rate of data to file. The default value is 10 sec. (minimum 2 sec.); if required, change to desired interval.
  - The [Log Data] switch in this box can be pressed to toggle on/off data logging to file.
  - The Elapsed Time indicator will operate from the moment the DAC program is launched. If required, the [Reset Elapsed Time] switch button can be pressed to zero the elapsed time.

#### 2.4 PID Control Panels – Pump Speed and Fluid Temperature Control

On the DEPLOY front panel display click on the **[Show PID Control Panels]** button to display the PID Panels5 HP.vi front panel.

The PID Control display is separated into seven separate closed loop PID controllers. The upper row of panels (Loop 1, 7, 2, and 3) are dedicated to pump speed (liquid flow rate) control, while the lower panels (Loop 4, 5 and 6) manipulate the temperature control of the three main liquid streams: oil, cooling, and heating, respectively.

---

The PID output signals (4-20mA) processed are sent to the control devices (VFD or SSR), through the SCXI-1124 output card.

The values for the PID control variables (gain, reset, and derivative) can be viewed and changed by first selecting the panel index of the cluster array box in the lower right of the display window. The [PID CONFIG] switch button will toggle on/off the display of the PID Control Parameters control.

The temperature control loops 4 to 6 are limited by low flow and high temperature alarm set levels. In either instance, if process flow rate is less than the low flow alarm setting or the process fluid temperature is greater than the high temperature alarm setting, the power controller voltage supply will be disconnected. The red disconnect button for the SSR power controller serving the particular process immersion heater may also be pressed IN, as well.

Pressing the [Trend] panel button will toggle on/off the display of the loop's waveform graph of the PID control parameters set point (SP), primary variable (PV), and PID output (OUT%).

**[LOOP BYPASS]** switch — temperature control panels 4-5-6:

The flow meters indicating cooling flow (FT02) and heating flow (FT03) are not inline when the test loop is isolated from the cooling and heating fluid system streams; that is, the cooling Pump2 and heating system Pump3 are operating in bypass mode circulating fluid locally in the tank. The zero indicated flow rate will trigger a low flow alarm and the PID panel control will disconnect the power (open contactor at SSR box) to the immersion heater at the cooling fluid system tank (H2) and heating fluid system tank (H3). The [Loop Bypass] switch will over-ride the low flow alarm disconnect and allow H2 and H3 to be operated during the zero flow indicated situation. Therefore, when the switch is:

---

ON = flow meter is bypassed, no flow indication observed, SSR contactors can be closed to energize H2 and H3

OFF = flow meter not bypassed, flow indication observed, SSR contactors can be closed to energize H2 and H3 — normal operation during flow through the test loop

The **[PID CONFIG]** button toggles on/off the display of the alarm control settings and PID parameter controls.

The **[STOP ALL PID]** button, will allow the operator to shut down all control loops in case of emergency. The user is prompted with a confirmation dialog if this button is clicked, to allow him to bypass this operation if the button is accidentally pressed.

The user exits the PID control panel interface by clicking on the **[RETURN TO MAIN]** button switch.

### 3.0 System Filling and Preparation — Stage “b”

#### 3.1 Cooling Process Fluid System Start-Up — Tank TK-2 Skid Unit

##### 3.1.1 Add cooling process fluid to the system:

- For testing below 90°C (194°F) a fluid mixture of 60% ethylene glycol in water will be appropriate. With a required total volume of approximately 170 liters, use 100L glycol and 70L water. If HEX3 will be used in testing, an additional 80L will be required to fill the shell volume and the copper inlet/outlet piping manifolds of HEX3.
- At the cooling liquid tank TK-2 skid assembly:
  - Close the following valves:
    - Hose 4 liquid return isolation valve HV39

- 
- Hose 5 liquid return isolation valve HV71
  - SEC1 cooling supply isolation valve HV44
  - Bypass drain valve HV43
  - HV46 — SEC1 cold finger return line (Hose 2)
- 
- Open the following valves:
    - TK-2 lower outlet HV37 to Pump2 suction inlet
    - Bypass recirculation valve HV38
    - TK-2 liquid return isolation valve HV42
- 
- Add cooling liquid (glycol and water mixture) to fill tank TK-2 to a level just above the liquid return line at HV42 elevation (approximately 170L).

3.1.2 Begin recirculation of the “cooling liquid” at TK-2 in bypass mode to mix the ethylene glycol-water mixture thoroughly:

- Ensure that Pump2 stop buttons located at the pump and at the DAC cabinet front panel are pulled OUT.
- PID panel 2 “CLG” controls the speed of the cooling supply pump to the deposition SEC-1. Leave this controller in “MAN” (manual) control mode and adjust the OUT% control upwards to approximately 40-50% to achieve a nominal recirculation flow rate. Since the cooling flow meter FT02 is being bypassed at this stage, the PV panel indicator will not show a value.
- Open the closed isolation return valves to TK-2 (HV39, HV44, HV46, HV71) and close the bypass valve HV38 at Pump-2 to direct flow through the loop to fill The central pipe in the main deposition unit SEC-1.
- Increase cooling flow rate and open upper section vent valves to remove all entrained air.
- Once the system is filled, stop circulation through the loop. Cooling system is now ready for operation.

---

### 3.1.3 Heating the cooling system fluid

#### **If heating of the cooling glycol is required:**

- Turn ON cooling Pump2 circulating flow through the loop or in bypass mode.
- On PID panel #5 ensure loop control OUT% is zero
- If SEC1 cold finger is being bypassed, then press the [Loop Bypass] switch ON. This allows the SSR power controller for the in-line HTR2 to be used when no flow is being indicated.
- Pop out the SSR2 button at the power control box by slightly turning the button head. This button disconnects the 24Vdc required to energize the coil for the SSR2 contactor relay power supply.
- Adjust the set point (SP) value and press the MAN button to toggle control to automatic (AUTO) PID. Display the trending for the PID panel to monitor the SP, PV and OUT% variables. Adjustments to the gain, reset (integral) and derivative may be made at the configuration window.
- Monitor over time the temperature of the recirculating cooling liquid either at the main DAC front panel or the PID front panel. When the set point temperature is achieved the cooling liquid will be ready for circulation in the main loop. Continue bypassed circulation for now.

### 3.1.4 Operation of the refrigeration unit — maintaining a chilled fluid temperature

During standard test procedures, the cooling fluid will not be required to be heated, but chilled by the refrigeration unit and maintained at temperature in bypass mode until it is required to flow through the cold-finger of the deposition test SEC1 unit.

- Setup cooling system fluid to circulate in bypass mode.
  - At tank TK-2 close HV44 and HV46, open HV37, HV38, and HV42
  - Activate Pump2 flow control



- 
- Open pneumatic supply pressure to the refrigeration liquid bypass control valve controller.
  - Open HV40 and HV41, then switch ON power to chiller recirculation Pump4 (Grundfos)
  - Energize the chiller's PID controller mounted in the front panel of the DAC cabinet in the control room, adjust the temperature control setpoint, and put controller in automatic operation mode.
  - Energize the refrigeration unit by operating its disconnect switch.

The compressor of the refrigeration unit will operate in an on/off cycling mode with a  $\pm 1.8^{\circ}\text{C}$  control.

### 3.2 Heating Process Fluid System Start-Up — Tank TK-3 Skid Unit

#### 3.2.1 Add heating process fluid to the system.

- For testing below  $90^{\circ}\text{C}$  ( $194^{\circ}\text{F}$ ) a fluid mixture of 60% ethylene glycol in water will be appropriate.
- For testing above  $90^{\circ}\text{C}$ , a stable, thermal fluid at maximum  $160^{\circ}\text{C}$  ( $320^{\circ}\text{F}$ ) must be used. High temperature heat transfer fluid, of similar properties is suggested.

#### 3.2.2 At the TK-3 skid assembly:

- Close the following valves:
  - Hose 7 liquid return isolation valve HV52
  - Hose 8 liquid return isolation valve HV53
  - Hose 9 liquid return isolation valve HV62
  - SEC1 heating supply isolation valve HV55
  - Bypass drain valve HV54
  - TK-3 drain valve HV72

- 
- Open the following valves:
    - TK-3 lower outlet HV49 to Pump3 suction inlet
    - Bypass recirculation valve HV50
    - TK-3 liquid return isolation valve HV51
  - Charge the specified heating liquid to TK-3 to a level just above the liquid return line at HV51 elevation (approximately 170L).

3.2.3 Begin recirculation of the heating liquid at TK-3 in bypass mode and heat to the required temperature.

- Ensure that both Pump3 stop buttons located at the pump at the DAC cabinet front panel are pulled OUT.
- PID Panel 3 “HTG” controls the speed of the heating liquid supply Pump3 to the deposition SEC-1. Leave this controller in “MAN” (manual) control mode and adjust the loop OUT% control upwards to approximately 40-50% to achieve a nominal recirculation flow rate. Since the cooling flow meter FT03 is being bypassed at this stage, the PV panel indicator will not show a value.
- On PID panel #6 ensure OUT% is zero and then press the [Bypass] switch ON. This allows the SSR power controller for the in-line HTR3 to be used when no flow is being indicated.

When Bypass is “Off” during normal flow conditions through the loop a low alarm flow level or high temperature alarm will disconnect SSR3.

- Pop out the SSR3 button at the power control box by slightly turning the button head. This button disconnects the 24Vdc required to energize the coil for the SSR3 contactor relay power supply.
- Adjust the set point (SP) value and press the MAN button to toggle control to automatic (AUTO) PID. If you display the PID trend now you will see that

---

the OUT% to HTR3 will increase to 100% output until the SP and PV values come closer.

- Monitor over time the temperature of the recirculating heating liquid either at the main DAC front panel or the PID front panel. When the set point temperature is achieved the heating liquid will be ready for circulation in the main loop. Continue bypassed circulation for now.

### 3.3 Waxy Crude Oil System

#### 3.3.1 Crude Oil Supply Preparation

- Transfer approximately 120L of heated oil to TK-5.
- Make all connections from TK-5 to progressive cavity transfer pump and to main oil tank TK-1 at HV11, including the 100 psig air supply hose to the pump.
- Upon completion of Step 6 (System Heating and Heat Tracing) transfer ~85 liters of oil to tank TK-1 monitoring the level via the LabVIEW DAC front panel.
  - Open the TK-1 upper vent valve HV6, and lower drain/fill valve HV11
  - Open supply drain valve of TK-5 to the transfer pump, open-air supply valve for the pump and begin transfer of oil to TK-1.
  - Monitor oil level indicated by the DAC interface
  - When oil transfer is complete, close HV11.
  - Disconnect and drain out any oil from the transfer pump to the supply tank.

#### 3.3.2 Pressure Sensors

The tubing for the high and low legs of the pressure sensors must be filled with a suitable fluid to eliminate air (gas) in these lines. Use the high-pressure manual hydraulic pump to do this:

- Fill the supply bottle with the liquid to be filled,

- 
- Attach the high pressure stainless flexible ¼-inch tubing to the isolation valve fitting and tighten,
  - Open the isolation valve and pump supply valves
  - Pump in a suitable amount of liquid to insure the sensor leg is filled
  - Close the transmitter isolation valve and replace the safety cap onto the fitting.
  - Depressurize the pump hose, detach the hose
  - Repeat for all transmitter legs,
  - Oil Reservoir tank TK-1 level transmitter DPT01: the low-pressure leg of this transmitter senses the gas cap pressure of TK-1 through PT01 and must not be liquid filled. Liquid fill only the high-pressure sensor leg of DPT01.
  - Zero the DPT01 level signal when the high-pressure sensor leg is filled and the level in TK-1 is at a minimum level. Do this locally by pressing the “Z” button at the transmitter or trimming the zero with the Rosemount 275 HART interface.

### 3.3.3 Circulation of Oil in the Loop

Once the prepared oil under test has been transferred to the main reservoir tank TK-1 it can be injected through the main loop piping sections using either oil Pump1 or Pump5. The test piping is separated into two sections designed for low flow rate (1-inch pipe size) and high flow rate (2-inch pipe size) regimes. Depending on the flow regime used the piping sections not used may be isolated and not filled with oil. Certain units, such as the DP-1 oil differential pressure test section or the HEX-1 heat exchanger may not be required, also can be isolated if not required for the testing.

#### 3.3.3.1 Oil Pump 1 Operation — Low Flow Rates, 1-inch Pipe Section

- Isolate Oil Pump5 and all 2-inch pipe sections, including HEX3
  - Close valves HV76 at the oil tank TK-1 and valve HV83 at the deposition section SEC-1 oil inlet
  - Close valves HV84 at the SEC-1 oil outlet and oil return HV22 at oil tank TK-1

- 
- Open all oil 1-inch pipe sections through Pump1, FT01, HEX-1, SEC-1 and return to TK-1.
    - Open HV10, HV12, HV14, HV24 (DP-1 bypass), HV31 (SEC-1 inlet), HV35, and HV23
  - Close FT01 bypass HV16
  - Isolate the oil-gas mixing venturi section: close HV17, HV18, HV19, HV20
  - Ensure that the heating and cooling fluid hose connections for the shell of HEX1 and HEX2 are correctly installed.
  - With Pump1 adjustable speed drive VFD1 (Baldor) in remote operation mode, click the icon for Pump1 on the GUI front panel (LabVIEW) to switch Pump1 status ON, then select the PID Control Panels to adjust the speed of Pump1 (Panel1), in manual mode, to begin circulation of oil through the loop.

#### 3.3.3.2 Oil Pump 5 Operation — High Flow Rates, 2-inch Pipe Section

- Isolate Oil Pump1 and all 1-inch pipe sections, including HEX1
  - Close valve HV10 at the oil tank TK-1 outlet and valves HV21, HV31, HV91 at the deposition section SEC-1 oil inlet
  - Close valves HV84 at the SEC-1 oil outlet and oil return HV22 at oil tank TK-1
- Close all 2-inch line drain and vent valves at Pump5 and FT04: HV77, HV78, HV79, HV80
- Close all other 2-inch line drain and vent valves: HV92 at SEC1 oil outlet, and HV85 at HEX3 outlet
- At this time, isolate the 1-inch tubing bypass flow to the DP-1 test section through FT01: close HV81 and HV91
- Open all oil 2-inch pipe sections through Pump5, FT04, SEC-1, HEX3 and return to TK-1.
  - Open HV76 (Pump5 suction), HV83, HV84 (SEC-1 inlet), and HV22
- Ensure that the heating and cooling fluid hose connections for the shell of HEX2 and HEX3 are correctly installed.

- 
- With Pump5 adjustable speed drive VFD1 (WEG) in remote operation mode, click the icon for Pump5 on the GUI front panel (LabVIEW) to switch Pump5 status ON, then select the PID Control Panels to adjust the speed of Pump5 (Panel 7), in manual mode, to begin circulation of oil through the loop.

### 3.4 DP-1 Test Section Operation

The differential pressure test section DP-1 is constructed using two parallel lengths of process tubing, one 0.500”O.D. x 0.065”W and one 0.750” x 0.65”W, inside a 3-inch pipe shell (see Appendix for full specifications). The DP-1 test section can be used when either oil Pump1 or Pump5 is being used.

Flow rate is directed through DP-1 by first opening the isolation valves for the tube string to be used; for example, HV27 and HV28 opens the ¾-inch tube section. Open heating fluid flow to the shell of DP-1 and maintain the outlet temperature above the oil WAT.

If Pump1 is being operated (1-inch pipeline):

- Close DP-1 section bypass isolation valve HV24 (bypass)
- Open DP-1 outlet HV90 (If the ¾-inch isolation valve HV91 at the oil inlet to SEC-1 is closed, oil flow will be directed through HEX1 before entering SEC-1)
- Open DP-1 HV27 and HV28 for ¾” tubing flow or
- Open DP-1 HV29 and HV30 for ½” tubing flow.

If Pump2 is being operated (2-inch pipeline):

- At the 1-inch flow meter unit, FT01, close HV12, HV13, HV15, and HV16
- The venturi flow stream will not be required: close HV17, HV18, HV19 and HV20
- At the DP-1 section close bypass HV24 and outlet HV90
- At the outlet of the 1½-inch flow meter, FT04, direct flow into the 1-inch tubing bypass line towards FT01: open HV81 and HV82
- Open HV91 at the oil inlet to SEC-1
- Monitor oil flow rate through DP-1 using FT01 or FT04

- 
- Oil flow rate can be controlled by reducing Pump5 speed or choking the 2-inch valve HV83 at the SEC-1 oil inlet

#### 4.0 System Heating and Pressurization — Stage “c”

##### 4.1 System Heating

##### 4.1.1 Open SEC-1 to “cooling liquid” recirculation at elevated temperature as prepared in procedure 6.1:

- Open SEC-1 isolation valves HV44, HV46, and HV75 (all near FT02)
- Close TK-2 bypass valve HV38
- Open HEX-2 jacket to TK-2 cooling liquid recirculation (Hose 3)
  - Open branch HV45, jacket inlet HV48, and TK-2 return HV39.
- Continue to maintain TK-2 elevated temperature above WAT as defined in procedure 6.1.1.

##### 4.1.2 Open SEC-1 to heating liquid recirculation at elevated temperature as prepared in procedure 6.2

- Open SEC-1 isolation valves for the heating jacket: HV55, HV56, HV61, HV74, and HV62
- Close heating TK-3 bypass valve HV50
- Open heating liquid recirculation to oil temperature trim HEX-1 and HEX-2 units by:
  - Closing HV65 (HEX-2 inlet) and HV66, HV67, HV69 (HEX-1)
  - Opening HV63 (at SEC-1 jacket outlet) branch, HV64, HV68, and HV53
- Continue to maintain TK-2 elevated temperature above oil cloud point as defined in procedure 6.2.3.

##### 4.1.3 Open DP-1 section heating jacket to heating fluid recirculation from TK3

- Close DP-1 jacket drain valves HV58, HV59

- 
- Open jacket inlet valve HV57 and TK-3 liquid return HV52 (Hose 7)

#### 4.2 Heat Tracing

Prior to injection of the prepared waxy crude oil into the system loop via the high pressure TK-1 reservoir, the auxiliary heat tracing will be required to preheat TK-1 and oil recirculation piping to a temperature above the WAT of the oil.

The high pressure oil vessel TK-1 is wrapped with a 2.09 kW flexible silicon heating tape (240V) and is temperature controlled using the Power Control Box 2 holding the Omega CN76000 PID controller and SCR power controller.

- Energize the PID controller and set the required TK-1 surface temperature
- Connect heating tape HT-1 to the power supply cable
- By pulling out the red disconnect button on the PCB-2 front panel, HT-1 will be energized.
- Monitor heating and adjust control parameters as required via the PID controller
- Maintain the body temperature of the TK-1 vessel at the required set point until the moment oil will be injected, at which time HT-1 will be de-energized: push in the disconnect button on PCB-2 and disconnect the power cable from HT-1. The PID controller can be placed into manual mode and set for zero percent output.
- Continue monitoring TK-1 surface temperature via the PID controller.

The heat trace units HT-2, HT-3, HT-4, HT-5, and HT-6 (Omega HTWC102-010), are individually controlled by dedicated percentage power controllers at the plug end of the tapes. Plug these units into power feed cables as required and manually adjust the power supply to the heat trace tapes, monitoring the pipe surface temperatures. It is recommended to use low controller settings of 30-50% for slow heating. Monitor the temperature of the pipe surface and adjust amount of power to the heat trace as required.

Once the pipeline is sufficiently heated to a temperature above the WAT of the oil, heating may be removed and oil circulated into the loop (see Step 6.3.1).



---

### 4.3 System Pressurization

The oil loop section is pressurized with gas (nitrogen) with the “Wainbee” gas booster system. This system is designed to take gas flow from 100 psig at the inlet up to a 2500 psig discharge pressure. A gas bottle on the discharge side of the system allows for storage of the high-pressure gas (up to 2500 psig).

### 5.0 System Shutdown — Stage “d”

5.1 Continue to operate the heating and cooling liquid flow regimes.

5.2 Isolate SEC-1 from normal oil flow circulation:

- Open SEC-1 oil bypass HV36
- Close choke valve HV21, HV31, and HV35

5.3 The oil system will be allowed to depressurize slowly:

- Depressurize oil vessel TK-1 ~ 25 psig lower than present operating pressure value by opening slightly HV6 to vent gas to atmosphere,
- Open upper TK-1 isolation valve HV6A,
- Return oil from SEC-1 to TK-1 by opening slightly regulating isolation valve HV33
- Allow pressures in SEC-1 and TK-1 to equalize.
- Repeat until atmospheric pressure is obtained.

5.4 Stop oil flow – Pump1 or Pump5

- On the operator front panel, click on the pump icon to toggle to “OFF” state (red),
- On PID panel 1, adjust in “MANual” mode the output to zero %,
- Press “Stop” at Pump1 motor speed controller VFD1, and locally at the pump location,
- Shut off power to oil HTR1 by making output % zero on PID Panel4, and pressing in the power disconnect button at the SSR1 panel.

- 
- 5.5 Once the system has depressurized, drain fully the oil from units SEC-1, HEX-1, and DP-1, collecting the oil and transferring to suitable container.
- Install suitable drain hose to drain valve HV13 at the oil flow meter FT01 manifold,
  - If FT01 is used, then open its upper vent HV15 and drain HV13. If FT04 is used, then open its upper vent HV80 and drain HV79
  - If HEX-3 is used, then open its oil drain HV85
- 5.6 If required, the oil from vessel TK-1 can be drained now:
- Open upper TK-1 vent valve HV6
  - Install suitable drain hose to TK-1 drain HV11
  - Open HV11, transferring oil to suitable container/drum.
- 5.7 Drain oil from the in-line immersion heater HTR1 section
- Install drain hose to lower drain valve HV73
  - Open HV73, transferring oil to suitable container/drum.
- 5.8 Turn off removing any heat tracing to TK-1 or other oil piping sections.
- 5.9 Turn off the “cooling liquid” system:
- Switch off the power to compressor/chiller unit at TK-2 skid.
  - Stop Pump2 using PID Panel 2 making output % zero and pressing the “Stop” button at VFD2.
  - Isolate the “cooling liquid” circulation piping at the deposition SEC-1 unit from TK-2.
  - Open TK-2 bypass line valve HV38 at pump 2
  - Close cooling liquid supply valves HV44, HV45, and HV75
  - Close TK-2 liquid return isolation valve HV42
  - Place a 20-liter container at the drain at valve HV43 near Pump2, open the valve and drain all fluid from the SEC-1 cooling section transferring the ethylene glycol to a suitable container.
-

- 
- 5.10 Turn off the “heating liquid” system:
- Shut off heating to HTR3 by making output % zero on PID Panel 6 and pressing in the power disconnect button for SSR3.
  - Stop Pump3 using PID Panel3 making output % zero and pressing “Stop” button at VFD3.
- 5.11 Turn off the logging of data at the LabVIEW DAC front panel user interface:
- Press the [Log Data] switch OFF
  - Press the [STOP] button and then [YES] to confirm the shutdown (outputs to all process controllers – pump speed drives and heater SSR power controllers will be zeroed and stopped).

## 6.0 Data Acquisition Shut Down

Pressing the “STOP” button on the front panel of the DAC controller will initiate closing of the process control and reset all outputs to zero (all VFDs and SSRs), and close the logging file. The data file logged is in spreadsheet text format and can be opened and processed within Excel readily. A header file in Excel .xls format has been created and can be opened, placing the column identifiers above the data. Resave the new file in Excel .xls format.

---

## **APPENDIX D: Working Fluids Properties**

The physical properties of the working fluids (oil and water-glycol mixture) used in the experimental program of this study are determined via standard test method. In order to ensure the consistency of the working fluid properties, the properties of each fluid were measured twice, one time with a fresh sample (before it used in the system) and another one with a used sample taken at the end of the experimentation.

### ***Density measurement***

The D 4052 – 96 standard test method is used for the determination of the density of the working fluids used in the experimental program of this study.

A small volume (approximately 0.7 ml) of liquid sample is introduced into an oscillatory sample tube and the change in oscillatory frequency caused by the change in the mass of the tube is used in conjunction with calibration data to determine the density of the sample.

### ***Kinematic viscosity measurement***

D 445 – 06 standard test method is used for measuring the kinematic viscosity (and calculation of the dynamic viscosity) of the working fluids. By measuring the time for a volume of liquid to flow under gravity through a calibrated glass capillary viscometer. The dynamic viscosity,  $\mu$ , can be obtained by multiplying the kinematic viscosity,  $\nu$ , by the density,  $\rho$ .

The time is measured for a fixed volume of liquid to flow under gravity through the capillary of a calibrated viscometer under a reproducible driving head and at a closely controlled and known temperature. The kinematic viscosity (determined value) is the product of the measured flow time and the calibration constant of the viscometer. Two

such determinations are needed from which to be calculate kinematic viscosity result that is the average of two acceptable determined values.

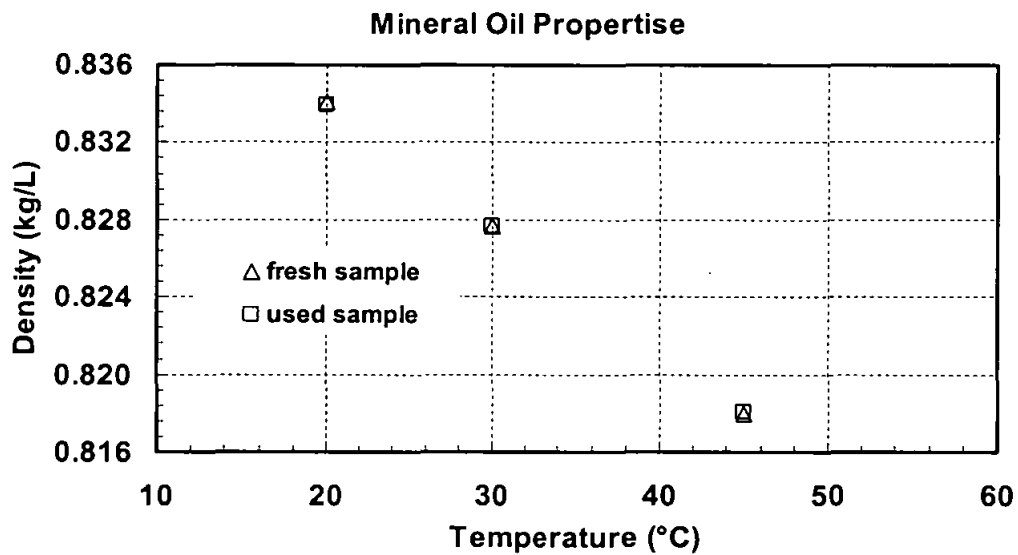


Figure D.1: Mineral oil density measurements

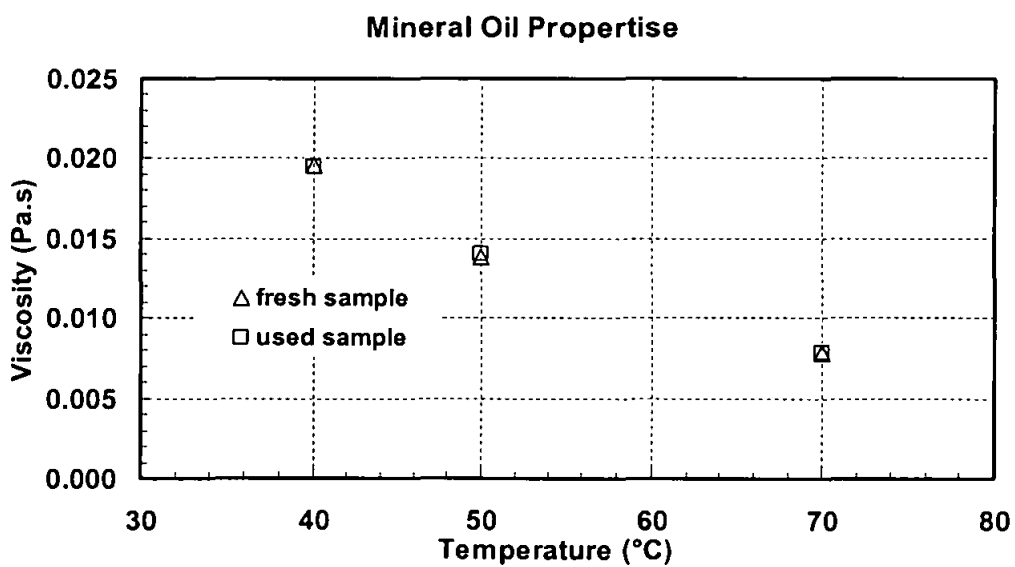


Figure D.2: Mineral oil Kinematic viscosity measurements

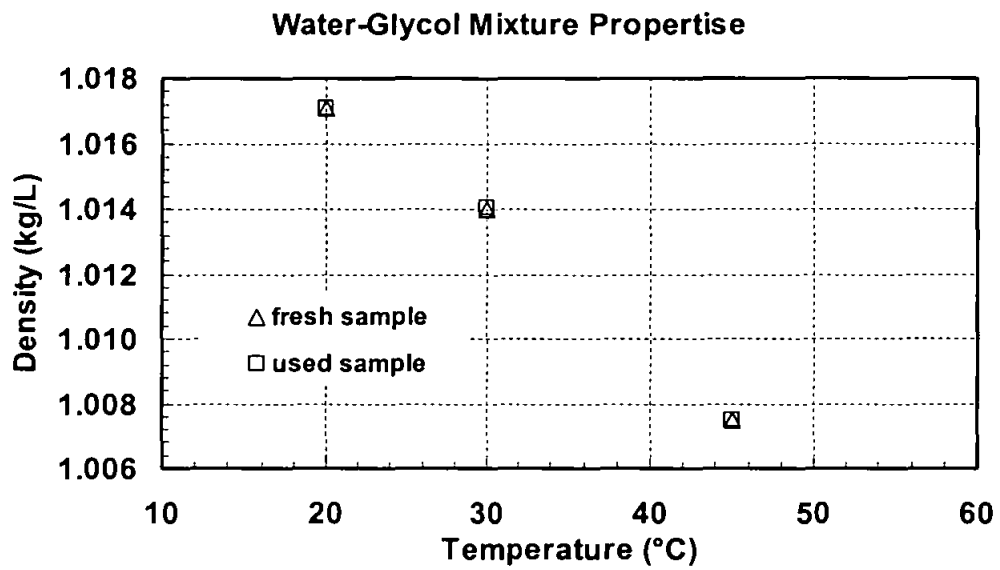


Figure D.3: Water-glycol mixture density measurements

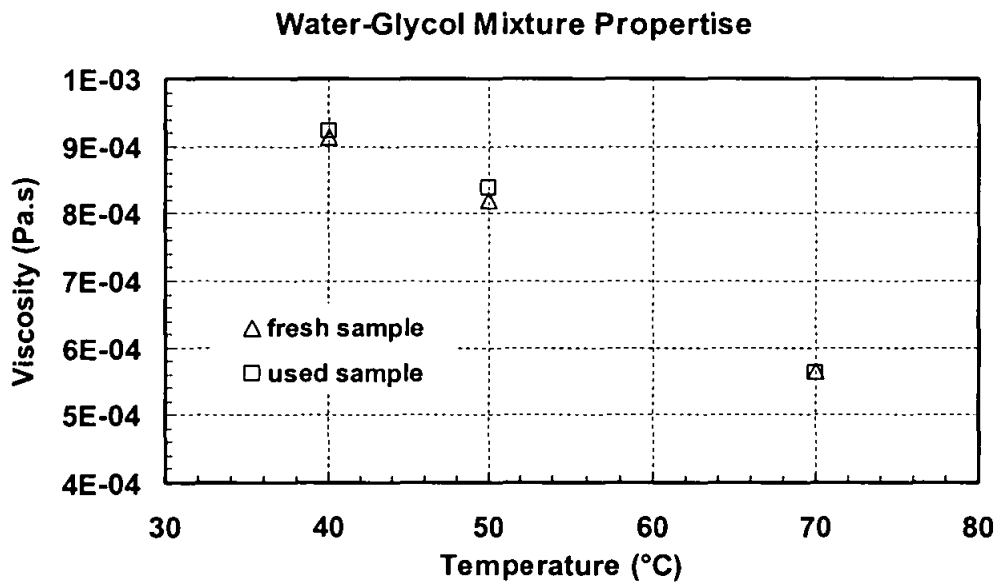


Figure D.4: Water-glycol mixture kinematic viscosity measurements

Table D.1: thermal properties of the working fluid.

fluid	Property	Correlation	Comment
Oil	Specific Heat, $C_p$ (Kj/Kg. °C)	$(0.6811 - 0.308 \times S) + T$ $(0.000815 - 0.000306 \times S) \times$ $(0.055 \times k + 0.35)$	A relationship developed by Bland and Davidson, 1967. S, is the specific density and k is the Watson characterization defined as: $K = (T_B)^{1/3} / S$ Where TB is the average of five temperature (10, 30, 50, 70, 90% vaporized) in degrees Rankin.
	Thermal conductivity, K (W/m. °C)	$(0.117/S) \times (1 - 0.00054 \times T)$	
Glycol-water	Specific Heat, $C_p$ (Kj/Kg. °C)	$(0.000009 \times T^3 - 0.001 \times T^2 + 0.0275 \times T + 2.2575) \times \alpha + (1 - \alpha) \times (0.000006 \times T^2 - 0.0003 \times T + 4.1825)$	The specific heat of the water-glycol mixture is calculated with the compositional regression as a function of glycol average temperature T. $\alpha$ , is the glycol/water ratio, and this value resulted after the measured mixture density-temperature was compared to the compositional density.

---

## APPENDIX E: Statistical Error Analysis

This error analysis is utilized to check the accuracy of the models. The statistical parameters used in the present work are:

### 1. Average Percent Relative Error

It is the measure of relative deviation from the experimental data, defined by:

$$E_r = \frac{1}{n} \sum_{i=1}^n E_i$$

where  $E_i$  is the relative deviation of the calculated value from the measured value.

$$E_i = \left( \frac{(DP)_{calc} - (DP)_{meas}}{(DP)_{calc}} \right) \times 100$$
$$i = 1, 2, 3, \dots, n$$

where:  $(DP)_{calc}$  is the calculated pressure drop  
 $(DP)_{meas}$  is the measured pressure drop

### 2. Average Absolute Percent Relative Error (AAPE)

It measures the relative absolute deviation from the measured value, defined by:

$$E_a = \frac{1}{n} \sum_{i=1}^n |E_i|$$

This will be considered as the main criterion in statistical error analysis in this study.

### 3. Minimum and Maximum Absolute Percent Error

$$E_{\min} = \min_{i=1}^n |E_i|$$

$$E_{\max} = \max_{i=1}^n |E_i|$$



#### 4. Root Mean Square Error

Measure the data dispersion around zero deviation, defined by:

$$RMSE = \left[ \frac{1}{n} \sum_{i=1}^n E_i^2 \right]^{0.5}$$

#### 5. Standard Deviation Error

It is measure of dispersion and is expressed as:

$$STD = \sqrt{\frac{1}{(m-n-1)} \sum_{i=1}^m \left[ \left( \frac{(DP)_{calc} - (DP)_{meas}}{(DP)_{calc}} \right) \times 100 \right]^2}$$

where (m-n-1) represents the degree of freedom in multiple regression. A lower value of standard deviation indicates a smaller degree of scatter.

#### 6. The Correlation Coefficient

It represents the degree of success in reducing the standard deviation by regression analysis, defined by:

$$R = 1 - \frac{\sum_{i=1}^n [(DP)_{calc} - (DP)_{meas}]}{\sum_{i=1}^n (DP)_{meas} - \overline{\Delta DP}}$$

Where:

$$\overline{\Delta DP} = \frac{1}{n} \sum_{i=1}^n [(\Delta DP)_{act}]_i$$

“R” value range between 0 and 1. The closer value to 1 represents perfect correlation correlations whereas 0 indicates no correlation at all among the independent variables.

# APPENDIX F: The Moody Experimental Diagram

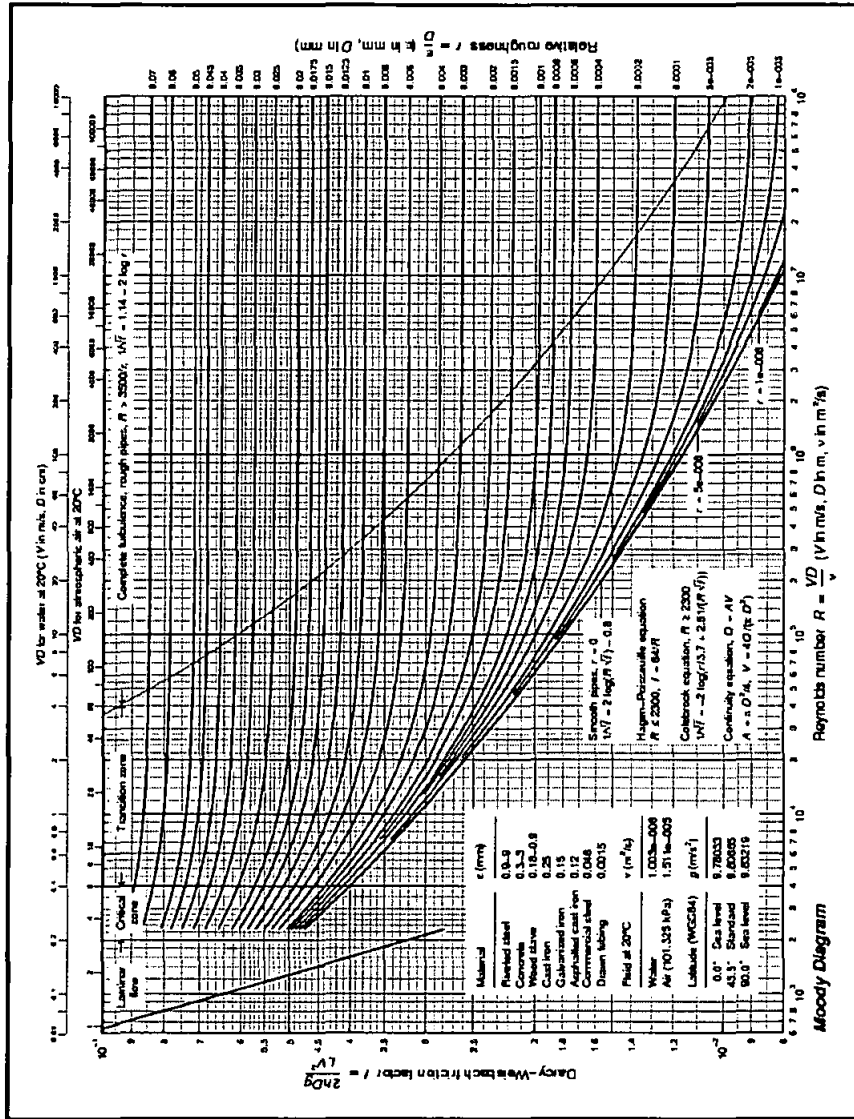


Figure F.27: Friction factor as function of Reynolds number and relative roughness - Moody experimental chart for smooth and rough circular pipes (White, 1998).